Universidade Federal de Minas Gerais

Departamento de Fśica
Instituto de Ciências Exatas

A Thesis Submitted for the Degree of Doctor of Philosophy in Physics

Propagation of Higher Order Correlation Beams in Turbulent Atmosphere

Candidate:
Hakob Avetisyan

Thesis Supervisor:
Prof. Carlos H. Monken

ABSTRACT

This Thesis deals with theoretical aspects of atmospheric propagation of correlation beams. The correlation beam is prepared in the process of low gain spontaneous parametric down-conversion in the two photon regime within the thin crystal approximation with the correlated direct detection scheme. The joint detection probability amplitude has a beam-like behavior of spatial correlations in two-photon states, hence the name. The correlation beam is the most practical tool in various quantum communication protocols, thus, studying its propagation in the atmosphere is of practical and fundamental interest opening a possibility of performing a global quantum communication. Moreover, one can prepare two-qudit states to implement a communication with large alphabets. To this end, we analytically calculated the atmospheric two-photon joint detection probability when the pump represents a coherent Hermite- or Laguerre Gaussian mode of any order as well as a partially coherent beam from a Gaussian-Schell model source. As an important side result, we showed that the joint probability for the latter case is a convex combination of the former ones. Our results show that the expressions for fourth-order correlation functions are similar to those of intensities of classical beams: a manifestation of the concept of the correlation beam. Additionally, we showed that with the strength of the turbulence the amount of the HG_{00} mode is appreciable even in moderate turbulence, meaning that the cross-talk between modes increases with turbulence degrading the dimensionality of the alphabet based on higher-order Gaussian modes.

To quantify the crosstalk between different modes, which is inevitable when propagating in the atmosphere, we made a mode analysis of the correlation beam. An operational procedure to implement projective measurements on two-photon multimode states is also given. Because of the mathematical difficulty, we considered only the zeroth order Gaussian pump.

We calculated the probability of single photodetections and compared with the two-photon joint detection probability. The former probability degrades rapidly after short distances of propagation, whereas the latter one is considerable even after five or more kilometers of propagation. The analytical approach used in this Thesis enables one to deal with the subject more deeply.

Finally, we set up two approached to solve certain problems. One of them concerns the correction of the corrupted two-photon wave phase using Zernike polynomials. The other – the inference of atmospheric parameters by measuring the correlation beam. Certainly, the

parameters that can be inferred only with fourth order statistics, e.g., the scintillation index, the intensity correlation width, are easier to infer using a correlation beam, which is a fourth-order phenomenon.

to my parents

ACKNOWLEDGEMENTS

I express my sincere gratitude to my supervisor Prof. Dr. Carlos Henrique Monken for his continuous support during my PhD study. I am grateful for his patience, motivation, and immense knowledge that I have gained while collaborating with him. Prof. Monken's guidance was especially beneficial for my research and preparation of this Thesis.

I would also like to thank my qualification exam committee members, Prof. Dr. Pablo Lima Saldanha, Prof. Dr. Ronald Dickman, and Prof. Dr. Leonardo Teixeira Neves, for their insightful comments and encouragement as well as for motivating questions which helped me to deepen my understanding and widen my research from various perspectives. Prof. Dr. Pablo Lima Saldanha and Prof. Dr. Ronald Dickman were also in my PhD defence committee with Prof. Dr. Daniel Schneider Tasca and Prof. Dr. Stephen Patrick Walborn pointing out interesting additional viewpoints of the results of this Thesis that I failed to see before. Thank you. Apart from the committee members, I thank the professors of the courses I have taken in the first two years of my PhD studies.

I acknowledge the stimulating discussions with my colleagues and friends, Davi, Ana Paula, Marcello Nery, Gláucia, Eliel, Raul, Natália, Tassius, André Tanus, Thiago Maciel, Érico, Marcelo Pereira, Renan, Paula, Mario, Roberto, Gilberto, Artur.

My sincere gratefulness to the fellows from Maracatu, people who changed my life bringing closer to Brazilian culture, Daniela Ramos, the leader of Trovão das Minas, Mirna, for constantly being in my life during my last months in Brazil, Eliel, Joilson, Andreij, the physicist triple in Maracatu; João, Phillip, Pedro, Atila, Lucas, Ellen, Livia, Letícia and the rest of my awesome friends!

I am grateful to my flatmates Alisson and Aroldo for their kindness and patience in living together and friendship during my stay in Brazil. Thank you guys!

I thank Luis and his family for their friendship and Colombian breakfasts we had together. I also thank two Armenian families that live here in Belo Horizonte. Alexandre, Shoghik, Andranik and Lulu, thank you for your friendship and many dinners we had together. Violinists Ara and Anahit, thank you for your friendship and invitations for concerts in Orquestra Filarmónica. Thank you!

I wholeheartedly thank my friends from Armenia, Armen, Davit, Anna, Ruben who had a huge and encouraging influence in many of my life decisions and in my personal development.

Last, I would like to thank my family: my parents, Samvel and Susana, and my sisters, Armineh and Siranush, for supporting me throughout these four years abroad. Without the help of all of my colleagues, professors, friends and family members this Thesis could not have been accomplished. Thank you all!

DECLARATION

I, HAKOB AVETISYAN, declare that this thesis titled, 'PROPAGATION OF HIGHER ORDER CORRELATION BEAMS IN TURBULENT ATMOSPHERE' and the work presented in it are my own. I confirm that:

- This work was done wholly or mainly while in candidature for a research degree at this University.
- Where any part of this thesis has previously been submitted for a degree or any other qualification at this University or any other institution, this has been clearly stated.
- Where I have consulted the published work of others, this is always clearly attributed.
- Where I have quoted from the work of others, the source is always given. With the exception of such quotations, this thesis is entirely my own work.
- I have acknowledged all main sources of help.
- Where the thesis is based on work done by myself jointly with others, I have made clear exactly what was done by others and what I have contributed myself.

Signed: _____

Date: _____

CONTENTS

1

INTRODUCTION

The study of the effects of turbulent or random media on the propagation of non-classical light has gained a considerable interest due to the possibility of implementing quantum optical communication links with entangled photons [1, 2].

In order to avoid absorption effects in long–distance quantum optical communications, one needs to exploit satellite–based free-space distribution of single photons or entangled photon pairs. In this scheme, photonic quantum states are first sent through the atmosphere, then reflected from one satellite to another, and finally sent back to a ground station. Since the effective thickness of the atmosphere is of the order of $5 - 10$ km (i.e., the whole aerosphere is equivalent to $5 - 10$ km ground atmosphere) and photon losses and decoherence are negligible in outer space, one can achieve global free-space quantum communication as long as the quantum states survive after penetrating the atmosphere.

Transmission through free space can be used as a channel for high - dimensional quantum communication if an orthogonal propagating mode set is used as a d-level system (qudit). In this context, electromagnetic beams carrying orbital angular momentum open an opportunity for communication with large alphabets [3]. Unfortunately, unlike polarization, transverse mode profiles can be severely distorted by turbulence. Transmission through turbulence could thus be regarded as a decohering channel for the transverse spatial degrees of freedom [4, 5]. Several theoretical studies have been devoted to the investigation of turbulence effects on the propagation of electromagnetic beams carrying orbital angular momentum [6–9]. An experiment in which orbital angular momentum states in free space propagation were used as a multiplexing resource for classical communication was performed with radio waves (at a wavelength λ = 12.5 cm) at a 442 m propagation distance [10]. In the optical domain, free-space classical communication using orbital angular momentum has been demonstrated in Ref. [11]. Quantum key distribution through free space should also be considered, since it is possible to distill secure final keys even in the presence of some noise in the quantum channel [12]. The transport of orbital-angular-momentum entanglement through a turbulent atmosphere has been studied experimentally using a turbulence chamber [13]. Alignment-free quantum key

distribution through free space for a distance of 210 m exploiting orbital angular momentum in combination with polarization to encode the quantum bits has been demonstrated [14]. A recent experiment demonstrating a distribution of quantum entanglement encoded in orbital angular momentum over a turbulent intra-city link of 3 kilometers has been done [15].

The effects of the atmospheric turbulence can be simulated in the laboratory by artificially inducing random phase fluctuations in optical beams. This become possible due to Keskin et al. [16] who designed a turbulence generator. They showed experimentally that it can emulate basically any turbulence strength. Most theoretical and experimental studies [17–20] of the effects of atmospheric turbulence on the modal entanglement of photon pairs are based on the single phase screen approach, which uses a single phase screen to model the turbulent atmosphere [21]. The random phase function of such a phase screen represents the phase modulation caused by the turbulence under weak scintillation conditions. An alternative approach valid in all scintillation conditions, the multiple phase screen approach, was recently used to derive first-order differential equations that enable the study of turbulence-induced decoherence of transverse spatial mode entanglement of photon pairs [7, 22]. According to [7], the parameter dependence in the atmospheric decoherence process is more complex than what is found in the single phase screen approach [6].

An appreciable research activity on other related topics has been observed, including: communication [23–28], entanglement in orbital angular momentum [20, 29]; negative correlations [30–32]; two-photon speckle [33–36]; spatial correlations [37, 38, 41]; ghost imaging [40, 42–44]; interference, anti-bunching and symmetry properties [45, 46], and high-dimensional quantum cryptography [47].

To the best of our knowledge, no analytical study considering the propagation of *pairs* of entangled photons (two-photon beams) through a turbulent atmosphere is available. In this Thesis we study the optical turbulence effects on a transverse-mode entangled two-photon beam generated by the parametric down-conversion process in a nonlinear $\chi^{(2)}$ crystal [48]. As a result, we calculate the *atmospheric* fourth-order correlation function (the so called two-photon speckle) in the cases when the $\chi^{(2)}$ crystal is pumped by any coherent Hermite or Laguerre-Gauss beam or by a partially coherent beam. In the former case, the higher-order correlation beams can be used for quantum communication tasks with large alphabets if the quantum correlations maintain after propagating through atmosphere. The later case is particularly interesting because the beams produced by partially coherent sources spread less in the random medium than coherent beams [49–51].

The Thesis is organized as follows: a short review of SPDC process and correlation beams is presented as well as the highlights of the main aspects of the theory of optical turbulence in Ch.2. The development of the study of correlation beams in the atmosphere is presented in Ch.3. There we consider the cases when the source (pumping the $\chi^{(2)}$ crystal) of the correlation beams is coherent Hermite-Gauss as well as partially coherent beam. These results are published in our paper [138]. As is known, the twin photons generated from the spontaneous parametric down-conversion process are entangled in transverse Hermite-Gaussian modes and the mode indices of the pump and the down-converted photons obey selection rules. In Ch.4 we calculated the joint probability of detecting the down-converted photons in different modes and analyzed the modal properties of correlation beams after propagating through atmosphere. Some open problems are discussed in Chapters 6 and 7. Finally, in the appendices we give information on HG and LG beams, on generation of LG beams and provide some derivations of the results that are discussed in Chapters 3 and 4.

Part I

BACKGROUND THEORIES

2

BACKGROUND THEORIES

2.1 SPONTANEOUS PARAMETRIC DOWN-CONVERSION PROCESS

According to the classical description of three-wave mixing within a nonlinear crystal, for *spontaneous* parametric down conversion, no non-zero field except for the pump field appears in the solution of the equations [52, ch. 7]. And yet, experience shows that new waves do indeed appear. The phenomenon is called spontaneous parametric down-conversion (SPDC) or parametric fluorescence. The process of spontaneous parametric down-conversion has been observed for the first time by Burnham and Weinberg [53]. This process *emerges as amplification of the vacuum fluctuations associated with the non commutation of the field operators* [55–57], *and is analogous to spontaneous emission by an excited atom. Like the latter, it can only be handled by a purely quantum theoretical approach*. It can be understood as splitting of the pump photon into two lower energy photons, called *signal* and *idler*, when passing through a nonlinear and non centrosymmetric medium. The downconverted photons sometimes are called twins because they are "born" together. Energy and momentum conservation laws of the form

$$\omega_p = \omega_s + \omega_i, \tag{1}$$

$$\mathbf{k}_p = \mathbf{k}_s + \mathbf{k}_i \tag{2}$$

are only met when the phase matching condition is satisfied. Here ω_j and $\mathbf{k}_j$, $j = p, s, i$ are the frequencies and wave-vectors of the pump, signal and idler photons, respectively.

The condition (2) does not need to be rigorously fulfilled. For one thing, in a crystal of finite thickness L, it actually has the form $\Delta k \leq \pi/L$, with $\Delta\mathbf{k} = \mathbf{k}_p - \mathbf{k}_s - \mathbf{k}_i$, and for another, the mixing process has a non-zero amplitude even if the condition is not satisfied. It thus has a quite different status to the relation $\omega_p = \omega_s + \omega_i$, which holds exactly when monochromatic beams are used. (The situation is quite different with ultra-short pulses, where the frequency dispersion is high.)

The down-converted beams usually do not propagate in the same direction; instead, they emerge from the non-linear birefringent medium at some small angle determined by the phase matching conditions (1), (2). In a uniaxial crystal, there are two ways of satisfying the phase matching condition, known as type I and type II. In type I phase matching, a pump photon polarized in the ordinary (extraordinary) o(e) direction creates two extraordinarily(ordinarily) e(o) polarized photons, whereas in type-II, the down-converted photons have orthogonal polarizations. Because of birefringence different polarized photons "see" different refractive indices.

The theoretical treatment is based on perturbative expansion in the interaction picture [58]. The quantum state of the two down-converted photons is non-separable, meaning that it cannot be written as a product of two one-photon states. Thus the two-photon, or biphoton state must be regarded as a single entity, which results in a plethora of interesting quantum phenomena. This non-separability arises from the various constraints and conservation laws present in the SPDC process.

Under certain approximations the post selected two photon state generated in the SPDC process is given by [48]

$$|\psi_{SPDC}\rangle = \sum_{\sigma_s,\sigma_i} \int d\omega_s \int d\omega_i \int d\mathbf{q}_s \int d\mathbf{q}_i \Phi_{\sigma_s,\sigma_i}(\mathbf{q}_s, \mathbf{q}_i, \omega_s, \omega_i) |\mathbf{q}_s, \omega_s, \sigma_s\rangle |\mathbf{q}_i, \omega_i, \sigma_i\rangle, \quad (3)$$

where $|\mathbf{q}_j, \omega_j, \sigma_j\rangle$, $j = s, i$ is a one-photon state in the mode defined by the transverse component $\mathbf{q}_j$ of the wave vector, by the frequency ω_j and by the polarization σ_j. $\Phi_{\sigma_s,\sigma_i}(\mathbf{q}_s, \mathbf{q}_i, \omega_s, \omega_i)$ represents the joint probability amplitude of signal and idler photons. It strongly depends on the phase matching conditions and the birefringence of the nonlinear crystal. phase matching Φ is a symmetric function For rigorous treatment of spatial correlations in parametric down-conversion and applications see [48] and the references therein.

2.1.1 *The Correlation Beam.*

In general, quantities involving both operators and state vectors take the same form in either the Schrödinger or the Heisenberg representation. For example, the single photodetection probability in the Schrödinger representation is given by

$$P_1(\mathbf{R}, t) \propto s\langle\psi(t)|\mathbf{E}^{(-)}(\mathbf{R}) \cdot \mathbf{E}^{(+)}(\mathbf{R})|\psi(t)\rangle. \quad (4)$$

In the Heisenberg picture, this becomes,

$$P_1(\mathbf{R}, t) \propto s\langle\psi|\mathbf{E}^{(-)}(\mathbf{R}, t) \cdot \mathbf{E}^{(+)}(\mathbf{R}, t)|\psi\rangle \quad (5)$$

where $s \leq 1$ represents the sensitivity of the detector. $\mathbf{E}^{(+)}(\mathbf{R},t)$ and $\mathbf{E}^{(-)}(\mathbf{R},t)$ are so called positive and negative frequency parts of the field operator, which, in travelling plane wave basis takes the form

$$\begin{aligned}\mathbf{E}(\mathbf{R},t) &= \sum_{\ell} i\mathbf{e}_{\ell}\sqrt{\frac{\hbar\omega_{\ell}}{2\varepsilon_0 L^3}}\left(a_{\ell}e^{i(\mathbf{k}_{\ell}\cdot\mathbf{R}-\omega_{\ell}t)} - a_{\ell}^{\dagger}e^{-i(\mathbf{k}_{\ell}\cdot\mathbf{R}-\omega_{\ell}t)}\right) \\ &\equiv \mathbf{E}^{(+)}(\mathbf{R},t) + \mathbf{E}^{(-)}(\mathbf{R},t),\end{aligned} \tag{6}$$

where $\mathbf{E}^{(+)}$ and $\mathbf{E}^{(-)}$ are the positive and negative frequency components of the field operator and they are hermitian conjugates of each other. To a certain extent the non-Hermitian operators $\mathbf{E}^{(+)}$ and $\mathbf{E}^{(-)}$ play the role of configuration space annihilation and creation operators at the space-time point (R,t). They correspond very closely to the analytic signals used in the classical treatment. The real field is often difficult to measure in the optical domain and beyond. Most observations in optics are based on the absorption of light, either through the use of a photodetector, or a photographic plate or even the eye. It is therefore not surprising that the annihilation operator $\mathbf{E}^{(+)}(\mathbf{R},t)$, rather than the real field $\mathbf{E}(\mathbf{R},t)$ operator, plays the dominant role in the description of quantum optical experiments.

When one considers joint photodetection rates, the Heisenberg picture is more general because it allows one to express the rate of joint detections at two different times t_1 and t_2 as follows:

$$P_2(\mathbf{R}_1,t_1,\mathbf{R}_2,t_2) \propto s_1 s_2 \langle\psi|\mathbf{E}^{(-)}(\mathbf{R}_1,t_1)\mathbf{E}^{(-)}(\mathbf{R}_2,t_2)\mathbf{E}^{(+)}(\mathbf{R}_2,t_2)\mathbf{E}^{(+)}(\mathbf{R}_1,t_1)|\psi\rangle \tag{7}$$

The fields appearing in this expression are written in time- and normally ordered fashion.

There exist correspondences between the fourth order correlation for the parametric down-conversion field and the second-order correlation for the pump beam as shown in P. L. Saldanha's Master's dissertation [59]. In the degenerate parametric down-conversion process, Saldanha has shown theoretically and experimentally, that the two-photon detection probability amplitude $A(\mathbf{R}_1,\mathbf{R}_2)$ (or, equivalently, the fourth-order correlation amplitude) behaves as a Huygens-Fresnel integral for the electromagnetic field of the pump propagating from the point $\mathbf{S}$ at the crystal ($z=0$) plane to the point $\mathbf{r}$ at the detectors' plane,

$$A(\mathbf{R}_1,\mathbf{R}_2) \propto e^{ik_p z}\int d\mathbf{S} E_p(\mathbf{S}) e^{\frac{ik_p}{2z}(\mathbf{r}-\mathbf{S})^2}. \tag{8}$$

Here, E_p is the transverse (x,y) profile of the pump beam field, k_p is the wavenumber of the pump beam, $k_s = k_i = k_p/2$, $\mathbf{r} = (\mathbf{r}_1+\mathbf{r}_2)/2$ and $\mathbf{S} = (\mathbf{s}_1+\mathbf{s}_2)/2$. In other words,

$$A(\mathbf{R}_1,\mathbf{R}_2) \propto E_p\left(\frac{\mathbf{r}_1+\mathbf{r}_2}{2},z\right). \tag{9}$$

We use a notation where three dimensional position vector $\mathbf{R}$ is represented as a set composed of two dimensional transverse vector $\mathbf{r}$ and the z distance from the origin

$$\mathbf{R} = (\mathbf{r},z). \tag{10}$$

Thus we see that the fourth-order correlation amplitude for the field generated by spontaneous parametric down-conversion process resembles a field propagation integral, hence the expression *"correlation beam"*. This effect is a consequence of the transfer of angular spectrum of pump to the downconverted field [60].

2.2 OPTICAL TURBULENCE

2.2.1 *Overview*

In fluid mechanics the Reynolds number is used to help predict similar flow patterns in different fluid(gas) flow situations. The Reynolds number is defined as the ratio of momentum forces to viscous forces and quantifies the relative importance of these two types of forces for given flow conditions. A turbulent flow occurs at high Reynolds numbers and is dominated by inertial forces, which tend to produce chaotic eddies, vortices and other flow instabilities. Turbulent air motion represents a set of vortices, or eddies, of various scale sizes, extending from a large scale size L_0 called the *outer scale* of turbulence to a small scale size l_0 called the *inner scale* of turbulence. Under the influence of inertial forces, large eddies break up into smaller ones, forming a continuous cascade of scale sizes between L_0 and l_0 known as the *inertial range*. Scale sizes smaller than the inner scale belong to the *dissipation range*. In the simplest case, when an optical wave propagates through turbulence, the diffraction and scattering effects occur on these eddies of different size (those by molecules or aerosols are neglected). A propagating beam will deflect encountering an eddy that is larger than the beams transverse size, and will expand - encountering an eddy smaller than its size, giving rise to intensity and phase fluctuations, respectively, in the observation plane.

Turbulence is a nonlinear process as is described by the Navier-Stokes equation. Because of mathematical difficulties in solving these equations, Kolmogorov [61] developed a statistical theory of turbulence that relies on dimensional analysis and additional simplifications and approximations. Thus, turbulence theory as we know it today is not derived from first principles.

In the *optical turbulence* the most important process in optical wave propagation is the *index-of-refraction fluctuations*. The theoretical framework of optical turbulence is based on the classical theory of turbulence concerning velocity fluctuations. Fluctuations in the index of refraction are related to corresponding temperature and pressure fluctuations. In particular, for optical and IR wavelengths, the index of refraction for the atmosphere can be written according to [62]

$$n(\mathbf{R}) \simeq 1 + 7.9 \times 10^{-5} \frac{P(\mathbf{R})}{T(\mathbf{R})}, \tag{11}$$

where P is the pressure in millibars, and T is the temperature in Kelvin. Because pressure fluctuations are usually negligible, we see that index-of-refraction fluctuations associated with the visible and near-IR region of the spectrum are due primarily to random temperature fluctuations (humidity fluctuations only contribute in the far-IR region). Changes in the optical signal due to absorption or scattering by molecules or aerosols are not considered.

Since the refractive index fluctuations are very small, it is expected that the electric field will propagate very much like a field in free space except for small perturbations or fluctuations about the free space value. A quantitative model for optical scintillation (irradiance fluctuations) requires a model for the turbulence. There are a number of such models [21, 64–67, 71] depending on whether one includes the effects of the inner scale and the outer scale. The simplest model is the Kolmogorov model, which is valid in the inertial range between the inner and outer scales.

By using dimensional analysis, Kolmogorov showed that the structure function of the index of refraction $D_n(\mathbf{R}_1, \mathbf{R}_2) = \langle [n(\mathbf{R}_1) - n(\mathbf{R}_2)]^2 \rangle$ obeys a $2/3$ power law in the inertial range, the same as obtained for temperature and longitudinal velocity fluctuations. The angular brackets denote an ensemble average. The corresponding inertial range behavior of the three-dimensional power spectrum of index-of-refraction fluctuations is described by a $-11/3$ power law, viz., the *Kolmogorov spectrum*

$$\Phi(\kappa) = 0.033 C_n^2 \kappa^{-11/3}, \qquad 1/L_0 \ll \kappa \ll 1/l_0, \tag{12}$$

where C_n^2 is called the *structure constant* of the index of refraction (in units of $\mathrm{m}^{-2/3}$). It determines the strength of turbulence, with values ranging from $10^{-17}\mathrm{m}^{-2/3}$ for weak turbulence, to about $10^{-13}\mathrm{m}^{-2/3}$ for strong turbulence. The Kolmogorov spectrum is the most commonly used spectrum in theoretical analyses but it is appropriate only over wave numbers within the inertial range. To account for the behavior of the power spectrum outside the inertial range, various spectral models have been proposed. These models include the *Tatarskii spectrum* [63]:

$$\Phi(\kappa) = 0.033 C_n^2 \kappa^{-11/3} \exp\left(-\frac{\kappa^2}{\kappa_m^2}\right), \qquad \kappa \gg 1/L_0; \qquad \kappa_m = 5.92/l_0, \tag{13}$$

the (modified) *von Kármán spectrum* [68]:

$$\Phi(\kappa) = 0.033 C_n^2 \kappa^{-11/3} \frac{\exp(-\kappa^2/\kappa_m^2)}{(\kappa^2 + 1/L_0^2)^{11/6}}, \qquad 0 \le \kappa < \infty; \qquad \kappa_m = 5.92/l_0, \tag{14}$$

and the *modified atmospheric spectrum* [69]:

$$\begin{aligned} \Phi(\kappa) = 0.033 C_n^2 \kappa^{-11/3} &\left[1 + 1.802(\kappa/\kappa_l) - 0.254(\kappa/\kappa_l)^{7/6}\right] \\ &\times \frac{\exp(-\kappa^2/\kappa_l^2)}{\left(\kappa^2 + 1/L_0^2\right)^{11/6}}, \qquad 0 \le \kappa < \infty; \qquad \kappa_l = 3.3/l_0. \end{aligned} \tag{15}$$

These latter models are not based on rigorous calculations outside the inertial range, but more on mathematical convenience and tractability.

2.2.2 *Theory for Propagation Through Random Media.*

Maxwell's equations for the vector amplitude $\mathbf{E}(\mathbf{R})$ of a propagating sinusoidal electromagnetic wave is given by [155]

$$\nabla^2\mathbf{E}(\mathbf{R}) + k^2 n^2(\mathbf{R})\mathbf{E} + 2\nabla[\mathbf{E}\cdot\nabla \ln n(\mathbf{R})] = 0, \tag{16}$$

where $\mathbf{R} = (x, y, z)$, $k = 2\pi/\lambda$ is the wavenumber, λ is the wavelength, $n(\mathbf{R})$ is the index of refraction. The time variations of the index of refraction are usually suppressed, meaning that the wave maintains a single frequency as it propagates. The last term in (16) which contains the interaction terms between the orthogonal components of the field is the one that gives rise to (de)polarization effects. It is shown to be negligible in the atmosphere [70] so that it can be dropped. This means that the equation (16) may be decomposed into three scalar equations for each component of the field. In most approaches, the starting point for describing the propagation of a monochromatic optical/IR wave through a turbulent medium with random index of refraction $n(\mathbf{R})$ is the *stochastic reduced (Helmholtz) wave equation*

$$\nabla^2 U + k^2 n^2(\mathbf{R})U = 0, \tag{17}$$

where $U = U(\mathbf{R})$ is the transverse scalar component of the electric field. Basically all approaches to optical/IR propagation through a random media rely on a simple set of fundamental assumptions:

(*i*) depolarization effects can be neglected
(*ii*) backscattering of the wave can be neglected
(*iii*) the wave equation may be approximated by the parabolic (paraxial) equation
(*iv*) the refractive index is delta correlated in the direction of propagation.

Assumptions (*i*) and (*ii*) are valid because the wavelength λ for optical/IR radiation is much smaller than the smallest scale of turbulence (i.e., the inner scale l_0), the maximum scattering angle is roughly $\lambda/l_0 \sim 10^{-4}$ rad, also that the fluctuations in the refractive index about its mean value are very small [70]. The assumption (*iii*) is based on the notion that the propagation distance along the z axis is much greater than the transverse spreading of the wave. Under assumption (*iv*), the refractive index is expressed as

$$n(\mathbf{R}) = n_0 + n_1(\mathbf{R}), \tag{18}$$

where $n_0 = \langle n(\mathbf{R})\rangle \cong 1, \langle n_1(\mathbf{R})\rangle = 0$, and that the covariance function – delta correlated in the direction of propagation along the positive z-axis can be expressed as ($\mathbf{R} = (\mathbf{r}, z)$)

$$\langle n_1(\mathbf{R}_1)n_1(\mathbf{R}_2)\rangle \cong \delta(z_1 - z_2)A_n(\mathbf{r}_1 - \mathbf{r}_2). \tag{19}$$

Eq. (19) is often referred to as the *Markov approximation*. In writing it, it is assumed that the covariance is statistically homogeneous so it is a function of only the difference $\mathbf{R}_1 - \mathbf{R}_2$, where $\mathbf{R}_j = (\mathbf{r}_j, z_j)$, $j = 1, 2$, and $A_n(\mathbf{r}_1 - \mathbf{r}_2)$ is the corresponding two-dimensional covariance function. We further recognize that if $n_1(\mathbf{R})$ is statistically homogeneous in three dimensions, it is also statistically homogeneous in two dimensions.

2.2.3 *Weak and strong fluctuation conditions.*

In optical wave propagation through turbulence the researchers traditionally classified the problems into weak and strong fluctuation regimes. In the study of plane waves or spherical waves that have propagated over a path of length L, it is customary to distinguish between these cases by values of the *Rytov variance* defined as

$$\sigma_R^2 = 1.23 C_n^2 k^{7/6} L^{11/6}. \tag{20}$$

Weak fluctuations are associated with $\sigma_R^2 \ll 1$, and then the Rytov variance physically represents the irradiance fluctuations associated with an unbounded plane wave. *Moderate fluctuation* conditions are characterized by $\sigma_R^2 \sim 1$, *strong fluctuations* are associated with $\sigma_R^2 \gg 1$, and the so-called *saturation regime* is defined by the condition $\sigma_R^2 \to \infty$. For a Gaussian-beam wave, weak fluctuation regimes correspond to the set of conditions $\sigma_R^2 < 1, \quad \sigma_R^2 \Lambda^{5/6} < 1$, where $\Lambda = 2L/kW^2$ is the output beam parameter (see Sec. 2.2.8) and W is the beam radius at the receiver in the vacuum. If either of these conditions fails to exist, the fluctuations are classified as moderate to strong.

2.2.4 *Born approximation.*

Writing the square of the index of refraction term as

$$n^2(\mathbf{R}) = [n_0 + n_1(\mathbf{R})]^2 \cong 1 + 2n_1(\mathbf{R}), \qquad |n_1(\mathbf{R})| \ll 1 \tag{21}$$

and assuming the possibility to express the optical field at $z = L$ as a sum of terms of the form

$$U(\mathbf{R}) = U_0(\mathbf{R}) + U_1(\mathbf{R}) + U_2(\mathbf{R}) + \ldots, \tag{22}$$

$U_0(\mathbf{R})$ denotes the unperturbed (unscattered) portion of the field in the absence of turbulence and the remaining terms represent first-order scattering, second-order scattering, etc., caused by random inhomogeneities. It is assumed that $|U_2(\mathbf{r}, L)| \ll |U_1(\mathbf{r}, L)| \ll |U_0(\mathbf{r}, L)|$. Eq. (17) reduces to the system of equations after equating the terms of the same order

$$\begin{aligned} \nabla^2 U_0 + k^2 U_0 &= 0, \\ \nabla^2 U_1 + k^2 U_1 &= -2k^2 n_1(\mathbf{R}) U_0(\mathbf{R}), \\ \nabla^2 U_2 + k^2 U_2 &= -2k^2 n_1(\mathbf{R}) U_1(\mathbf{R}), \\ &\cdots \end{aligned} \tag{23}$$

and so on for higher-order perturbations. Eq. (22) is known as Born approximation. The solutions of set (23) are

$$U_m(\mathbf{r}, L) = \frac{k^2}{2\pi} \int_0^L dz \iint_{-\infty}^{\infty} d^2s \exp\left[ik(L-z) + \frac{ik|\mathbf{s}-\mathbf{r}|^2}{2(L-z)}\right] U_{m-1}(\mathbf{s}, z) \frac{n_1(\mathbf{s}, z)}{L-z} \quad (24)$$
$$m = 1, 2, 3, \ldots$$

Unlike the first-order perturbation, one can see that $\langle U_m(\mathbf{r}, L)\rangle \neq 0$, $m > 1$.

2.2.5 *Rytov approximation.*

Historically, the first approach to solving Eq. (17) was based on the *method of Green's function*, reducing it to an integral equation [67]. More tractable solutions, however, can be obtained by the *geometrical optics method*, the *Born approximation* and the *Rytov approximation* (also known as the *method of smooth perturbations* in the Russian literature) [71]. The geometrical optics method is simple in that it ignores diffraction effects, but is generally limited to propagation paths in which $L \ll l_0^2/\lambda$, where l_0 is the inner scale of turbulence. Diffraction effects, important in the analysis of irradiance fluctuations sensitive to small scale sizes on the order of the Fresnel zone $\sqrt{\lambda L}$, are taken into account in both the Born and Rytov approximations, but the Born approximation was found to be restricted to extremely weak scattering conditions. The first method to give good agreement with scintillation data in the weak fluctuation regime was the Rytov approximation, which is the standard method used today under these conditions.

In the Rytov method, the solution of Eq.(17) is assumed to take the form

$$U(\mathbf{R}) \equiv U(\mathbf{r}, L) = U_0(\mathbf{r}, L) \exp[\psi_1(\mathbf{r}, L) + \psi_2(\mathbf{r}, L) + \cdots], \quad (25)$$

where $U_0(\mathbf{r}, L)$ is the unperturbed field and $\psi_1(\mathbf{r}, L)$ and $\psi_2(\mathbf{r}, L)$ represent first-order and second-order perturbations, respectively. These perturbations are directly related to the normalized Born approximations according to

$$\psi_1(\mathbf{r}, L) = \frac{U_1(\mathbf{r}, L)}{U_0(\mathbf{r}, L)} \equiv \Phi_1(\mathbf{r}, L),$$

$$\psi_2(\mathbf{r}, L) = \frac{U_2(\mathbf{r}, L)}{U_0(\mathbf{r}, L)} - \frac{1}{2}\left[\frac{U_1(\mathbf{r}, L)}{U_0(\mathbf{r}, L)}\right]^2 \equiv \Phi_2(\mathbf{r}, L) - \frac{1}{2}\Phi_1^2(\mathbf{r}, L), \quad (26)$$

where $\Phi_m(\mathbf{r}, L) \equiv U_m(\mathbf{r}, L)/U_0(\mathbf{r}, L)$, $m = 1, 2, 3, \ldots$ are called normalized Born perturbations.

Although direct use of the Born approximation to the optical wave propagation problem is not generally applicable, it is interesting that

the Born approximation can play such a central role in the Rytov method. In particular, the three integrals

$$E_1(\mathbf{r},\mathbf{r}) = E_1(0,0) \equiv \langle \psi_2(\mathbf{r},L)\rangle + \frac{1}{2}\langle \psi_1^2(\mathbf{r},L)\rangle = -2\pi^2 k^2 \int_0^L dz \int_0^\infty d\kappa\kappa\Phi_n(\kappa,z), \tag{27}$$

$$E_2(\mathbf{r}_1,\mathbf{r}_2) \equiv \langle \psi_1(\mathbf{r}_1,L)\psi_1^*(\mathbf{r}_2,L)\rangle = 4\pi^2 k^2 \int_0^L dz \int_0^\infty d\kappa\kappa\Phi_n(\kappa,z) \times J_0(\kappa|\gamma\mathbf{r}_1 - \gamma^*\mathbf{r}_2|)\exp\left[-\frac{i\kappa^2}{2k}(\gamma-\gamma^*)(L-z)\right], \tag{28}$$

$$E_3(\mathbf{r}_1,\mathbf{r}_2) \equiv \langle \psi_1(\mathbf{r}_1,L)\psi_1(\mathbf{r}_2,L)\rangle = -4\pi^2 k^2 \int_0^L dz \int_0^\infty d\kappa\kappa\Phi_n(\kappa,z) \times J_0(\gamma\kappa|\mathbf{r}_1 - \mathbf{r}_2|)\exp\left[-\frac{i\kappa^2\gamma}{k}(L-z)\right] \tag{29}$$

that define second-order statistics for both the Born and Rytov approximations are used to describe the fundamental statistical behavior (means, covariances, etc.) of an optical wave propagating in a random medium. Here

$$\gamma \equiv 1 - (\overline{\Theta} + i\Lambda)(1 - z/L), \qquad 0 \le z \le L,$$

with $\overline{\Theta}$ and Λ output beam parameters to be defined in Sec. 2.2.8.

For horizontal propagation paths the refractive-index structure parameter C_n^2 can be treated as constant so that one can set $\Phi(\kappa,z) = \Phi(\kappa)$ in various expressions.

2.2.6 *Strong fluctuation theory.*

For more general turbulence conditions, other methods must be employed like the parabolic equation method [72, 80] extended Huygens-Fresnel principle [78, 79], or Feynman path integral method [76, 81]. Strong fluctuation conditions were reviewed by Strohbehn [70] and by Yura [77] and shown that, up to second-order moments of the field, these methods are equivalent to each other under appropriate restrictions. Only asymptotic results have been obtained thus far by any of these methods for the fourth-order field moment [73–76]. We will use the extended Huygens-Fresnel principle to calculate the fourth-order correlation function for the correlation beams in the SPDC process in the next chapters.

The condition $\lambda \ll l$ plays the most important role in strong fluctuation theory, where l is the size of inhomogeneities of the medium. As a consequence, the interaction with a single inhomogeneity results in predominantly forward scattering, and the scattered radiation is concentrated in a narrow angular range around the original direction of propagation. Under these circumstances random interference occurs

between the scattered waves, leading to drastic intensity changes in the plane of observation. The area where the intensity fluctuations reach their maximum (where a concentration of random caustics occur) is the region of random focusing, so called because the focusing effect of the large-scale inhomogeneities appears here in the strongest form. With increasing path length or the strength of inhomogeneities the phase fluctuations within the first Fresnel zone become substantial, and the individual components of the wave front arrive out of phase and add up incoherently. Therefore, the focusing is weakened, the fluctuations slowly begin to decrease, saturating at a given level. In general terms, this gives a qualitative picture of strong fluctuations.

The function $n_1(\mathbf{R})$ (see Eq.(18)) describes a random field, obeying $\langle n_1 \rangle = 0$. The random field $n_1(\mathbf{R})$ is fully determined if all statistical moments of the form $\langle n_1(\mathbf{R}_1) \cdots n_1(\mathbf{R}_n) \rangle$ are given. For simplicity it is assumed that the $n_1(\mathbf{R})$ is a Gaussian random field. In this case it is sufficient to know the mean value ($\langle n_1 \rangle = 0$) and the correlation function $B(\mathbf{R}, \mathbf{R}') = \langle n_1(\mathbf{R}) n_1(\mathbf{R}') \rangle$, since all higher moments can be expressed in terms of B. In a turbulent medium, for very large Reynolds numbers, $n_1(\mathbf{R})$ is a statistically locally isotropic homogeneous field [83, 84]. For such a field, it is customary to use, instead of the correlation function B, the structure function $D(\mathbf{R}') = \langle (n_1(\mathbf{R} + \mathbf{R}') - n_1(\mathbf{R}))^2 \rangle$.

2.2.7 *Extended Huygens-Fresnel principle.*

One approach to solving Eq. (17) by a different method was developed in the United States by Lutomirski and Yura [78] and in the former Soviet Union by Feizulin and Kravtsov [79]. In the *extended Huygens-Fresnel principle*, the field that propagates from the source located in the plane $z = 0$ to the observation point $\mathbf{r} = (x, y)$ at the plane $z = L$ is determined via the expression

$$U(\mathbf{r}, L) = \frac{k e^{ikL}}{2\pi i L} \int \int_{-\infty}^{\infty} d^2 s \; U_0(\mathbf{s}, 0) \exp\left[\frac{ik|\mathbf{s} - \mathbf{r}|^2}{2L} + \psi(\mathbf{r}, \mathbf{s}) \right], \tag{30}$$

where $\psi(\mathbf{r}, \mathbf{s})$ is the random part of the complex phase of a spherical wave propagating in the turbulent medium from the point $(\mathbf{s}, 0)$ to the point $(\mathbf{r}, L)$. We recognize Eq. (30) as an extended version of the Huygens-Fresnel formula, hence its name. Now it reads: the field at the point $(\mathbf{r}, z)$ in the atmosphere is a superposition of spherical waves originated at the source plane $z = 0$, $(\mathbf{s}, 0)$ with amplitudes $U_0(\mathbf{s}, 0)$ while during the propagation suffered phase and amplitude distortions represented by stochastic complex function $\psi(\mathbf{r}, \mathbf{s})$ that depends on points of source and observation planes.

It has been shown that the extended Huygens-Fresnel principle is applicable through first-order and second-order field moments under weak or strong fluctuation conditions of atmospheric turbulence. In fact, it has been established that, up to second-order field moments,

the *parabolic equation method* [80] and the extended Huygens-Fresnel principle yield the same results. We will use this latter method to develop results for fourth-order moments under general atmospheric conditions. For the fourth-order moment of the field, however, it has not been demonstrated that Eq. (30) is equivalent to the parabolic equation method or that Eq. (30) is applicable except under weak fluctuation conditions.

The Rytov approximation is the most widely used method, but is limited to regimes of weak irradiance fluctuations. When the propagation channel involves moderate-to-strong irradiance fluctuations, the parabolic equation method and extended Huygens-Fresnel principle have generally been the most successful. Yet, the mathematical complications associated with both of these methods precludes the complete analysis for moderate levels of irradiance fluctuations that is often required in many applications.

If the random medium is *statistically homogeneous* and *isotropic*, the statistical quantities are now given by [21, 82]

$$E_1(0,0;0,0) \equiv E_1(0) = \langle \psi_2(\mathbf{r},\mathbf{s})\rangle + \frac{1}{2}\langle \psi_1^2(\mathbf{r},\mathbf{s})\rangle = -2\pi^2 k^2 L \int_0^\infty d\kappa \kappa \Phi_n(\kappa), \tag{31}$$

$$\begin{aligned} E_2(\mathbf{r}_1,\mathbf{r}_2;\mathbf{s}_1,\mathbf{s}_2) &= \langle \psi_1(\mathbf{r}_1,\mathbf{s}_1)\psi_1^*(\mathbf{r}_2,\mathbf{s}_2)\rangle \\ &= 4\pi^2 k^2 L \int_0^1 \int_0^\infty \kappa \Phi_n(\kappa) J_0(\kappa|(1-\xi)\mathbf{p} + \xi\mathbf{Q}|) d\kappa d\xi, \end{aligned} \tag{32}$$

$$\begin{aligned} E_3(\mathbf{r}_1,\mathbf{r}_2;\mathbf{s}_1,\mathbf{s}_2) &= \langle \psi_1(\mathbf{r}_1,\mathbf{s}_1)\psi_1(\mathbf{r}_2,\mathbf{s}_2)\rangle \\ &= -4\pi^2 k^2 L \int_0^1 \int_0^\infty \kappa \Phi_n(\kappa) J_0(\kappa|(1-\xi)\mathbf{p} + \xi\mathbf{Q}|) \\ &\times \exp\left[-\frac{iL\kappa^2}{k}\xi(1-\xi)\right] d\kappa d\xi, \end{aligned} \tag{33}$$

where $\mathbf{Q} = \mathbf{s}_1 - \mathbf{s}_2$ and $\mathbf{p} = \mathbf{r}_1 - \mathbf{r}_2$ are input and output plane variables, respectively.

In the next chapters we will extensively use these important functions to calculate second and fourth order correlation functions for the SPDC light propagating through turbulent (random) medium. Assuming the random part of the index-of-refraction is Gaussian random field, for which $\langle \exp(\psi)\rangle = \exp\left[\langle\psi\rangle + \frac{1}{2}\left(\langle\psi^2\rangle - \langle\psi\rangle^2\right)\right]$ holds, Eqs. (31)–(33) will help us to calculate important statistical averages like

$$\langle \exp[\psi(\mathbf{r},\mathbf{s})]\rangle = \exp[E_1(0)], \tag{34}$$

$$\langle \exp[\psi(\mathbf{r}_1,\mathbf{s}_2) + \psi^*(\mathbf{r}_2,\mathbf{s}_2)]\rangle = \exp[2E_1(0) + E_2(\mathbf{r}_1,\mathbf{r}_2;\mathbf{s}_1,\mathbf{s}_2)], \tag{35}$$

$$\begin{aligned} &\langle \exp[\psi(\mathbf{r}_1,\mathbf{s}_2) + \psi^*(\mathbf{r}_2,\mathbf{s}_2) + \psi(\mathbf{r}_3,\mathbf{s}_3) + \psi^*(\mathbf{r}_4,\mathbf{s}_4)]\rangle = \\ &= \exp\Big[4E_1(0) + E_2(\mathbf{r}_1,\mathbf{r}_2;\mathbf{s}_1,\mathbf{s}_2) + E_2(\mathbf{r}_1,\mathbf{r}_4;\mathbf{s}_1,\mathbf{s}_4) \\ &+ E_2(\mathbf{r}_3,\mathbf{r}_2;\mathbf{s}_3,\mathbf{s}_2) + E_2(\mathbf{r}_3,\mathbf{r}_4;\mathbf{s}_3,\mathbf{s}_4) + E_3(\mathbf{r}_1,\mathbf{r}_3;\mathbf{s}_1,\mathbf{s}_3) + E_3^*(\mathbf{r}_2,\mathbf{r}_4;\mathbf{s}_2,\mathbf{s}_4)\Big]. \end{aligned} \tag{36}$$

2.2.8 *Input and Output Plane Beam Parameters.*

Sometimes it is useful to express equations in terms of *input and output plane beam parameters*. The input beam parameters are defined as

$$\Theta_0 = 1 - \frac{z}{F_0}, \qquad \Lambda_0 = \frac{2z}{kW_0^2}. \tag{37}$$

and the output beam parameters as

$$\Theta = 1 + \frac{z}{F} = \frac{\Theta_0}{\Theta_0^2 + \Lambda_0^2}, \qquad \Lambda = \frac{2z}{kW^2} = \frac{\Lambda_0}{\Theta_0^2 + \Lambda_0^2}, \qquad \overline{\Theta} = 1 - \Theta, \tag{38}$$

where W_0, F_0 and W, F are the spot radius and the phase front radius of curvature of the TEM_{00} beam at the input and output planes, respectively. $k = 2\pi/\lambda$ is the wave number at the transmitter ($z = 0$).

These new parameters are somewhat non-intuitive, although they have interesting geometrical representation on the complex planes (Λ_o, Θ_0) and (Λ, Θ) from which one can identify different characteristics of a convergent, collimated and divergent beam. For more information about the input-output beam parameters see [21]. They also facilitate the description of Gaussian-beam waves in the presence of optical turbulence.

The type of beam is designated the following way:

- *collimated beam*: $\Theta_0 = 1$,
- *convergent beam*: $\Theta_0 < 1$,
- *divergent beam*: $\Theta_0 > 1$.

Another important feature of these parameters is the possibility of describing, as limiting cases, a plane wave ($\Theta = 1$, $\Lambda = 0$) and a spherical wave ($\Theta = 0$, $\Lambda = 0$).

2.2.9 *Wave structure functions. Scintillation index.*

For future use, we need some expressions for wave structure functions (*WSF*) as well as for scintillation index for a spherical wave. Definitions:
the spherical *WSF*

$$D_{sp}(Q) = 8\pi^2 k^2 z \int_0^1 d\xi \int_0^\infty d\kappa \kappa \Phi(\kappa) \left[1 - J_0(\kappa \xi Q)\right]. \tag{39}$$

It is the real part of the complex degree of coherence.
The two-point spherical *WSF*

$$D_{sp}(\mathbf{p}, \mathbf{Q}) = 8\pi^2 k^2 z \int_0^1 d\xi \int_0^\infty d\kappa \kappa \Phi(\kappa) \left[1 - J_0(\kappa |(1-\xi)\mathbf{p} + \xi \mathbf{Q}|)\right], \tag{40}$$

and the scintillation index of spherical wave

$$\sigma_{sp}^2(z) = 8\pi^2 k^2 z \int_0^1 d\xi \int_0^\infty d\kappa \kappa \Phi(\kappa) \left[1 - \cos\left(\frac{z\kappa^2}{k} \xi (1-\xi)\right)\right]. \tag{41}$$

It is the intensity variance scaled by the square of the mean intensity.

For the von Kármán spectrum (14), Eq. (39) is found to be, [21, ch.6]

$$D_{sp}(Q) = \begin{cases} 1.093 C_n^2 k^2 z l_0^{-1/3} Q^2, & z \gg z_i, \\ 1.093 C_n^2 k^2 z Q^{5/3}, & z \ll z_i, \end{cases}$$

which is valid for $\kappa_0 = 0$ or $L_0 = \infty$. The quantity $z_i \sim \left(C_n^2 k^2 l_0^{5/3}\right)^{-1}$ represents the propagation distance at which the transverse coherence radius of the optical wave is on the order of the inner scale l_0. In most practical situations the propagation path length satisfies $z \ll z_i$. For this reason, to proceed analytically, a commonly accepted approximation is

$$1.093 C_n^2 k^2 z Q^{5/3} \cong \frac{1.78 \sigma_R^2}{\Lambda_0 W_0^2} Q^2 = \frac{1.58 \sigma_{R,p}^2}{\Lambda_{0,p} W_0^2} Q^2, \tag{42}$$

where, in the last part of Eq.(42) we expressed the Rytov variance (see Eq.(20)) and input beam parameter Λ_0 in terms of pump wave number k_p. We will use the last expression for D_{sp}, viz.

$$D_{sp}(Q) \cong \frac{1.58 \sigma_{R,p}^2}{\Lambda_{0,p} W_0^2} Q^2. \tag{43}$$

The two-point spherical WSF can be evaluated to be [21, ch.7]

$$D_{sp}(\mathbf{p}, \mathbf{Q}) = \frac{2}{3\rho_{pl}^2} \left(p^2 + Q^2 + \mathbf{p} \cdot \mathbf{Q}\right), \tag{44}$$

where $\rho_{pl} = (1.45 C_n^2 k^2 z)^{-3/5} = (0.36 C_n^2 k_p^2 z)^{-3/5}$ $(z \ll z_i)$ is called a plane wave coherence radius.

Part II

ATMOSPHERIC PROPAGATION: THE FOURTH ORDER CORRELATION FUNCTION AND MODE ANALYSIS.

3

CORRELATION BEAMS IN THE TURBULENT ATMOSPHERE

3.1 COHERENT CORRELATION BEAMS IN THE TURBULENT ATMOSPHERE

3.1.1 *Overview*

The area of quantum optical communication [1] with entangled photons [2] is rich in experimental implementations. Therefore, studying the effects of turbulent or random medium on non-classical light has gained a considerable interest. There have been investigations in areas such communication [23], conservation of orbital angular momentum [6, 7, 20, 29, 85], noise transport and negative correlations [30]; two-photon speckle [33, 36]; spatial correlations [37, 38, 41]; ghost imaging [39, 42–44]; interference and anti-bunching and symmetry properties [45, 46].

To our knowledge, there is no analytical result involving turbulent medium in *both*, signal *and* idler arm. In this Thesis we investigate the problem analytically in a more general context. As a result, we calculate the *atmospheric* fourth-order correlation function (or, the two-photon speckle, which is proportional to two-photon joint detection probability, therefore, a measurable quantity) in the cases when the $\chi^{(2)}$ crystal is pumped either by any coherent Hermite/Laguerre-Gaussian beam (Secs.3.1.6, 3.1.7) or by a partially coherent beam (Sec.3.2). The latter case is particularly interesting because the beams produced by partially coherent sources spread less in the random medium than coherent beams [49–51, 138].

3.1.2 *The Biphoton*

Though the two-photon probability amplitude or, so called the Biphoton, is not a coherence function, it does obey the Wolf equations [86], and therefore exhibits propagation and diffraction phenomena analogous to those of the second-order coherence function, including the van Cittert–Zernike theorem [58, 87, 88].

A duality accompanied with mathematical similarity between the two-photon probability amplitude and the second-order coherence function for the incoherent source has been highlighted before [89]. The smaller the size of an incoherent source, the more separable is the

coherence function and the more coherent is the field, and therefore the higher the visibility of ordinary interference fringes. In contrast, the narrower the size of a two-photon source (the pump at the thin crystal), the more separable is the wave function and the less entangled is the state, and therefore the lower the visibility of two-photon interference fringes.

Light in a two-photon pure quantum state is described in a Hilbert space with a continuum of spatiotemporal, also transverse, modes occupied by a total of exactly two photons. It is a superposition of multimode states, each of which has the two photons occupying a different pair of modes, with all other modes empty. Two-photon light is generated, for example, by a low gain spontaneous parametric down-conversion process in a second-order nonlinear optical crystal. Phase matching conditions dictate that the state be entangled spectrally, spatially and in transverse modes.

3.1.3 *Two-Photon Speckle*

Replacing the simple optical system by a random medium and assuming that the coincidence rate P_2 is measured as a function of the positions $\mathbf{R}_1$ and $\mathbf{R}_2$ of the two detectors at times t_1 and t_2, one arrives at the concept of the two-photon speckle pattern $P_2(x_1, x_2)$, where $x_i = (\mathbf{R}_i, t_i)$ [36]. It is important to realize that P_2 corresponds to a single realization of the random medium. It is therefore a random quantity and fluctuates from one realization of disorder to another. To obtain a deterministic quantity, one must average P_2 over an ensemble of realizations of the random medium.

The two-photon speckle is given by the square magnitude of the two-photon wave function:

$$P_2(x_1, x_2) = |A(x_1, x_2)|^2 = |\langle 0, 0|\hat{E}_2^{(+)}(x_2)\hat{E}_1^{(+)}(x_1)|\psi\rangle|^2, \tag{45}$$

where $x_1 = (\mathbf{r}_1, z_1, t_1)$ and $x_2 = (\mathbf{r}_2, z_2, t_2)$. $\hat{E}_1^{(+)}(x_1)$ and $\hat{E}_2^{(+)}(x_2)$ are $+z$ propagating, scalar, quasi-monochromatic, paraxial, positive-frequency field operators [1] at x_1, x_2. They are expressed in terms of the annihilation operators $\hat{a}_s(x)$ and $\hat{a}_i(x)$ at the source plane (the crystal) and the amplitude-response functions of the signal and idler systems [89]:

$$\hat{E}_1^{(+)}(x_1) = \int d\mathbf{r} h_s(\mathbf{r}_1, \mathbf{r})\hat{a}_s(\mathbf{r}, t_1 - z_1/c), \tag{46}$$

$$\hat{E}_2^{(+)}(x_2) = \int d\mathbf{r} h_i(\mathbf{r}_2, \mathbf{r})\hat{a}_i(\mathbf{r}, t_2 - z_2/c), \tag{47}$$

with amplitude-response functions for signal and idler systems:

$$h_j(\mathbf{r}_j, \mathbf{r}) = \frac{k_j e^{ik_j z_j}}{i2\pi z_j} \exp\left\{\frac{ik_j}{2z_j}|\mathbf{r}_j - \mathbf{r}|^2 + \psi^{(j)}(\mathbf{r}_j, \mathbf{r}; k_j)\right\}, \qquad j = s, i. \tag{48}$$

Finally, $|\psi\rangle$ is the two-photon SPDC state vector in the thin crystal approximation

$$\begin{aligned} |\psi\rangle &= \iint d\mathbf{r}d\mathbf{r}' E_p\left(\frac{\mathbf{r}+\mathbf{r}'}{2}\right)\delta(\mathbf{r}-\mathbf{r}')\hat{a}_s^\dagger(\mathbf{r})\hat{a}_i^\dagger(\mathbf{r}')|0,0\rangle \\ &= \int d\mathbf{r} E_p(\mathbf{r})|1_\mathbf{r}, 1_\mathbf{r}\rangle, \end{aligned} \tag{49}$$

which is maximally entangled in the configuration space variables and $|1_\mathbf{r}\rangle = \frac{1}{(2\pi)^2}\int d\mathbf{k} e^{i\mathbf{k}\cdot\mathbf{r}}|1_\mathbf{k}\rangle$, $|1_\mathbf{k}\rangle$ being the single photon Fock state of mode $\mathbf{k}$.

Pictorially, the system is presented in Figure 1 below, where, for completeness, we added an amplitude-response system for the pump as well. The remote coincidence identification of the two remote lo-

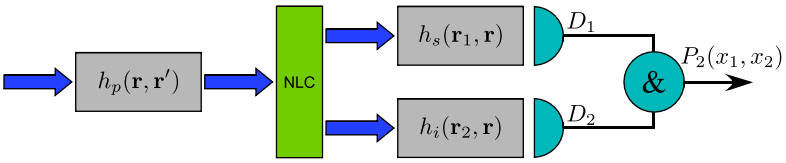

Figure 1: *Schematic diagram of the system considered. NLC represents a nonlinear crystal, h_p, h_s and h_i represent the amplitude response functions for the pump beam (p) and for the down-converted photons (s, i). D_1 and D_2 represent the detectors and P_2 represents the fourth order correlation function, a measurable quantity which is proportional to the two-photon joint detection probability.*

cations without dedicated coincidence hardware is settled using the time correlation of the photon pairs [90].

When substituting Eqs.(46)–(49) into Eq.(45), the joint detection probability density function takes the following form:

$$\begin{aligned} P_2(x_1,x_2) = \frac{k_s k_i}{4\pi^2 z_1 z_2}\iint d\mathbf{r}'d\mathbf{r}'' E_p(\mathbf{r}', t_1 - z_1/c)E_p^*(\mathbf{r}'', t_2 - z_2/c) \\ \times \exp\left\{\frac{ik_s}{2z_s}\left[|\mathbf{r}_1-\mathbf{r}'|^2 - |\mathbf{r}_1-\mathbf{r}''|^2\right] + \frac{ik_i}{2z_i}\left[|\mathbf{r}_2-\mathbf{r}'|^2 - |\mathbf{r}_2-\mathbf{r}''|^2\right]\right\} \\ \times \exp\left[\psi(\mathbf{r}',\mathbf{r}_1;k_s) + \psi^*(\mathbf{r}'',\mathbf{r}_1;k_s) + \psi(\mathbf{r}',\mathbf{r}_2;k_i) + \psi^*(\mathbf{r}'',\mathbf{r}_2;k_i)\right]. \end{aligned} \tag{50}$$

To proceed further one must account for statistical average over an ensemble of realizations of turbulent medium

$$\begin{aligned} P_2(x_1,x_2) = \frac{k^2}{4\pi^2 z^2}\iint d\mathbf{r}'d\mathbf{r}'' E_p(\mathbf{r}', t_1 - z_1/c)E_p^*(\mathbf{r}'', t_2 - z_2/c) \\ \times \exp\left\{\frac{ik}{2z}\left[|\mathbf{r}_1-\mathbf{r}'|^2 - |\mathbf{r}_1-\mathbf{r}''|^2 + |\mathbf{r}_2-\mathbf{r}'|^2 - |\mathbf{r}_2-\mathbf{r}''|^2\right]\right\} \\ \times \left\langle \exp\left[\psi(\mathbf{r}',\mathbf{r}_1) + \psi^*(\mathbf{r}'',\mathbf{r}_1) + \psi(\mathbf{r}',\mathbf{r}_2) + \psi^*(\mathbf{r}'',\mathbf{r}_2)\right]\right\rangle, \end{aligned} \tag{51}$$

where we assumed the degenerate case, $k \equiv k_s = k_i = k_p/2$, and chose the detection plane at $z \equiv z_1 = z_2$.

With the help of Eq.(36), the last exponential in Eq.(51) takes the form

$$\begin{aligned}\langle \exp[...] \rangle = \exp\left[4E_1(0) + 2E_2(0,0;\mathbf{r}',\mathbf{r}'') + E_2(\mathbf{r}_1,\mathbf{r}_2;\mathbf{r}',\mathbf{r}'')\right] \\ \times \exp\left[E_2(\mathbf{r}_2,\mathbf{r}_1;\mathbf{r}',\mathbf{r}'') + 2\mathrm{Re}E_3(\mathbf{r}_1,\mathbf{r}_2;0,0)\right],\end{aligned} \tag{52}$$

where the functions E_1, E_2, E_3 are defined in (31)-(33). Using Tatarskii spectrum (13) we evaluated the integral in Eq.(59) (for details, see the Appendix B). Now Eq.(51) amounts to

$$\begin{aligned}P_2(x_1,x_2) = \frac{k^2}{4\pi^2 z^2}\iint d\mathbf{r}'d\mathbf{r}''E_p(\mathbf{r}')E_p^*(\mathbf{r}'') \\ \times \exp\left\{\frac{ik}{2z}\left[|\mathbf{r}_1-\mathbf{r}'|^2-|\mathbf{r}_1-\mathbf{r}''|^2+|\mathbf{r}_2-\mathbf{r}'|^2-|\mathbf{r}_2-\mathbf{r}''|^2\right]\right\} \\ \times \exp\Bigg[-\frac{1}{2}\left[D_{sp}(\mathbf{p},\mathbf{Q}) + D_{sp}(-\mathbf{p},\mathbf{Q})\right] \\ + D_{sp}(p) - D_{sp}(Q) - 0.043\pi^2 C_n^2 z^3 p^{-7/3}\Bigg].\end{aligned} \tag{53}$$

Finally, using Eqs.(43) and (44) we arrive at

$$\begin{aligned}P_2(x_1,x_2) = \frac{k^2}{4\pi^2 z^2}\exp\left[\left(\frac{1.58\sigma_{R,p}^2}{\Lambda_{0,p}W_0^2} - \frac{2}{3\rho_{pl}^2}\right)p^2 - 0.043\pi^2 C_n^2 z^3 p^{-7/3}\right] \\ \times \iint d\mathbf{S}d\mathbf{Q}E_p(\mathbf{S}+\mathbf{Q}/2)E_p^*(\mathbf{S}-\mathbf{Q}/2) \\ \times \exp\left\{\frac{ik_p}{z}(\mathbf{S}\cdot\mathbf{Q}-\mathbf{r}\cdot\mathbf{Q})\right\}\exp\left[-\left(\frac{1.58\sigma_{R,p}^2}{\Lambda_{0,p}W_0^2} + \frac{2}{3\rho_{pl}^2}\right)Q^2\right].\end{aligned} \tag{54}$$

In Eq.(54) we used (43), (44) and made the following change of variables

$$\mathbf{Q} = \mathbf{r}' - \mathbf{r}'', \qquad \mathbf{S} = \frac{1}{2}(\mathbf{r}' + \mathbf{r}''), \qquad Q = |\mathbf{Q}|, \qquad S = |\mathbf{S}|, \tag{55}$$

for the source plane, and

$$\mathbf{p} = \mathbf{r}_1 - \mathbf{r}_2, \qquad \mathbf{r} = \frac{1}{2}(\mathbf{r}_1 + \mathbf{r}_2), \qquad p = |\mathbf{p}|, \qquad r = |\mathbf{r}|, \tag{56}$$

for the observation plane. Using these, we also simplified the expression in the first exponential in Eq.(53), viz.

$$\frac{ik_p}{z}(\mathbf{S}\cdot\mathbf{Q}-\mathbf{r}\cdot\mathbf{Q}) = \frac{ik}{2z}\left[|\mathbf{r}_1-\mathbf{r}'|^2-|\mathbf{r}_1-\mathbf{r}''|^2+|\mathbf{r}_2-\mathbf{r}'|^2-|\mathbf{r}_2-\mathbf{r}''|^2\right],$$

which is easily checked. Note that we are in the degenerate regime $k_p = 2k$.

3.1.4 *Two Photon Absorber.*

First, let us calculate the two-photon speckle for the case $x_1 = x_2$. Experimentally, it can be measured using, e.g., a two-photon absorber [58].

We have

$$
\begin{aligned}
P_2(x,x) = \frac{k^2}{4\pi^2 z^2} \iint d\mathbf{r}' d\mathbf{r}'' E_p(\mathbf{r}', t - z/c) E_p^*(\mathbf{r}'', t - z/c) \\
\times \exp\left\{ \frac{ik}{z} \left[|\mathbf{r} - \mathbf{r}'|^2 - |\mathbf{r} - \mathbf{r}''|^2 \right] \right\} \\
\times \exp\left[4E_1(0) + 4E_2(0,0;\mathbf{r}',\mathbf{r}'') + 2\mathrm{Re}E_3(0) \right].
\end{aligned}
\tag{57}
$$

From now on we are going to omit the time dependence of the fields. Adding and subtracting $4E_1(0)$ in the above exponent, we recognize

$$
2\mathrm{Re}E_3(0) - 4E_1(0) = \sigma_{sp}^2(z),
$$

the scintillation index for a spherical wave, and

$$
4E_2(0,0;\mathbf{r}',\mathbf{r}'') + 8E_1(0) = -2D_{sp}(|\mathbf{r}' - \mathbf{r}''|, z),
$$

the spherical wave structure function. They are defined in the previous chapter (see Eqs.(39),(155)). For different models of turbulence power spectrum $\Phi(\kappa)$, they are given in the Appendix III of Ref. [21] expressed in turbulence parameters.

With these quantities, $P_2(x,x)$ takes the form

$$
\begin{aligned}
P_2(x,x) = & \frac{k^2 e^{\sigma_{sp}^2(z)}}{4\pi^2 z^2} \iint d\mathbf{r}' d\mathbf{r}'' E_p(\mathbf{r}') E_p^*(\mathbf{r}'') \\
& \times \exp\left\{ \frac{ik}{z} \left[|\mathbf{r} - \mathbf{r}'|^2 - |\mathbf{r} - \mathbf{r}''|^2 \right] - 2D_{sp}(|\mathbf{r}' - \mathbf{r}''|) \right\}.
\end{aligned}
\tag{58}
$$

Going back to the more general case we recognize in Eq.(52)

$$
4E_1(0) + E_2(\mathbf{r}_1,\mathbf{r}_2;\mathbf{r}',\mathbf{r}'') + E_2(\mathbf{r}_2,\mathbf{r}_1;\mathbf{r}',\mathbf{r}'') = -\frac{1}{2}\left[D_{sp}(\mathbf{p},\mathbf{Q}) + D_{sp}(-\mathbf{p},\mathbf{Q}) \right],
$$

and

$$
\begin{aligned}
& 2E_2(0;\mathbf{r}',\mathbf{r}'') + 2\mathrm{Re}E_3(\mathbf{r}_1,\mathbf{r}_2;0) \\
& \quad = 8\pi^2 k^2 z \int_0^1 d\xi \int_0^\infty d\kappa \kappa \Phi(\kappa) \left[J_0(\kappa\xi Q) - J_0(\kappa\xi p) \cos\left(\frac{z\kappa^2}{k} \xi(1-\xi) \right) \right] \\
& \quad = D_{sp}(p) - D_{sp}(Q) + 4\pi^2 z^3 \int_0^1 d\xi \int_0^\infty d\kappa \kappa^5 \Phi(\kappa) J_0(\kappa\xi p) \xi^2 (1-\xi)^2.
\end{aligned}
\tag{59}
$$

In the last line of Eq.(59), to have an analytical expression, we used geometrical optics approximation, viz. $z\kappa^2/k \ll 1$, to replace $\cos\alpha$ by $1 - \alpha^2/2$ ([21], Ch.9). In geometrical optics approximation one neglects diffraction effects, it is generally limited to propagation paths in which $L \ll l_0^2/\lambda$, where l_0 is the inner scale of turbulence. The geometrical optics method produces similar results as diffraction theories because phase fluctuations are most sensitive to large scale sizes. This method is extensively used in astronomical applications.

3.1.5 *Two-Photon versus One-Photon Speckle. Quantum versus Classical Correlations. Comparison.*

In vacuum, P_2 factorizes for two independent photons: $P_2(x_1, x_2) = P_1(x_1)P_1(x_2)$, where $P_1(x_i)$ is the probability to detect a photon at a position r_i at a time t_i, $i = 1, 2$. It describes the one-photon speckle pattern and is proportional to the intensity of light at x_i. As mentioned already, in the atmosphere, the ensemble averaged P_2 does not factorize. Note that even for two *independent* photons, $P_2(x_1, x_2) \neq P_1(x_1)P_1(x_2)$ does not factorize into a product of P_1's (in contrast to the non-averaged P_2) because $P_1(x_i)$ can have nontrivial (classical) correlations in both space and time [129]. Therefore, the ensemble-averaged two-photon speckle $P_2(x_1, x_2)$ combines properties due to the quantum nature of the incident light and those arising from the classical correlations between photons at two different positions (or times). Let us compare the two photon speckle with the one-photon speckle which is obtained in single photocounts (second order effect). The single-photon probability density is given by [130]

$$P_1(x_1) = \int d\mathbf{r} |E_p(\mathbf{r}, t_1 - r/c)|^2 |h_1(\mathbf{r}_1, \mathbf{r})|^2, \tag{60}$$

where $x_1 = (\mathbf{r}_1, z_1, t_1)$ is the detector's coordinate $\mathbf{r}_1$ at time t_1, and

$$h_1(\mathbf{r}_1, \mathbf{r}) = -\frac{ik}{2\pi z} e^{ikz} \exp\left[\frac{ik}{2z}|\mathbf{r}_1 - \mathbf{r}|^2 + \psi(\mathbf{r}_1, \mathbf{r}; k)\right], \tag{61}$$

is the impulse-response function with $\psi(\mathbf{r}_1, \mathbf{r}; k)$ being the Rytov's (complex) random function representing the amplitude and phase fluctuations of the field due to the random (turbulent) medium. Considering it in (60) one arrives at

$$P_1(x_1) = \left(\frac{k}{2\pi z}\right)^2 \int d\mathbf{r} |E_p(\mathbf{r}, t_1 - r/c)|^2 \exp\left[\psi(\mathbf{r}_1, \mathbf{r}; k) + \psi^*(\mathbf{r}_1, \mathbf{r}; k)\right]. \tag{62}$$

Expanding ψ, as always, up to the second order, $\psi_1 + \psi_2$, $\psi_2 \ll \psi_1$, and making an ensemble average of the exponent we obtain

$$\langle \exp\left[\psi(\mathbf{r}_1, \mathbf{r}; k) + \psi^*(\mathbf{r}_1, \mathbf{r}; k)\right] \rangle = \exp\left[2\sigma_{r_1}^2 - T\right], \tag{63}$$

where $\sigma_{r_1}^2$ describes the atmospherically induced change in the mean intensity profile in the transverse direction, and T describes the change in the on-axis mean intensity at the receiver plane caused by turbulence [21, Ch. 6]. The one-photon speckle now looks like

$$\begin{aligned} P_1(\mathbf{r}_1) &= \left(\frac{k}{2\pi z}\right)^2 \exp\left[2\sigma_{r_1}^2 - T\right] \int d\mathbf{r} |E_p(\mathbf{r})|^2 \\ &= \left(\frac{k}{2\pi z}\right)^2 \exp\left[2\sigma_{r_1}^2 - T\right] \exp\left[-\frac{2r^2}{W_p^2}\right]. \end{aligned} \tag{64}$$

The term $\exp\left[2\sigma_{r_1}^2 - T\right]$ represents the turbulence induced spread of the one-photon field. Same expression holds for $P_1(\mathbf{r}_2)$. They are

proportional to the pump intensity at the crystal ($z = 0$), additionally affected by the turbulence parameters represented by σ_r^2 and T. We see that their product is different from the expression for $P_2(\mathbf{r}_1, \mathbf{r}_2)$, Eq.(54), moreover, the marginal probability of Eq.(54) is not the same as Eq.(64).

In the attempt to separate quantum effects from classical ones, the authors of Ref. [36] found out that properties of two-photon speckle are conditioned by the following phenomena: the indistinguishability of photons, the quantum nature of the incident light, the classical correlations between photons, induced by the fact that they propagate through the same random medium. These phenomena determine the overall behavior of $P_2(x_1, x_2)$ whatever the state of the incident light. As a result, the P_2 calculated for two-photon entangled and non-entangled states, as well as for the coherent state look very similar, with, however, one notable exception. Entanglement allows to modify the symmetry of the state with respect to the exchange of the two photons [46, 132].

Consider the two-particle state,

$$|\psi\rangle = \iint dxdy f(x,y)|x\rangle|y\rangle, \tag{65}$$

Where $|x\rangle = |1\rangle_x$ indicates a single particle in mode x, and $|y\rangle = |1\rangle_y$ indicates a particle in a distinct mode y. When these particles are interfered, the paths are rendered partially distinguishable if $f(x,y)$ is not symmetric under exchange of its arguments, because auxiliary measurements of the properties x and y may reveal "which path" information. On the other hand, the state

$$|\psi\rangle_S = \iint dxdy[f(x,y) + e^{iu} f(y,x)]|x\rangle|y\rangle, \tag{66}$$

obtained by coherently superposing two states of the form Eq. (65) contains no such distinguishing information [132].

3.1.6 *Pumping the Crystal with Coherent Hermite-Gaussian Beams of any Order.*

Next, we calculate the two-photon speckles (58) and (54) for the case when pump $E_p(\mathbf{r})$ is chosen as one of the Hermite-Gaussian modes,

$$U_{mn}^{HG}(r_x, r_y, 0) = B_{m,n} H_m\left(\frac{\sqrt{2}}{W_0} r_x\right) H_n\left(\frac{\sqrt{2}}{W_0} r_y\right) \exp\left(-\frac{r^2}{W_0^2}\right), \tag{67}$$

where $B_{m,n} = [W_0\sqrt{\pi 2^{m+n-1} m!\, n!}]^{-1}$ is the normalization constant, $H_k(\rho)$ is the Hermite polynomial and W_0 is the pump's beam radius at the

crystal. Changing the variables with the help of Eq.(55), Eq. (58) takes the following form

$$
\begin{aligned}
P_2(x,x) = |B_{m,n}|^2 \frac{k^2 e^{\sigma_{sp}^2(z)}}{4\pi^2 z^2} \iint d\mathbf{S} d\mathbf{Q} H_m\left[\frac{\sqrt{2}}{W_0}\left(S_x + \frac{Q_x}{2}\right)\right] H_m\left[\frac{\sqrt{2}}{W_0}\left(S_x - \frac{Q_x}{2}\right)\right] \\
\times H_n\left[\frac{\sqrt{2}}{W_0}\left(S_y + \frac{Q_y}{2}\right)\right] H_n\left[\frac{\sqrt{2}}{W_0}\left(S_y - \frac{Q_y}{2}\right)\right] \\
\times \exp\left[-\frac{2}{W_0^2}\left(S_x^2 + S_y^2\right)\right] \exp\left[-\frac{1}{2W_0^2}\left(Q_x^2 + Q_y^2\right)\right] \\
\times \exp\left[\frac{ik_p}{z}\left(S_x Q_x + S_y Q_y\right)\right] \exp\left[-\frac{ik_p}{z}\left(r_x Q_x + r_y Q_y\right)\right] \\
\times \exp\left[-\frac{3.16\sigma_{R,p}^2}{\Lambda_{0,p} W_0^2}\left(Q_x^2 + Q_y^2\right)\right],
\end{aligned}
\tag{68}
$$

where σ_{sp}^2 is the scintillation index for a spherical wave (155). In the Appendix C we evaluated this integral analytically. The result is

$$
P_2(x,x) = \frac{e^{\sigma_{sp}^2(z) - \frac{2r^2}{W_{LT}^2}}}{2\pi W_{LT}^2} \sum_{k=0}^{m}\sum_{l=0}^{n} \binom{m}{k}\binom{n}{l} \frac{(W/W_{LT})^{2k+2l}}{2^{k+l} k!\, l!} H_{2k}\left[\frac{\sqrt{2}}{W_{LT}} r_x\right] H_{2l}\left[\frac{\sqrt{2}}{W_{LT}} r_y\right],
\tag{69}
$$

where W represents the spot size of the pump beam on the observation plane in the absence of turbulence. We also made the following definition:

$$
W_{LT} \equiv W\sqrt{1 + 6.32\sigma_{R,p}^2 \Lambda}
$$

Note that, as one would expect, in no turbulence limit, $\sigma_{sp}^2(z) \to 0$, $W_{LT} \to W$, and Eq.(69) reduces to

$$
P_2(x,x) = |B_{m,n}|^2 \frac{W_0^2}{W^2} H_m^2\left[\frac{\sqrt{2}}{W} r_x\right] H_n^2\left[\frac{\sqrt{2}}{W} r_y\right] \exp\left[-\frac{2r^2}{W^2}\right],
\tag{70}
$$

where we used the identity [128]

$$
H_m^2(x) = 2^m (m!)^2 \sum_{k=0}^{m} \frac{H_{2k}(x)}{2^k (k!)^2 (m-k)!}.
\tag{71}
$$

We have found a similar result for Eq.(54):

$$
\begin{aligned}
P_2(x_1,x_2) = \frac{1}{2\pi W_{LT1}^2} \exp\left[\left(\frac{1.58\sigma_{R,p}^2}{\Lambda_p W^2} - \frac{2}{3\rho_{pl}^2}\right) p^2 - 0.043\pi^2 C_n^2 z^3 p^{-7/3}\right] e^{-\frac{2r^2}{W_{LT1}^2}} \\
\times \sum_{k=0}^{m}\sum_{l=0}^{n} \binom{m}{k}\binom{n}{l} \frac{(W/W_{LT1})^{2k+2l}}{2^{k+l} k!\, l!} H_{2k}\left[\frac{r_{x2} + r_{x1}}{\sqrt{2} W_{LT1}}\right] H_{2l}\left[\frac{r_{y1} + r_{y2}}{\sqrt{2} W_{LT1}}\right],
\end{aligned}
\tag{72}
$$

where

$$
W_{LT1} = W\sqrt{1 + 6.32\sigma_{R,p}^2 \Lambda + \frac{4\Lambda^2 W^2}{3\rho_{pl}^2}}.
$$

Eq.(72), too, reduces to a similar expression for the vacuum limit

$$P_2(x_1,x_2) = |B_{m,n}|^2 \frac{W_0^2}{W^2} H_m^2\left[\frac{\sqrt{2}}{W}\left(\frac{r_{x2}+r_{x1}}{2}\right)\right] H_n^2\left[\frac{\sqrt{2}}{W}\left(\frac{r_{y1}+r_{y2}}{2}\right)\right] \exp\left[-\frac{2r^2}{W^2}\right], \tag{73}$$

with $r = |\mathbf{r}_1 + \mathbf{r}_2|/2$. The results (69), (72) show that for an Hermite-Gaussian pump the joint detection probability of down-converted photons is a weighted convex sum of lower, even order Hermite-Gaussian modes, all of them having scaled Hermite functions and the same long term averaged Gaussian part $\exp[-2r^2/W_{LT}^2]$.

It is interesting to analyse the $m = 1,\ n = 0$ case. In that case, Eq.(69) takes the form

$$\begin{aligned} P_2^{(10)}(x,x) &= \frac{e^{\sigma_{sp}^2(z)}}{2\pi W_{LT}^2} \exp\left[-\frac{2r^2}{W_{LT}^2}\right] \sum_{k=0}^{1} \frac{(W/W_{LT})^{2k}}{2^k} H_{2k}\left[\frac{\sqrt{2}}{W_{LT}} r_x\right] \\ &= \frac{e^{\sigma_{sp}^2(z)}}{2\pi W_{LT}^2} \exp\left[-\frac{2r^2}{W_{LT}^2}\right] \left(1 + \frac{W^2}{2W_{LT}^2} H_2\left[\frac{\sqrt{2}}{W_{LT}} r_x\right]\right) \\ &= \frac{e^{\sigma_{sp}^2(z)}}{2\pi W_{LT}^2} \exp\left[-\frac{2r^2}{W_{LT}^2}\right] \left(1 + \frac{W^2}{2W_{LT}^2}\left[4\frac{2r_x^2}{W_{LT}^2} - 2\right]\right) \\ &= \frac{e^{\sigma_{sp}^2(z)}}{2\pi W_{LT}^2} \exp\left[-\frac{2r^2}{W_{LT}^2}\right] \left(1 + \frac{4W^2}{W_{LT}^4} r_x^2 - \frac{W^2}{W_{LT}^2}\right), \end{aligned} \tag{74}$$

where we have used identities $H_0(x) = 1$ and $H_2(x) = 4x^2 - 2$.

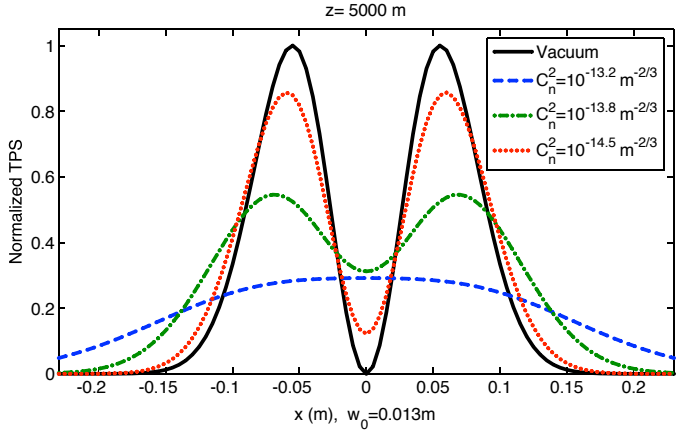

Figure 2: *The normalized two-photon speckle (TPS) for the HG_{10} pump case under turbulence conditions: strong (dashed), strong-to-moderate (dashed-dotted), moderate (dotted) and no turbulence (solid). The normalization is made by dividing Eq. (74) by its maximum value $(1/\pi W^2 e)$ in the absence of turbulence. For simplicity, we took $\sigma_{sp}^2(z) = 0.4\sigma_R^2$ for the Kolmogorov spectrum.*

We plotted the normalized version of Eq.(74) as a function of r_x and $r_y = 0$ corresponding to the cases: vacuum, moderate turbulence,

moderate-to-strong and strong turbulence for a propagation distance of $z = 5\text{km}$. The normalization is made by dividing Eq.(74) by its maximum value $(1/\pi W^2 e)$ in the absence of turbulence. The result is:

$$P_2^{N(10)}(x,x) = \frac{eW^2}{2W_{LT}^2} \exp\left[-\frac{2r^2}{W_{LT}^2}\right]\left(1 + \frac{4W^2}{W_{LT}^4} r_x^2 - \frac{W^2}{W_{LT}^2}\right), \tag{75}$$

The plot resembles the result [21, ch.17] for HG_{10} laser beam intensity. This is again a manifestation of the beam-like behavior of spatial correlations in two-photon states generated by spontaneous parametric down-conversion. We see that the coincident counts reduce significantly in the strong turbulence regime. Another important conclusion can be drawn from this result: the amount of the HG_{00} mode is appreciable even in moderate turbulence, meaning that cross-talk between modes increases with turbulence, degrading the dimensionality of the alphabet based on higher-order Gaussian modes. The dimensionality degradation of Laguerre-Gauss modes due to turbulence has been experimentally demonstrated in Ref. [13].

3.1.7 *Pumping the crystal with Coherent Laguerre-Gaussian Beams of any Order.*

In calculating the two-photon speckle we have used Hermite-Gauss functions to represent the transverse profile of the pump. We have done so due to relatively simpler manipulations that Hermite-Gauss functions permit, which lacks when dealing with Laguerre-Gauss functions. The normalized Laguerre-Gaussian modes in polar coordinates are given by [91]

$$\begin{aligned} U_{pl}^{LG}(r,\theta,z) = \sqrt{\frac{2p!}{\pi(|l|+p)!}} \frac{1}{W(z)} \left(\frac{\sqrt{2}r}{W(z)}\right)^{|l|} L_p^{|l|}\left(\frac{2r^2}{W^2(z)}\right) e^{il\theta} \\ \times \exp[i(2p+|l|+1)\phi(z)] \exp\left(ikz - \frac{r^2}{W^2(z)} + i\frac{kr^2}{2F(z)}\right), \end{aligned} \tag{76}$$

where the various parameters are defined in the Appendix A.

Instead of using Eq.(76) in (51), one can use the fact that HG and LG modes are converted one into another by a basis change [92]

$$|LG_{l.p}\rangle = \sum_{m=0}^{\infty}\sum_{n=0}^{\infty} |HG_{m,n}\rangle\langle HG_{m,n}|LG_{l.p}\rangle, \tag{77}$$

and

$$|HG_{l.p}\rangle = \sum_{l=-\infty}^{\infty}\sum_{p=0}^{\infty} |LG_{l,p}\rangle\langle LG_{l,p}|HG_{m,n}\rangle, \tag{78}$$

where

$$\langle HG_{m,n}|LG_{l.p}\rangle = \langle LG_{l,p}|HG_{m,n}\rangle^* = \begin{cases} i^m b\left(\frac{N+l}{2}, \frac{N-l}{2}, m\right), & 2p+|l| = m+n, \\ 0, & 2p+|l| \neq m+n, \end{cases}$$

and the coefficients $b(m,n,k)$ are defined as

$$b(m,n,k) = \sqrt{\frac{(m+n-k)!\,k!}{2^{m+n}m!\,n!}}\frac{1}{k!}\frac{d^n}{dt^n}\left[(1-t)^m(1+t)^n\right]_{t=0}, \tag{79}$$

so that

$$U^{LG}_{mn}(x,y,z) = \sum_{k=0}^{N} i^k b(m,n,k) U^{HG}_{N-k,k}(x,y,z), \tag{80}$$

with $N = m+n = 2p+|l|$, called the mode order. The indices l and p of the LG mode resulting from mode conversion of a HG mode are related to the indices n and m of the original HG mode through the equations

$$l(m,n) = m-n, \qquad p(m,n) = \min(m,n),$$

and the inverse relation

$$m(N,l) = \frac{N+l}{2}, \qquad n(N,l) = \frac{N-l}{2}.$$

Using the relation (80) one immediately has a solution for the two-photon speckle for a Laguerre-Gaussian pump of any order.

3.1.8 *Coordinates Inversion*

Let us make a transverse coordinates inversion in the signal, say, photon, $\mathbf{r}_2' \to -\mathbf{r}_2'$. Also choose the detectors at $\mathbf{r}_1 = -\mathbf{r}_2 \equiv \mathbf{r}$. The experimental implementation of this has been made in Ref. [37]. Then the Biphoton at the observation plane, in the thin crystal approximation, takes the following form

$$\begin{aligned} A^{\text{inv}}(\mathbf{r},-\mathbf{r}) &= \left(\frac{k}{2\pi z}\right)^2 \iint d\mathbf{r}_1' d\mathbf{r}_2' E_p\left(\frac{\mathbf{r}_1'-\mathbf{r}_2'}{2}\right)\delta(\mathbf{r}_1'+\mathbf{r}_2') \\ &\times \exp\left[\frac{ik}{2z}\left(|\mathbf{r}-\mathbf{r}_1'|^2+|\mathbf{r}+\mathbf{r}_2'|^2\right)\right]\exp\left[\psi^s(\mathbf{r}_1',\mathbf{r})+\psi^i(\mathbf{r}_2',-\mathbf{r})\right] \\ &= \left(\frac{k}{2\pi z}\right)^2 \int d\mathbf{r}' E_p(\mathbf{r}')\exp\left[\frac{ik}{z}|\mathbf{r}-\mathbf{r}'|^2\right]\exp\left[\psi^s(\mathbf{r}',\mathbf{r})+\psi^i(-\mathbf{r}',-\mathbf{r})\right]. \end{aligned} \tag{81}$$

We see from Eq.(81) that the total perturbation is now symmetric with respect to the z axis; that is to say, the antisymmetric part of ψ is canceled out. In particular, the wavefront tilt $(ik/2L)(\mathbf{r}'-\mathbf{r})\cdot\mathbf{d}$, where d is a random displacement, vanishes.

The two-photon speckle takes the form

$$\begin{aligned} P_2^{\text{inv}}(\mathbf{r},-\mathbf{r}) &= \left(\frac{k}{2\pi z}\right)^2 \iint d\mathbf{r}' d\mathbf{r}'' E_p(\mathbf{r}')E_p^*(\mathbf{r}'')\exp\left[\frac{ik}{z}\left(|\mathbf{r}-\mathbf{r}'|^2-|\mathbf{r}-\mathbf{r}''|^2\right)\right] \\ &\times\left\langle\exp\left[\psi(\mathbf{r}',\mathbf{r})+\psi^*(\mathbf{r}'',\mathbf{r})+\psi(-\mathbf{r}',-\mathbf{r})+\psi^*(-\mathbf{r}'',-\mathbf{r})\right]\right\rangle. \end{aligned} \tag{82}$$

With the help of Eq.(36) we find the ensemble average to be

$$\begin{aligned} \langle\exp[\ldots]\rangle &= \exp\left[4E_1(0)+E_2(0,0;\mathbf{r}',\mathbf{r}'')+E_2(\mathbf{r},-\mathbf{r};\mathbf{r}',-\mathbf{r}'')+E_2(-\mathbf{r},\mathbf{r};-\mathbf{r}',\mathbf{r}'')\right] \\ &\times\exp\left[E_2(-\mathbf{r},-\mathbf{r};-\mathbf{r}',-\mathbf{r}'')+E_3(\mathbf{r},-\mathbf{r};\mathbf{r}',-\mathbf{r}')+E_3(\mathbf{r},-\mathbf{r};\mathbf{r}'',-\mathbf{r}'')\right]. \end{aligned} \tag{83}$$

By grouping the second term with the fifth, the third with the fourth and using Eqs.(31)–(33), one can show that Eq.(83) results in

$$\begin{aligned}\langle \exp[...]\rangle = &-8\pi^2k^2z\int_0^\infty d\kappa\kappa\Phi(\kappa) + \left(8\pi^2k^2z\int_0^\infty d\kappa\kappa\Phi(\kappa) - 8\pi^2k^2z\int_0^\infty d\kappa\kappa\Phi(\kappa)\right)\\ &+8\pi^2k^2z\int_0^1 d\xi\int_0^\infty d\kappa\kappa\Phi(\kappa)\left[J_0(\kappa\xi|\mathbf{r}-\mathbf{r}'|)\right]\\ &+8\pi^2k^2z\int_0^1 d\xi\int_0^\infty d\kappa\kappa\Phi(\kappa)\left[J_0(\kappa|(1-\xi)(2\mathbf{r})+\xi(\mathbf{r}'+\mathbf{r}'')|\right]\\ &-4\pi^2k^2z\int_0^1 d\xi\int_0^\infty d\kappa\kappa\Phi(\kappa)\left[J_0(\kappa|(1-\xi)(2\mathbf{r})+\xi(2\mathbf{r}')|\right]\exp\left[-i\frac{z\kappa^2}{k}\xi(1-\xi)\right]\\ &-4\pi^2k^2z\int_0^1 d\xi\int_0^\infty d\kappa\kappa\Phi(\kappa)\left[J_0(\kappa|(1-\xi)(2\mathbf{r})+\xi(2\mathbf{r}'')|\right]\exp\left[i\frac{z\kappa^2}{k}\xi(1-\xi)\right].\end{aligned} \tag{84}$$

In terms of wave structure functions (39) and (40), this has the form

$$\langle \exp[...]\rangle = -D_{sp}(|\mathbf{r}'-\mathbf{r}''|) + D_{sp}(2\mathbf{r},\mathbf{r}'+\mathbf{r}'') - \frac{1}{2}\left[D_{sp}(2\mathbf{r},2\mathbf{r}') + D_{sp}(2\mathbf{r},2\mathbf{r}'')\right]. \tag{85}$$

In passing from Eq.(84) to Eq.(85) we again made the geometrical optics approximation [21, ch.8], $z\kappa^2/k \ll 1$, to replace the exponential functions in the fourth and fifth lines of Eq.(84) by one. The two-photon speckle, in the changed variables (55) now becomes

$$\begin{aligned}P_2^{\text{inv}}(\mathbf{r},-\mathbf{r}) = &\left(\frac{k}{2\pi z}\right)^2\iint d\mathbf{S}d\mathbf{Q}E_p\left(\mathbf{S}+\frac{\mathbf{Q}}{2}\right)E_p^*\left(\mathbf{S}-\frac{\mathbf{Q}}{2}\right)\exp\left[\frac{2ik}{z}(\mathbf{S}\cdot\mathbf{Q}-\mathbf{r}\cdot\mathbf{Q})\right]\\ &\times\exp\left\{-D_{sp}(Q)+D_{sp}(2\mathbf{r},2\mathbf{S})-\frac{1}{2}\left[D_{sp}(2\mathbf{r},2\mathbf{S}+\mathbf{Q})+D_{sp}(2\mathbf{r},2\mathbf{S}-\mathbf{Q})\right]\right\},\end{aligned} \tag{86}$$

which, using the approximated expressions (43) and (44), takes the form

$$\begin{aligned}P_2^{\text{inv}}(\mathbf{r},-\mathbf{r}) = &\left(\frac{k}{2\pi z}\right)^2\iint d\mathbf{S}d\mathbf{Q}E_p\left(\mathbf{S}+\frac{\mathbf{Q}}{2}\right)E_p^*\left(\mathbf{S}-\frac{\mathbf{Q}}{2}\right)\\ &\times\exp\left[\frac{2ik}{z}(\mathbf{S}\cdot\mathbf{Q}-\mathbf{r}\cdot\mathbf{Q})\right]\exp\left[-\left(\frac{2}{3\rho_{pl}^2}+\frac{0.79\sigma_{R,p}^2}{\Lambda_{0,p}W_0^2}\right)Q^2\right].\end{aligned} \tag{87}$$

We see that this expression has a simpler form than Eq.(54), the latter having an exponential degrading modulation in front. This is so not only because of the symmetric observation points, but also because of the coordinate inversion we made in one of the signal or idler fields at the source plane. This explains the raise of coincidences observed in [37].

3.2 Partially coherent correlation beams in the turbulent atmosphere

3.2.1 *Cross-Spectral Density and its Coherent-Mode Representation.*

Because of the spreading of a light travelling in the atmosphere the detection becomes a difficult task when propagation distance is increased. One would need larger telescopes to detect the incoming

signal. Although partially coherent beams spread more than coherent beams when propagating in vacuum, it is the opposite when they propagate in the atmosphere, in a relative manner. After some propagation distance, coherent beams start spreading faster than partially coherent ones. In this sense, partially coherent beams are more resistant to the atmosphere [49–51]. Particularly, it has been shown that the angular spread of partially coherent Hermite-cosh-Gaussian beams is less when the spatial correlation length ρ_0, the waist width W_0, the beam parameter (associated with the cosh part) Ω_0 are smaller and when the beam order m, n is larger [94]. This implies that the partial coherence of the pump field can be used as a parameter to prepare states that are optimal for a given quantum-information protocol and a given strength of turbulence. Therefore, using partially coherent sources to pump a $\chi^{(2)}$ crystal to produce correlation beams becomes a natural task, for the *pump field amplitude* shows up in the SPDC state (49). A review article on generation of various partially coherent beams and their propagation properties in turbulent atmosphere is given by Cai [101].

Partially coherent sources have been used before in SPDC process without– [102, 103] and with the presence of turbulent meduim [41–44].

The partially coherent sources are characterized by the cross-spectral density function defined by [58]

$$\langle U(\mathbf{r}_1,\omega)U^*(\mathbf{r}_2,\omega')\rangle = W^{(0)}(\mathbf{r}_1,\mathbf{r}_2,\omega)\delta(\omega-\omega'), \tag{88}$$

where angular brackets represent ensemble average over different realizations of the field and δ is the Dirac delta function.

The cross-spectral density functions satisfy Wolf equations for propagation of correlations in free space and for a large class of statistically stationary sources they have a coherent mode representation [58, 86]

$$W^{(0)}(\mathbf{r}_1,\mathbf{r}_2,\omega) = \sum_n \alpha_n(\omega)\varphi_n^*(\mathbf{r}_1,\omega)\varphi_n(\mathbf{r}_2,\omega). \tag{89}$$

Here, $\varphi_n(\mathbf{r},\omega)$ and $\alpha_n(\omega)$ are the eigenfunctions (eigenmodes) and eigenvalues of the (Fredholm) integral equation

$$\int_{source} W^{(0)}(\mathbf{r}_1,\mathbf{r}_2,\omega)\varphi_n(\mathbf{r}_1,\omega)d^2r_1 = \varphi_n(\mathbf{r}_2,\omega), \quad n=\{n_1,n_2\}. \tag{90}$$

As a set of mode functions one usually takes an orthonormal one:

$$\int_{source} \varphi_m^*(\mathbf{r},\omega)\varphi_n(\mathbf{r},\omega)d^2r = \delta_{m,n} \tag{91}$$

and $\alpha_n(\omega) \geq 0, \quad \forall n$.

A model for partially coherent source is the Gaussian-Schell-model (GSM). They are characterized by a cross-spectral density function of the form [50, 58]

$$W^{(0)}(\mathbf{r}_1,\mathbf{r}_2,\omega) = \sqrt{S^{(0)}(\mathbf{r}_1,\omega)S^{(0)}(\mathbf{r}_2,\omega)}\mu^{(0)}(\mathbf{r}_1,\mathbf{r}_2,\omega), \tag{92}$$

where

$$S^{(0)}(\mathbf{r},\omega) = M\exp\left[-\frac{|\mathbf{r}|^2}{2\sigma_s^2}\right], \quad \mu^{(0)}(\mathbf{r}_1,\mathbf{r}_2,\omega) = \exp\left[-\frac{|\mathbf{r}_1-\mathbf{r}_2|^2}{2\sigma_\mu^2}\right] \tag{93}$$

are the spectral density and the spectral degree of coherence of the source, respectively. M is a positive constant, σ_s and σ_μ are the effective widths of spectral density and spectral degree of coherence, respectively.

The authors of Ref.[51] prove a theorem according to which the spreading of a beam generated by a GSM source is independent of the coherence properties of the source, after it has travelled over a sufficiently long distance through a turbulent atmosphere. It means that there is no need to use high quality lasers for pointing, tracking and guiding through the atmosphere over long enough distances. A poor quality laser or a "mosaic" of independent lasers would do just as well. In order that such sources (GSM) generate a beam, the condition

$$1/(2\sigma_s^2) + 2/\sigma_\mu^2 \ll k^2$$

must be satisfied [58].

Another model of sources is the so called Collett-Wolf model [104–106]. These sources can produce fields as directional as a laser beam fields (in the quasi-homogeneity hypothesis), although the sources are nearly incoherent. Experimental realizations of Collett-Wolf sources are described in Refs. [107, 108].

The cross-spectral density function of a planar, rectangular GSM sources may have coherent-mode representation of the following form [50]

$$W^{(0)}(\mathbf{r}_1,\mathbf{r}_2,\omega) = \sum_m\sum_n \beta_{m,n}(\omega)\phi_m^{(0)*}(\mathbf{r}_1,\omega)\phi_n^{(0)}(\mathbf{r}_2,\omega), \tag{94}$$

where

$$\beta_{m,n}(\omega) = M\left(\frac{\pi}{a+b+c}\right)\left(\frac{b}{a+b+c}\right)^{m+n}, \tag{95}$$

with $a = 1/4\sigma_s^2$, $b = 1/2\sigma_\mu^2$, $c = \sqrt{a^2+2ab}$, and the coherent modes $\phi^{(0)}(\mathbf{r},\omega)$ are given by

$$\phi^{(0)}(\mathbf{r},\omega) = B_{m,n}H_m\left[\frac{\sqrt{2}}{W_0}r_x\right]H_n\left[\frac{\sqrt{2}}{W_0}r_y\right]\exp\left[-\frac{r_x^2+r_y^2}{W_0^2}\right]. \tag{96}$$

$H_m(\rho)$ are the Hermite polynomials and

$$B_{m,n} = \left[W_0\sqrt{\pi 2^{m+n-1}m!\,n!}\right]^{-1}, \qquad W_0 = 1/\sqrt{c}.$$

3.2.2 *Two-Photon Speckle: Partially Coherent Pump.*

When the $\chi^{(2)}$ crystal is pumped by a partially coherent beam, one must consider the ensemble averaged quantity $\langle E_p E_p^*\rangle$ over different realizations of fields in the expression for the two-photon speckle (50)

which is the cross-spectral density function $W^{(c)}(\mathbf{r}_1, \mathbf{r}_2)$. The superscript (c) means that the cross-spectral density is considered at the surface of the $\chi^{(2)}$ crystal.

The joint detection probability density function (53) now takes the following form

$$P_2(x_1, x_2) = \frac{k^2}{4\pi^2 z^2} \iint d\mathbf{r}' d\mathbf{r}'' W^{(c)}(\mathbf{r}', \mathbf{r}'') \exp\left\{\frac{ik}{2z}\left[|\mathbf{r}_1 - \mathbf{r}'|^2 - |\mathbf{r}_1 - \mathbf{r}''|^2 + |\mathbf{r}_2 - \mathbf{r}'|^2 - |\mathbf{r}_2 - \mathbf{r}''|^2\right]\right\} \times \exp\left[-\frac{1}{2}\left[D_{sp}(\mathbf{p}, \mathbf{Q}) + D_{sp}(-\mathbf{p}, \mathbf{Q})\right] + D_{sp}(p) - D_{sp}(Q) - 0.043\pi^2 C_n^2 z^3 p^{-7/3}\right], \tag{97}$$

where we have dropped the ω dependence.

For the case $x_1 = x_2$, Eq.(58) now takes the following form

$$P_2(x, x) = \frac{k^2 e^{-\sigma_{sp}^2(z)}}{4\pi^2 z^2} \iint d\mathbf{r}' d\mathbf{r}'' W^{(c)}(\mathbf{r}', \mathbf{r}'') \times \exp\left\{\frac{ik}{z}\left[|\mathbf{r} - \mathbf{r}'|^2 - |\mathbf{r} - \mathbf{r}''|^2\right] - 2D_{sp}(|\mathbf{r}' - \mathbf{r}''|)\right\}. \tag{98}$$

We now use the GSM model for the cross-spectral density function $W^{(c)}$ of the two photon source Eqs.(92) and (93) in Eq.(98)

$$\begin{aligned} P_2(x, x) &= \frac{k^2 e^{-\sigma_{sp}^2(z)}}{4\pi^2 z^2} \iint d\mathbf{S} d\mathbf{Q} W^{(c)}(\mathbf{S} + \mathbf{Q}/2, \mathbf{S} - \mathbf{Q}/2) \exp\left\{\frac{ik_p}{z}\left[\mathbf{S}\cdot\mathbf{Q} - \mathbf{r}\cdot\mathbf{Q}\right] - 2D_{sp}(Q)\right\} \\ &= \frac{Mk^2 e^{-\sigma_{sp}^2(z)}}{4\pi^2 z^2} \iint d\mathbf{S} d\mathbf{Q} \exp\left[-\frac{S^2}{2\sigma_s^2} - \frac{Q^2}{2\sigma_\Delta^2}\right] \exp\left\{\frac{ik_p}{z}\left[\mathbf{S}\cdot\mathbf{Q} - \mathbf{r}\cdot\mathbf{Q}\right] - 2D_{sp}(Q)\right\} \end{aligned} \tag{99}$$

where we made a change of variables (55), and defined

$$1/\sigma_\Delta^2 = 1/4\sigma_s^2 + 1/\sigma_\mu^2.$$

Integration in $\mathbf{S}$ variable is readily performed by using Fourier transform

$$\text{int in } d\mathbf{S}: \qquad 2\sigma_s^2 \exp\left(-\frac{\sigma_s^2 k_p^2}{2\pi^2 z^2} Q^2\right),$$

and, similarly, the integration in $\mathbf{Q}$ variable

$$\begin{aligned} &\int d\mathbf{Q} \exp\left[-\left(\frac{1}{2\sigma_\Delta^2} + \frac{\sigma_s^2 k_p^2}{2\pi^2 z^2} + \frac{1.58\sigma_{R,p}^2}{\Lambda_{0,p} W_0^2}\right) Q^2\right] \exp\left(-2\pi i \mathbf{Q}\cdot\mathbf{r}/\lambda_p z\right) \\ &\quad = \frac{2z^2}{\sigma_s^2 k_p^2 \Delta^2(z)} \exp\left\{-\frac{r^2}{2\sigma_s^2 \Delta^2(z)}\right\}, \end{aligned} \tag{100}$$

where we used Eq.(43) for D_{sp} and defined

$$\begin{aligned} \Delta^2(z) &= 1 + \frac{1}{(k_p \sigma_s \sigma_\Delta)^2} z^2 + \frac{2z^2}{\sigma_s^2 k_p^2} \cdot \frac{1.58\sigma_{R,p}^2}{\Lambda_{0,p} W_0^2} \\ &= 1 + \frac{1}{(k_p \sigma_s)^2}\left(\frac{1}{4\sigma_s^2} + \frac{1}{\sigma_\mu^2}\right) z^2 + \frac{1.58 C_n^2 k_p^{1/6}}{\sigma_s^2} z^{13/6}. \end{aligned} \tag{101}$$

Finally, for the two-photon absorber we have

$$P_2(x,x) = \frac{Me^{-\sigma_{sp}^2(z)}}{\Delta^2(z)} \exp\left\{-\frac{r^2}{2\sigma_s^2\Delta^2(z)}\right\}. \tag{102}$$

Note that with Eq.(102) we recover the result in Ref.[50] for a partially coherent beam intensity. Our result is for fourth order correlations: a manifestation of the concept of correlation beam. Eq.(101) depicts

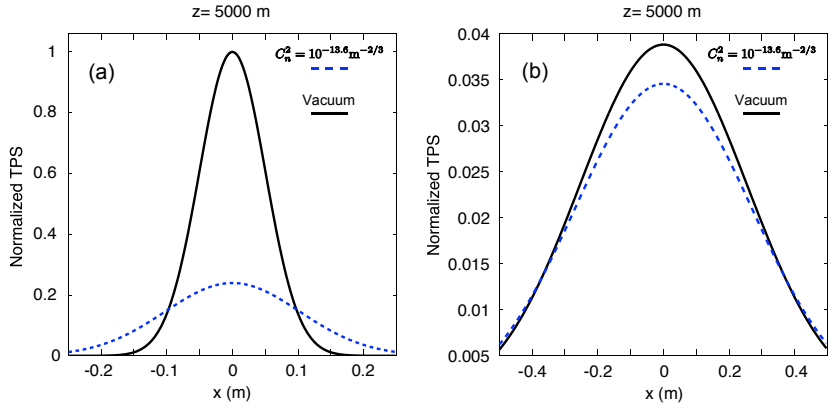

Figure 3: *Normalized two-photon speckle profile for the case when the* $\chi^{(2)}$ *crystal is pumped by (a) a fully coherent* ($\sigma_\mu \to \infty$) *Gaussian beam and (b) a partially coherent* ($\sigma_\mu = 2\mathrm{mm}$) *Gaussian beam, both under the conditions* $k_p = 10^{-7}\mathrm{m}^{-1}$, $C_n^2 = 10^{-13.6}\mathrm{m}^{-2/3}$, $l_0 = 0.01\mathrm{m}$, $\sigma_s = 5\mathrm{mm}$. *The detectors are at the same space-time points* $x_1 = x_2$.

the spread of a partially coherent beam in the atmosphere when the approximation $z \ll z_i$ is satisfied. Remember, that z_i represents the propagation distance at which the transverse coherence radius of optical wave is of the order of the inner scale l_0. For the other limit, $z \gg z_i$, Eq.(101) takes the following form

$$\Delta^2(z) = 1 + \frac{1}{(k_p\sigma_s)^2}\left(\frac{1}{4\sigma_s^2} + \frac{1}{\sigma_\mu^2}\right) z^2 + \frac{0.55C_n^2 l_0^{-1/3}}{\sigma_s^2} z^3. \tag{103}$$

The first two terms represent the vacuum induced spreading, the third term – the turbulence induced spreading. As we see from Eqs.(101) and (103), turbulence effects become dominant for long propagation distances. For a fully coherent Gaussian beam ($\sigma_\mu = \infty$), $\Delta^2(z)$ is larger, and Eq.(102) is appreciably changed in comparison with the beam propagating in free space. In Fig.3, we plotted the normalized version of (102) for both, partially and fully coherent Gaussian pump beam cases. The normalization is made by dividing it by the on-axis probability $P_2(\mathbf{r}=0,z)|_{C_n^2=0,\sigma_\mu=0} = M/(1+(\pi z/2k_p\sigma_s^2)^2)$:

$$P_2^N(x,x) = \frac{1+(\pi z/2k_p\sigma_s^2)^2}{\Delta^2(z)} \exp\left\{-\frac{r^2}{2\sigma_s^2\Delta^2(z)}\right\}. \tag{104}$$

As the figures show, the two-photon speckle for the partially coherent pump beam case is nearly the same as in vacuum, whereas that of the the fully coherent Gaussian pump beam case is appreciably changed in comparison with the propagation in vacuum. This result is consistent with that of Ref. [50] for the *intensity* distribution of a fully coherent beam and a beam generated by a GSM source.

3.2.3 *Two-Photon Speckle in Coherent-Mode Representation.*

Using Eqs.(94) and (96), the two-photon speckle (98) takes the form

$$\begin{aligned} P_2^{(p-coh)}(\mathbf{r},\mathbf{r}) = \frac{k^2 e^{-\sigma_{sp}^2(z)}}{4\pi^2 z^2} \sum_m \sum_n \beta_{m,n} |B_{m,n}|^2 \iint d\mathbf{r}' d\mathbf{r}'' H_m \left[\frac{\sqrt{2}}{W_0} r_x'\right] H_m \left[\frac{\sqrt{2}}{W_0} r_x''\right] \\ \times H_n \left[\frac{\sqrt{2}}{W_0} r_y'\right] H_n \left[\frac{\sqrt{2}}{W_0} r_y''\right] \exp\left[-\frac{r_x'^2 + r_x''^2 + r_y'^2 + r_y''^2}{W_0^2}\right] \\ \times \exp\left\{\frac{ik}{z}\left[|\mathbf{r}-\mathbf{r}'|^2 - |\mathbf{r}-\mathbf{r}''|^2\right] - 2D_{sp}(|\mathbf{r}'-\mathbf{r}''|)\right\}. \end{aligned} \tag{105}$$

We notice that the integral in (105) is exactly the one in Eq.(68) if one makes the change of variables (55), so that we can write in general

$$P_2^{(p-coh)}(x,x) = \sum_{m=0}^{\infty} \sum_{n=0}^{\infty} \beta_{m,n} |B_{m,n}|^2 P_2^{(coh)}(x,x), \tag{106}$$

which is an incoherent sum of probabilities of type (69) with $\beta_{m,n}$ given in Eq.(95).

As a perspective, one can consider the problem for different pump beam models, e.g. cosh-Gaussian, Hermite-cosh-Gaussian beams [94], Bessel and Bessel-Gaussian beams, etc. which have interesting properties and may be applied in communication schemes. As for the partially coherent case one can also consider the *phase screen model* [95] instead of the Gaussian-Schell model we considered here.

An important potential application of these results is the determination of the turbulence parameters: the strength of turbulence σ_R or C_n^2, the inner l_0 and outer L_0 scales, etc. by measuring the signal and idler photons in coincidence. We discuss this aspect in the last chapter of this Thesis.

The question whether the correlation beams are advantageous in comparison with a laser beams is still open. The extended Huygens-Fresnel principle that we extensively used for correlation beams can be applied in two-photon imaging systems, together with ABCD ray matrix formalism and Zernike polynomials [98], to calculate the first few turbulence induced aberrations such as piston, tilt, focus, astigmatism, coma and so forth. These aspects are discussed in the last chapters of this Thesis.

4

MODE ANALYSIS OF HIGHER ORDER TRANSVERSE-MODE CORRELATION BEAMS IN TURBULENT ATMOSPHERE

4.1 INTRODUCTION

The fact that the down-converted photons are entangled in transverse modes [109] justifies the question of finding the probability of detecting a signal photon in some transverse mode and an idler photon in another transverse mode after propagating through turbulent medium and check whether they are still correlated in modes. If that is the case, there opens a possibility of quantum communication with large alphabets. By writing the state of down-converted photons in the transverse mode basis and equip with mode detection scheme one could reach long distance, larger alphabet quantum communication.

The conventional (zero-order) Gaussian mode can be viewed as an LG (HG) mode with $l, p = 0$ ($m, n = 0$), which can be detected with the help of single-mode optical fibers used as mode filters. All other modes ($l \neq 0$) have a more complex spatial distribution, and therefore cannot be coupled into single-mode fibers. In order to detect higher-order modes, computer-generated holograms are used to transform them to zero-order Gaussian modes [110] that are further coupled to single-mode fibers for detection. The computer-generated holograms can be also used to project superposition states of LG modes to a particular state defined by the hologram, which is necessary to verify entanglement [3, 111]. As the hologram and a single mode fiber configuration is also sensitive to radial field distributions of source and detectors (related to the mode number p), there has been works on measurement of only the spiral spectrum of entangled two-photon states, e.g. [116] . These are the main reasons why the outcomes of previous works could not be directly compared with predictions of the well-known SPDC wave function. Full spatial entanglement has been accessed experimentally with practicable radial detection modes with negligible cross correlations [112, 113]. The expected perfectly correlated pure state from SPDC has the form

$$|\psi\rangle = \sum_{p=0}^{\infty} \sum_{l=-\infty}^{\infty} a_{p,l} |LG_p^l\rangle_s |LG_p^{-l}\rangle_i. \tag{107}$$

In contrast to the azimuthal modes, the radial modes do not necessarily represent Schmidt modes [122], but there has been found nonzero quantum correlations of detected modes with different p [112]. Considering only the azimuthal dependence, the nature of the OAM correlations can thus be expressed in the entangled state [114, 115]

$$|\psi\rangle = \sum_l \sqrt{P_l}|l\rangle_s|l_p - l\rangle_i, \tag{108}$$

where l_p is the pump's orbital angular momentum quantum number, P_l is the probability of finding a signal photon with orbital angular momentum l and an idler photon with $l_p - l$. It is important to stress once again that this decomposition refers to the whole generated state. The distribution of P_l, which is called the OAM spectrum of the two-photon field, is the quantity to be measured [116].

4.2 PROJECTIVE MEASUREMENTS.

For experimental verification of the transverse-mode correlations one must make projective measurements on the prepared states. We follow Ref.[117] for operational implementation of projective measurements in this section. In quantum mechanics, a projective measurement is a process where a projection operator, often composed of a single basis element which can be represented as $P = |\Phi_n\rangle\langle\Phi_n|$, operates on some input state. The result of this projection on an input state $|\psi\rangle$ is given by $P|\psi\rangle = |\Phi_n\rangle\langle\Phi_n|\psi\rangle$. When the input state is a photon state, at the moment the detector clicks, the measurement destroys the photon so that one can express the projection simply in terms of the inner product $\langle\Phi_n|\psi\rangle$. The measured quantity would be proportional to $|\langle\Phi_n|\psi\rangle|^2$. In other words, the implementation of a projective measurement in an optical system is in one to one correspondence with implementing an inner product. Although, the sources and the detectors of classical and quantum optical systems in general are different, the optical system between them will perform the same task in both cases. Different experimental setups accurately performing optical projective measurements are reported in [117].

Some applications of projective measurements are quantum state tomography [118–120], which is used to determine the density matrix of a quantum state, and measurements of mode spectra of output quantum states [121–123].

The inner product between two functions in two dimensions is

$$\langle f, g\rangle = \int_{\mathscr{D}} f(\mathbf{r})g^*(\mathbf{r})d^2r, \tag{109}$$

where $f(\mathbf{r})$ and $g(\mathbf{r})$ are two-dimensional normalized, complex-valued functions, $\mathbf{r}$ is the two-dimensional transverse position vector, $*$ denotes the complex conjugation, and $\mathscr{D}$ is the domain where f and g are defined. Experimentally, this inner product can be implemented

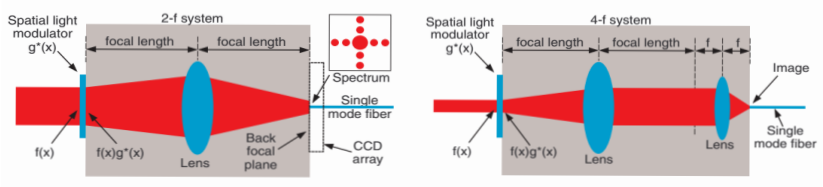

Figure 4: *Diagrams of systems that perform projective measurements. On the left, the 2-f system performes a projective measurement by coupling (the central part of) the Fourier transform of $f(x)g^*(x)$ into the single–mode fiber. On the right, the 4-f system does it by imaging the product $f(x)g^*(x)$ onto the end of the single–mode fiber.*

by doing an optical Fourier transform: passing a modulated optical field through a 2-f system and measuring the light at the center of the back focal Fourier plane: that will make the exponent in the integral vanish. Another method is to image the light onto the single mode fiber. The overlap integral gives the coupling coefficient. With the aid of 4-f system one images the product $f(\mathbf{r})g^*(\mathbf{r})$ onto the single mode fiber, using an appropriate demagnification, Fig.4 [117]. The resulting overlap integral is

$$\alpha = \mathcal{N} \int f(\mathbf{r})g^*(\mathbf{r})G(\mathbf{r};w)d^2r, \tag{110}$$

where $G(\mathbf{r};w) = \sqrt{2/\pi w^2}\exp(-|\mathbf{r}|^2/w^2)$ is the normalized mode of the single mode fiber, w being the size of the mode and $\mathcal{N}$ is the normalization constant. The expression (110) would be an inner product if one can eliminate the function $G(\mathbf{r};w)$ by, say, absorbing it into $g^*(\mathbf{r})$.

In quantum information protocols one usually realizes optical implementation of entangled photon pairs produced via parametric down-conversion process. Then the projective measurement is made on the pair of photons in coincidence. In this case one uses the same imaging technique in both, the signal and the idler systems: modulating the signal and idler fields with a spatial light modulator (SLM) and coupling into single mode fiber. Now, for the collinear PDC, the projective measurement is given by a three-way overlap

$$\alpha = \int M(\mathbf{r})M_1^*(\mathbf{r})M_2^*(\mathbf{r})d^2r, \tag{111}$$

where $M(\mathbf{r})$ is the mode profile of the pump beam in the crystal plane, and $M_1(\mathbf{r})$ and $M_2(\mathbf{r})$ are the two modes on the crystal plane used for the projective measurement in the signal and idler beams, respectively. Together with the Gaussian modes from two single mode fibers the actual integral becomes

$$\alpha = \int M(\mathbf{r})M_1^*(\mathbf{r})M_2^*(\mathbf{r})G^2(\mathbf{r};w)d^2r. \tag{112}$$

The Gaussian modes in (112) can be absorbed into the pump profile, which will modify the pump's mode size as follows:

$$\frac{1}{W_p^2} \to \frac{1}{W_p^2} + \frac{2}{w^2}. \tag{113}$$

4.3 THE JOINT DETECTION PROBABILITY OF TRANSVERSE-MODE CORRELATION BEAMS

Instead of the Laguerre-Gaussian modes basis, mathematically it is easier to deal with the Hermite-Gaussian modes. Then, since the HG modes form a complete basis, we can expand the two-photon state as

$$|\psi_{mn}\rangle = \sum_{j,k,u,t=0}^{\infty} C_{jkut}^{mn} |HG_{jk}\rangle_s |HG_{ut}\rangle_i \tag{114}$$

where $|\psi\rangle$ is the state prepared in SPDC process and

$$C_{jkut}^{mn} = {}_s\langle HG_{jk}|_i\langle HG_{ut}|\psi\rangle. \tag{115}$$

The expression for the joint detection probability, which is the squared modulus of C_{jkut}^{mn}, for signal and idler photons each in some transverse mode (e.g. HG_{mn}, LG_p^l) propagating in vacuum has been calculated before [109, 125, 126]. To account for the atmospheric effects on the state we follow Ref.[124] for the joint probability

$$P(M_1, M_2) = |\langle\psi_1, \psi_2|\psi\rangle|^2 \propto \left| \int d\mathbf{x}_1 \int d\mathbf{x}_2 M_1^*(\mathbf{x}_1) M_2^*(\mathbf{x}_2) E_p\left(\frac{\mathbf{x}_1 + \mathbf{x}_2}{2}\right) V(\mathbf{x}_1 - \mathbf{x}_2)\right|^2, \tag{116}$$

and the probability for finding a photon in signal or idler mode

$$\begin{aligned} P(M_{1,2}) = |\langle\psi_{1,2}|\psi\rangle|^2 \propto \int d\mathbf{x}_1 \int d\mathbf{x}_2 \int d\mathbf{x}_2' M_{1,2}(\mathbf{x}_2') M_{1,2}^*(\mathbf{x}_2) \\ \times E_p^*\left(\frac{\mathbf{x}_1 + \mathbf{x}_2'}{2}\right) E_p\left(\frac{\mathbf{x}_1 + \mathbf{x}_2}{2}\right) V^*(\mathbf{x}_1 - \mathbf{x}_2') V(\mathbf{x}_1 - \mathbf{x}_2), \end{aligned} \tag{117}$$

where

$$|\psi\rangle \propto \iint d\mathbf{x}_1 d\mathbf{x}_2 E_p\left(\frac{\mathbf{x}_1 + \mathbf{x}_2}{2}\right) V(\mathbf{x}_1 - \mathbf{x}_2) \hat{a}_1^\dagger(\mathbf{x}_1) \hat{a}_2^\dagger(\mathbf{x}_2)|0\rangle \tag{118}$$

is the two-photon state generated by SPDC [60] and

$$|\psi_{1,2}\rangle = \int d\mathbf{x}_{1,2} M_{1,2}(\mathbf{x}_{1,2}) \hat{a}_{1,2}^\dagger(\mathbf{x}_{1,2})|0\rangle. \tag{119}$$

is a one-photon state of the signal or idler associated with detecting it the mode $M_{1,2}$. It is important to note that we are considering the frequency degenerate SPDC state, that is, $\omega_s = \omega_i = \omega_p/2$. In Eq. (116) $M_1^*(\mathbf{x}_1)$ and $M_2^*(\mathbf{x}_2)$ represent the phase holograms, say, to be coupled with detection system.

The expressions (116) and (117) are independent of the detectors' positions. This is because the fields whose modal expansion is made up of arbitrary weighted (HG) modes is shape-invariant [106]. In the

presence of turbulence, the shape-invariant property will no longer hold.

Then the two photon wavefunction $E_p\left((\mathbf{x}_1+\mathbf{x}_2)/2\right)V(\mathbf{x}_1-\mathbf{x}_2)$ can be taken in the far field zone to calculate the above probabilities taking the effects of turbulence into account. To calculate (116) and (117), we write the two-photon wavefunction $E_p\left((\mathbf{x}_1+\mathbf{x}_2)/2\right)V(\mathbf{x}_1-\mathbf{x}_2)$ in the form [37]

$$\frac{1}{\lambda^2 z^2}\int d\mathbf{r}'\int d\mathbf{r}''E_p\left(\frac{\mathbf{r}'+\mathbf{r}''}{2}\right)\delta(\mathbf{r}'-\mathbf{r}'')\exp\left[\frac{ik}{2z}\left[|\mathbf{x}_1-\mathbf{r}'|^2+|\mathbf{x}_2-\mathbf{r}''|^2\right]\right] \times \exp[\psi(\mathbf{x}_1,\mathbf{r}')+\psi(\mathbf{x}_2,\mathbf{r}'')], \tag{120}$$

where $\psi(\mathbf{x},\mathbf{r})$ is a random function representing phase and amplitude distortions of signal and idler fields. With the help of (197) the probability (116) takes the form

$$\begin{aligned} P(M_1,M_2) = \mathscr{C}_0\int d\mathbf{x}_1\int d\mathbf{x}_1'\int d\mathbf{x}_2\int d\mathbf{x}_2'\int d\mathbf{r}'\int d\mathbf{r}'' \\ \times M_1^*(\mathbf{x}_1)M_1(\mathbf{x}_1')M_2^*(\mathbf{x}_2)M_2(\mathbf{x}_2')E_p(\mathbf{r}')E_p^*(\mathbf{r}'') \\ \times \exp\left[\frac{ik}{2z}\left(|\mathbf{x}_1-\mathbf{r}'|^2-|\mathbf{x}_1'-\mathbf{r}''|^2+|\mathbf{x}_2-\mathbf{r}'|^2-|\mathbf{x}_2'-\mathbf{r}''|^2\right)\right] \\ \times \left\langle\exp\left[\psi(\mathbf{x}_1,\mathbf{r}')+\psi^*(\mathbf{x}_1',\mathbf{r}'')+\psi(\mathbf{x}_2,\mathbf{r}')+\psi^*(\mathbf{x}_2',\mathbf{r}'')\right]\right\rangle, \end{aligned} \tag{121}$$

where $\mathscr{C}_0 = 1/(\lambda^4 z^4)$. The integration for a Gaussian pump and Hermite-Gaussian mode functions is provided in the Appendix B. The result is

$$P(HG_{m_s n_s}, HG_{m_i n_i}) = \Pi(m_s,m_i)\Pi(n_s,n_i), \tag{122}$$

where

$$\begin{aligned} \Pi(\mu,\nu) = &\frac{1}{\lambda^2 z^2\sqrt{\pi B_1}\mu!\,\nu!\,2^{\mu+\nu}}\sum_{k_1=0}^{\mu}\sum_{l_1=0}^{\nu}\sum_{k_3=0}^{\mu}\sum_{l_3=0}^{\nu}\mathscr{F}(\mu,\nu,k_1,l_1)\mathscr{F}^*(\mu,\nu,k_3,l_3) \\ &\times\mathscr{K}(\mu+\nu-k_1-l_1,\mu+\nu-k_3-l_3), \end{aligned} \tag{123}$$

with

$$\begin{aligned} \mathscr{F}(\mu,\nu,k,l) = &\binom{\mu}{k}\binom{\nu}{l}2^{\mu+\nu}i^{k+l}\sigma(k,l)\,\Gamma\left(\frac{k+l+1}{2}\right)\left(\frac{\sqrt{2}}{W}\right)^{\mu+\nu-k-l} \\ &\times\sqrt{1-\zeta}\left(\sqrt{\zeta}\right)^{k+l}{}_2F_1\left(-k,-l;\frac{1-k-l}{2};\frac{1}{2\zeta}\right), \end{aligned} \tag{124}$$

and

$$\begin{aligned}\mathscr{K}(\mu,\nu) =& \frac{1}{4}\left(\frac{1}{\sqrt{2}}\right)^{\mu+\nu}\sum_{p=0}^{\mu}\sum_{q=0}^{\nu}\binom{\mu}{p}\binom{\nu}{q}(-1)^{\nu-q}\left(\frac{1}{\sqrt{C_1}}\right)^{2+p+q}\left(\frac{1}{\sqrt{C_2}}\right)^{\mu+\nu-p-q}\\ &\times\left\{\sigma(0,p+q)\sigma(0,\mu+\nu-p-q)\sqrt{\frac{C_1}{C_2}}\,\Gamma\left(\frac{1+p+q}{2}\right)\right.\\ &\times\Gamma\left(\frac{1+\mu+\nu-p-q}{2}\right){}_2F_1\left(\frac{1+p+q}{2};\frac{1+\mu+\nu-p-q}{2},\frac{1}{2};C_4\right)\\ &-\frac{i\sigma(1,p+q)\sigma(1,\mu+\nu-p-q)(4C_1C_2+C_3^2)}{C_2C_3(1+p+q)(1+\mu+\nu-p-q)}\Gamma\left(\frac{2+p+q}{2}\right)\\ &\times\Gamma\left(\frac{2+\mu+\nu-p-q}{2}\right){}_2F_1\left(\frac{2+p+q}{2};\frac{2+\mu+\nu-p-q}{2},-\frac{1}{2};C_4\right)\\ &+\frac{i\sigma(1,p+q)\sigma(1,\mu+\nu-p-q)[4C_1C_2+C_3^2(4+\mu+\nu)]}{C_2C_3(1+p+q)(1+\mu+\nu-p-q)}\Gamma\left(\frac{2+p+q}{2}\right)\\ &\times\left.\Gamma\left(\frac{2+\mu+\nu-p-q}{2}\right){}_2F_1\left(\frac{2+p+q}{2};\frac{2+\mu+\nu-p-q}{2},\frac{1}{2};C_4\right)\right\}.\end{aligned} \tag{125}$$

For the definitions of the other quantities in the last equations see in the Appendix B.

We see from Eq.(122) that the joint two-mode detection probability for signal and idler photons is a product of functions that mix the indices of signal and idler which means that entanglement is preserved. It should be noticed that since the two-photon wavefunction in Eq. (197) is written in the paraxial approximation and, therefore, not properly normalizable, $\sum_{m_s}\sum_{n_s}\sum_{m_i}\sum_{n_i}P(HG_{m_sn_s},HG_{m_in_i})$ does not converge to 1.

One can arrange the values of Eq.(122) in a matrix. Below we constructed the matrix for the vacuum case.

$$\begin{pmatrix}
0.3131 & 0 & 0 & 0.0399 & 0 & 0.0399 & 0 & 0 & 0 & 0\\
0 & 0.0769 & 0 & 0 & 0 & 0 & 0.0294 & 0 & 0.0098 & 0\\
0 & 0 & 0.0769 & 0 & 0 & 0 & 0 & 0.0098 & 0 & 0.0294\\
0.0398 & 0 & 0 & 0.0434 & 0 & 0.0051 & 0 & 0 & 0 & 0\\
0 & 0 & 0 & 0 & 0.0189 & 0 & 0 & 0 & 0 & 0\\
0.0398 & 0 & 0 & 0.0051 & 0 & 0.0434 & 0 & 0 & 0 & 0\\
0 & 0.0294 & 0 & 0 & 0 & 0 & 0.0302 & 0 & 0.0037 & 0\\
0 & 0 & 0.0098 & 0 & 0 & 0 & 0 & 0.0107 & 0 & 0.0037\\
0 & 0.0098 & 0 & 0 & 0 & 0 & 0.0037 & 0 & 0.0107 & 0\\
0 & 0 & 0.0294 & 0 & 0 & 0 & 0 & 0.0037 & 0 & 0.0302
\end{pmatrix}$$

The elements of the matrix have double indices $ij = m_sn_s, m_in_i$ corresponding to mode numbers of signal and idler ranging as $m_kn_k = \{00,01,10,02,11,20,03,12,21,30\}$, $k = s,i$. We note that the matrix elements satisfy conditions obtained in [109, 126]

$$\text{parity}(m_s+m_i) = \text{parity}(m_p), \quad m_s+m_i \geq m_p, \tag{126}$$

$$\text{parity}(n_s+n_i) = \text{parity}(n_p), \quad n_s+n_i \geq n_p. \tag{127}$$

The matrix for a weak turbulence $\sigma_R^2 = 0.02$ regime, $z = 5$km propagation distance, the Fresnel ratio $\lambda = 0.8\mu$m and pump's spot size at the crystal $W_0 = 10cm$ has the form

$$\begin{pmatrix}
0.2262 & 0.0157 & 0.0157 & 0.0379 & 0.0011 & 0.0379 & 0.0077 & 0.0026 & 0.0026 & 0.0077 \\
0.0157 & 0.0439 & 0.0011 & 0.0009 & 0.0030 & 0.0026 & 0.0204 & 0.0001 & 0.0073 & 0.0005 \\
0.0157 & 0.0011 & 0.0439 & 0.0026 & 0.0030 & 0.0009 & 0.0005 & 0.0073 & 0.0001 & 0.0204 \\
0.0379 & 0.0009 & 0.0026 & 0.0275 & 0.0001 & 0.0063 & 0.0005 & 0.0019 & 0.0001 & 0.0013 \\
0.0011 & 0.0030 & 0.0030 & 0.0001 & 0.0085 & 0.0001 & 0.0014 & 0.0002 & 0.0002 & 0.0014 \\
0.0379 & 0.0026 & 0.0009 & 0.0063 & 0.0001 & 0.0275 & 0.0013 & 0.0001 & 0.0019 & 0.0005 \\
0.0077 & 0.0204 & 0.0005 & 0.0005 & 0.0014 & 0.0013 & 0.0191 & 0.0001 & 0.0034 & 0.0003 \\
0.0026 & 0.0001 & 0.0073 & 0.0019 & 0.0002 & 0.0001 & 0.0001 & 0.0053 & 3\times10^{-6} & 0.0034 \\
0.0026 & 0.0073 & 0.0001 & 0.0001 & 0.0002 & 0.0019 & 0.0034 & 3\times10^{-6} & 0.0053 & 0.0001 \\
0.0077 & 0.0005 & 0.0204 & 0.0013 & 0.0014 & 0.0005 & 0.0003 & 0.0034 & 0.0001 & 0.0191
\end{pmatrix}$$

We see that all elements are different from zero: the atmosphere causes crosstalk between different modes. The variation of the first two matrix elements with the strength of turbulence is shown in Fig.5.

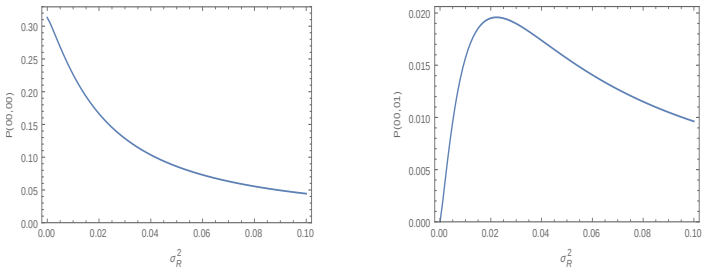

Figure 5: *The behaviour of the two-mode joint probabilities* $P(00,00)$ *ans* $P(00,01)$ *as turbulence strength increased. Because of the crosstalk between modes caused by atmosphere, the forbidden probabilities imposed by the selection-rules (126) increase. Accordingly, the allowed probabilities decrease to conserve the total probability.*

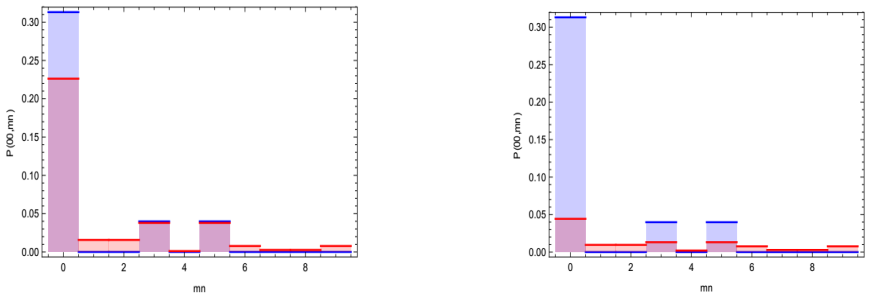

Figure 6: *The probabilities in the first lines of the matrices above are compared. On the left the comparison is made for* $\sigma_R^2 = 0,01$ *turbulence strength while on the right* $\sigma_R^2 = 0,1$.

For the first line of the matrix we compared with the vacuum case the behavior of the probabilities for two different turbulence conditions $\sigma_R^2 = 0.01$, $\sigma_R^2 = 0.1$ and same propagation distance, the Fresnel ratio and pump's spot size at the crystal as above, see Fig.6. One can see that the crosstalk between modes is not uniform: photons tend

to stay in some modes, e.g. {00,02} and {00,20}, conversely, crosstalk to some modes, e.g. {00,01}, {00,10} is more preferred than to others, e.g. {00,12} and {00,21}. Thus, in making quantum communication with Hermite-Gaussian alphabet, one has a definite choice of modes that can increase the fidelity of communication. One should also note that this is true for quite weak turbulence conditions as one can see from the right subfigure in Fig.6.

Part III

OPEN PROBLEMS FOR FUTURE CONSIDERATIONS

5

ANALYSIS OF THE SPDC WAVE PHASE CORRUPTED BY TURBULENCE

5.1 OVERVIEW.

The usual representation of optical elements by simple mathematical functions as "filter" functions in linear adaptive optics is for ideal, the so called Gaussian case. The manufactured optical elements or systems are not perfect causing wavefronts distortions when passing through such elements. If the optical elements have circular pupils the function representing the wavefront is usually expanded in Zernike polynomials to describe, and eventually to eliminate such distortions, Zernike polynomials are a set of orthogonal polynomials over a disc of unit radius and play an important role in the theory of diffraction and aberrations, beam optics, optometry, adaptive optics, etc. One of the principal uses of the Zernike polynomials is to represent fixed aberrations in an optical systems in the form of a generalized Fourier series in Zernike polynomials. The lower-order Zernike polynomials are then referred to by such names as *piston*, *tilt*, *focus*, *astigmatism*, *coma*, and so forth. They are also useful in adaptive optics systems designed for *atmospheric turbulence* decomposition [96, 97]. The approach was first used in the description of fixed aberrations where the phase was expanded using the lower-order Zernike polynomials [98].

5.2 ZERNIKE POLYNOMIALS AND FILTER FUNCTIONS

The Zernike polynomials represent a set of functions of two variables that are orthogonal over a circle with unit radius [99]. They are defined as

$$\left.\begin{array}{l} Z_i(\kappa) \\ Z_{i,\mathrm{even}}(r,\theta) = Z_{i,\mathrm{even}}[m,n] \\ Z_{i,\mathrm{odd}}(r,\theta) = Z_{i,\mathrm{odd}}[m,n] \end{array}\right\} = \sqrt{n+1} \left\{ \begin{array}{l} R_n^0(r)(m=0) \\ R_n^m(r)\sqrt{2}\cos(m\phi) \\ R_n^m(r)\sqrt{2}\sin(m\phi) \end{array}\right. ,$$

where

$$R_n^m(r) = \sum_{k=0}^{(n-|m|)/2} \frac{(-1)^k (n-k)!}{\left(\frac{n+m}{2}-k\right)!\left(\frac{n-m}{2}-k\right)!} \frac{r^{n-2k}}{k!}.$$

Lowest-order Zernike polynomials referred to as piston ($Z_1[0,0]$), tilt ($Z_2[1,1]$, $Z_3[1,1]$), (de)focus ($Z_4[0,2]$), astigmatism ($Z_5[2,2]$, $Z_6[2,2]$), coma, etc. are used to study aberrations of imaging systems. In the adaptive optics systems, the use of aperture filter functions are of particular interest in theoretical analysis of lower-order aberrations like piston and tilt. The aperture filter functions for an aperture of unit radius are defined by two-dimensional Fourier transform of the Zernike polynomials, scaled by the area of the aperture

$$G_i(\kappa,\phi) = \frac{1}{\pi}\int_0^1\int_0^{2\pi} e^{ir\kappa\cos(\theta-\phi)} Z_i(r,\theta) r d\theta dr. \tag{128}$$

To account for an aperture of diameter D, one can make a change of variable $r = 2\rho/D$ or, alternatively, replace κ with $\kappa D/2$. These filter functions are complex functions. In practice, it is often the absolute value squared of these expressions is needed, called simply the filter functions. Thus, the filter functions $F(\kappa) = |G(\kappa)|^2$ are defined by [21, Ch. 14.5.3]

$$\left.\begin{array}{l} F_i(\kappa) \\ F_{i,even}(\kappa,\phi) \\ F_{i,odd}(\kappa,\phi) \end{array}\right\} = (n+1)\left[\frac{2J_{n+1}(\kappa)}{\kappa}\right]^2 \left\{\begin{array}{l} 1(m=0) \\ 2\cos^2(m\phi) \\ 2\sin^2(m\phi) \end{array}\right.$$

Then various quantities are calculated removing the corresponding aberrations from their definitions, i.e., a term $1 - F_i$ is included in the integrals that include the power spectrum $\Phi(\kappa)$.

5.3 ABCD MATRIX FORMULATION

When optical elements such as aperture stops and lenses exist at various locations along the propagation path, the method of ABCD ray matrices can be used to characterize these elements, including the free-space propagation between elements [145]. By cascading the matrices in sequence, the entire optical path between the input and output planes can be represented by a single 2×2 matrix. The use of these ray matrices, which is based on the paraxial approximation, valid when the separation distance between optical elements is large compared with the transverse extent of the beam, greatly simplifies the treatment of propagation through several such optical elements. A configuration in which between the input and output plane there is a receiving lens is represented by a ray matrix

$$\begin{pmatrix} A & B \\ C & D \end{pmatrix} = \begin{pmatrix} 1 & L_2 \\ 0 & 1 \end{pmatrix}\begin{pmatrix} 1 & 0 \\ i\alpha_G & 1 \end{pmatrix}\begin{pmatrix} 1 & L_1 \\ 0 & 1 \end{pmatrix}$$

where L_1 is the distance between the input plane and the collecting lens, and L_2 is the distance between the collecting lens and the detector. α_G is a parameter describing the lens. For a Gaussian lens,

$\alpha_G = 2/(kW_G^2) + i/F_G$, where F_G is the real focal lenght and W_G is the effective transmission radius. An important property of all ray matrices is that $AD - BC = 1$, which is valid as long as input and output planes are in the same medium.

5.4 GENERALIZED AND EXTENDED HUYGENS-FRESNEL PRINCIPLE

Because we adopted the Huygens-Fresnel formalism for field propagation throughout this Thesis, now, with the ABCD ray matrix formalism it takes the following form [145]

$$U_0(\mathbf{r}, L) = -\frac{ik}{2\pi B}\exp(ikL)\iint_{\infty}^{\infty} d^2\mathbf{s}U_0(\mathbf{s}, 0)\exp\left[\frac{ik}{2B}(As^2 - 2\mathbf{s}\cdot\mathbf{r} + Dr^2)\right], \quad (129)$$

which is the so called *generalized* Huygens Fresnel integral. Note that when $A = D = 1$ and $B = L$, Eq.(129) reduces to the standard form of the Huygens-Fresnel integral. When fluctuating random medium is present only between the input plane and the receiving lens the quantities (31)-(33) that take care of the field's all statistical moments take the following form [82]

$$E_1(0,0;0,0) = -2\pi^2 k^2 L\int_0^{\infty} d\kappa\kappa\Phi(\kappa), \quad (130)$$

$$E_2(\mathbf{r}_1,\mathbf{r}_2;\mathbf{s}_1,\mathbf{s}_2) = 4\pi^2 k^2\int_0^L dz\int_0^{\infty} d\kappa\kappa\Phi(\kappa)\exp\left[-\frac{i\kappa^2\beta_i}{k}\right] \times J_0\left[\kappa\left|\mathrm{Re}\left(\frac{B_{0L_1}}{B}\right)\mathbf{p} + \mathrm{Re}\left(\frac{B_{L_1L}}{B}\right)\mathbf{Q} + 2i\mathrm{Im}\left(\frac{B_{0L_1}}{B}\right)\mathbf{r} + 2i\mathrm{Im}\left(\frac{B_{L_1L}}{B}\right)\mathbf{S}\right|\right], \quad (131)$$

$$E_3(\mathbf{r}_1,\mathbf{r}_2;\mathbf{s}_1,\mathbf{s}_2) = -4\pi^2 k^2\int_0^L dz\int_0^{\infty} d\kappa\kappa\Phi(\kappa)\exp\left[\frac{i\kappa^2\beta}{k}\right] J_0\left[\kappa\left|\frac{B_{0L_1}}{B}\mathbf{p} + \frac{B_{L_1L}}{B}\mathbf{Q}\right|\right], \quad (132)$$

where B_{0L_1}, B_{L_1L} and $B \equiv B_{0L}$ are the $B-$matrix elements for propagation through the system from 0 to L_1, from L_1 to L and from 0 to L, respectively. $L = L_1 + L_2$, $\beta \equiv B_{0L_1}B_{L_1L}/B$, $\beta_i = \mathrm{Im}[\beta]$, and

$$\begin{aligned} \mathbf{p} &= \mathbf{r}_1 - \mathbf{r}_2, \quad \mathbf{Q} = \mathbf{s}_1 - \mathbf{s}_2, \\ 2\mathbf{r} &= \mathbf{r}_1 + \mathbf{r}_2, \quad 2\mathbf{S} = \mathbf{s}_1 + \mathbf{s}_2. \end{aligned} \quad (133)$$

A desired aberration free quantities are calculated with the help of Eq.(130)–(132) making replacement of the power spectrum

$$\Phi(\kappa) \to \Phi(\kappa)\left[1 - \sum_i F_i(\kappa)\right], \quad (134)$$

where $F_i(\kappa)$ were introduced in the end of Section 5.2.

Now, generalizing the two photon wavefunction for ABCD matrix formalism and extended Huygens-Fresnel principle, one can write

$$A(\mathbf{r}_1,\mathbf{r}_2)\propto\int d\mathbf{s}_1\int d\mathbf{s}_2 E_p\left(\frac{\mathbf{s}_1+\mathbf{s}_2}{2}\right)V(\mathbf{s}_2-\mathbf{s}_2)\exp\left\{\psi(\mathbf{r}_1,\mathbf{s}_1;k_1)+\psi(\mathbf{r}_2,\mathbf{s}_2;k_2)\right\}$$
$$\times\exp\left\{\frac{ik_1}{2B_1}(A_1s_1^2-2\mathbf{s}_1\cdot\mathbf{r}_1+D_1r_1^2)\right\}\exp\left\{\frac{ik_2}{2B_2}(A_2s_2^2-2\mathbf{s}_2\cdot\mathbf{r}_2+D_2r_2^2)\right\}, \tag{135}$$

where $A_{1,2}$ $B_{1,2}$ $D_{1,2}$ are the ray-matrix elements for the signal and idler systems and $k_{1,2}$ - the wavenumbers of signal and idler. For the thin crystal approximation $V(\mathbf{s}_1-\mathbf{s}_2)$ can be taken as $\delta(\mathbf{s}_1-\mathbf{s}_2)$, then (135) takes the following form

$$A(\mathbf{r}_1,\mathbf{r}_2)\propto\int d\mathbf{s}E_p(\mathbf{s})\exp\left\{\frac{ik_1}{2B_1}(A_1s^2-2\mathbf{s}\cdot\mathbf{r}_1+D_1r_1^2)+\frac{ik_2}{2B_2}(A_2s^2-2\mathbf{s}\cdot\mathbf{r}_2+D_2r_2^2)\right\}$$
$$\times\exp\left\{\psi(\mathbf{r}_1,\mathbf{s};k_1)+\psi(\mathbf{r}_2,\mathbf{s};k_2)\right\}, \tag{136}$$

and for a particular case of $\mathbf{r}_1=\mathbf{r}_2=\mathbf{r}$, when the detectors are positioned in the same point, (136) becomes

$$A(\mathbf{r},\mathbf{r})\propto\int d\mathbf{s}E_p(\mathbf{s})\exp\left\{\frac{ik_1}{2B_1}(A_1s^2-2\mathbf{s}\cdot\mathbf{r}_1+D_1r_1^2)+\frac{ik_2}{2B_2}(A_2s^2-2\mathbf{s}\cdot\mathbf{r}_2+D_2r_2^2)\right\}$$
$$\times\exp\left\{\psi(\mathbf{r},\mathbf{s};k_1)+\psi(\mathbf{r},\mathbf{s};k_2)\right\}. \tag{137}$$

To simplify further we assume that the optical elements for the signal and idler are the same and positioned at the same distances from the detectors, also we consider the degenerate case, i.e. $k_1=k_2=k=k_p/2$ where k_p is the pump's wavenumber, then

$$A(\mathbf{r},\mathbf{r})\propto\int d\mathbf{s}E_p(\mathbf{s})\exp\left\{\frac{ik}{B}\left[As^2-2\mathbf{s}\cdot\mathbf{r}+Dr^2\right]\right\}\exp\left\{2\psi(\mathbf{r},\mathbf{s};k)\right\}. \tag{138}$$

The joint detection probability density function which represents the two-photon speckle is given by the modulus square of the two-photon wavefunction:

$$P_2(\mathbf{r},\mathbf{r})\propto\int d\mathbf{s}'\int d\mathbf{s}''E_p(\mathbf{s}')E_p^*(\mathbf{s}'')\left\langle\exp\left\{\psi(\mathbf{r},\mathbf{s}';k_p)+\psi^*(\mathbf{r},\mathbf{s}'';k_p)\right\}\right\rangle$$
$$\times\exp\left\{\frac{ik}{B}\left[A(s'^2-s''^2)-2(\mathbf{s}'-\mathbf{s}'')\cdot\mathbf{r}+D(r'^2-r''^2)\right]\right\}, \tag{139}$$

where in the passage from (138) to (139) we used the fact that $k_p=2k$ and $2\psi(\mathbf{r},\mathbf{s};k)=\psi(\mathbf{r},\mathbf{s};k_p)$, neglecting dispersion. The ensemble average is given by [21, Ch.7]

$$\left\langle\exp\left\{\psi(\mathbf{r},\mathbf{s}')+\psi^*(\mathbf{r},\mathbf{s}'')\right\}\right\rangle=\exp[2E_1(0,0;0,0)+E_2(\mathbf{r},\mathbf{r};\mathbf{s}',\mathbf{s}'')] \tag{140}$$

Thus, the main quantity of interest in this section is the modulus square of Eq.(135) a special case of which is Eq.(139). Care must be taken to make the replacement (134) when calculating the ensemble averages to get the desired aberration free expressions.

6

ON MEASURING TURBULENCE PARAMETERS WITH CORRELATION BEAMS

6.1 OVERVIEW.

This section is aimed to address the the inverse task as opposed to the rest of the Thesis, i.e. to deduce atmospheric parameters by detecting correlation beams. Fourth-order statistical quantities like the irradiance covariance function and the scintillation index (defined in Eqs.(147), (148)) are important quantities for determining atmospheric parameters. Knowledge of the scintillation index is crucial for determining system performance in a communication system. In particular, beam wander may be an important factor for scintillation, depending on whether or not the beam is tracked (i.e., whether beam wander is removed), and whether it is collimated or focused. From the covariance function one can deduce quantities like irradiance *correlation width* ρ_c associated with irradiance fluctuations, and the *temporal spectrum of irradiance* or *power spectral density* which is the Fourier transform of the temporal covariance function. The latter is a temporal statistical quantity for which the *Taylor frozen turbulence hypothesis* is applied that permits converting spatial statistics into temporal statistics by knowledge of the average wind speed transverse to the direction of observation. The scintillation index describes irradiance fluctuations at a single point in the receiver plane, while the covariance function of irradiance describes how the irradiance fluctuations at one point in the beam are correlated with those at another point. The covariance function is statistically inhomogeneous in that it depends on the location of the two points $\mathbf{r}_1$ and $\mathbf{r}_2$ within the beam. When $\mathbf{r}_1 = \mathbf{r}_2 = \mathbf{r}$, the covariance function reduces to the scintillation index. That is, the covariance function is a more general statistic that includes the scintillation index as a special case.

Several methods based on different types of measurements to determine the strength of turbulence (the Rytov variance, or, equivalntly, the structure constatnt) by means of optical measurements have been developed before: the scintillation index, which is the irradiance variance scaled by the square of the mean irradiance (measurable quantity), then the Rytov variance is deduced from the scintillation index.

Other methods to measure turbulence parameters are balloon-borne methods (not practical), SCIDAR, SLODAR techniques etc. [134–137].

The Rytov variance or the structure constant can be deduced from fourth order measurements (by detecting two photons at the same point in space). Better measurements can be obtained using two-photon fields having quantum properties (e.g. SPDS field) compared with classical fields second order measurements since two-photon fields can have advantage concerning the shot noise limit. This is because the fourth order correlation function for the SPDC field is proportional to modulus square of the two-photon probability amplitude (see Eq.(45)) while, for example, that of the thermal light has a dominating additional term, a product of second order correlation functions [89], which is interpreted as shot noise and which was the main difficulty in the Hanbury-Brown-Twiss experiment. Mathematically what was said is

$$\Gamma_4^{th}(\mathbf{r}_1,\mathbf{r}_1;\mathbf{r}_2,\mathbf{r}_2) = \Gamma_2(\mathbf{r}_1,\mathbf{r}_1)\Gamma_2(\mathbf{r}_2,\mathbf{r}_2) + |\Gamma_2(\mathbf{r}_1,\mathbf{r}_2)|^2, \tag{141}$$

$$\Gamma_4^{SPDC}(\mathbf{r}_1,\mathbf{r}_1;\mathbf{r}_2,\mathbf{r}_2) = |A(\mathbf{r}_1,\mathbf{r}_2)|^2. \tag{142}$$

Although $A(\mathbf{r}_1,\mathbf{r}_2)$ is not the same as $\Gamma_2(\mathbf{r}_1,\mathbf{r}_2)$ in (141), the authors of Ref.[89] showed a very close similarity between the two.

6.2 APPROACH

By considering specializations of the fourth-order field moment they can lead to the scintillation index, covariance function of irradiance, and the temporal spectrum of irradiance fluctuations. The general fourth-order cross-coherence function for a beam wave that has propagated a distance z is defined by the ensemble average

$$\Gamma_4(\mathbf{r}_1,\mathbf{r}_2,\mathbf{r}_3,\mathbf{r}_4,z) = \langle U(\mathbf{r}_1,z)U^*(\mathbf{r}_2,z)U(\mathbf{r}_3,z)U^*(\mathbf{r}_4,z)\rangle, \tag{143}$$

where $U(\mathbf{r},z)$ is the transverse profile of the electromagnetic field. In the Rytov theory, which is valid in the weak turbulence regime, the field is expressed as

$$U(\mathbf{r},z) = U_0(\mathbf{r},z)\exp[\psi(\mathbf{r},z)], \tag{144}$$

where ψ is a complex phase perturbation due to turbulence that takes the form

$$\psi(\mathbf{r},z) = \psi_1(\mathbf{r},z) + \psi_2(\mathbf{r},z) + ..., \tag{145}$$

with ψ_1 and ψ_2 being the first-order and second-order perturbations, respectively. With (144), Eq.(143) takes the form

$$\begin{aligned}\Gamma_4(\mathbf{r}_1,\mathbf{r}_2,\mathbf{r}_3,\mathbf{r}_4,z) = {} & U_0(\mathbf{r}_1,z)U_0^*(\mathbf{r}_2,z)U_0(\mathbf{r}_3,z)U_0^*(\mathbf{r}_4,z) \\ & \times \langle \exp[\psi(\mathbf{r}_1,z) + \psi^*(\mathbf{r}_2,z) + \psi(\mathbf{r}_3,z) + \psi^*(\mathbf{r}_4,z)]\rangle.\end{aligned} \tag{146}$$

The ensemble averages in (146) are usually computed using the power spectrum of index-of-refraction fluctuations. Depending on the problem type one can use different models of power spectra: Kolmogorov, Tatarskii, von Kármán, etc. [21]. In strong turbulence regime one must adopt one of the aproaches: the extended Huygens-Fresnel principle, the parabolic equation method or the asymptotic theory or the extended Rytov theory [21].

The covariance function of irradiance is defined by the normalized quantity

$$B_I(\mathbf{r}_1,\mathbf{r}_2,z)=\frac{\Gamma_4(\mathbf{r}_1,\mathbf{r}_1,\mathbf{r}_2,\mathbf{r}_2,z)-\Gamma_2(\mathbf{r}_1,\mathbf{r}_1,z)\Gamma_2(\mathbf{r}_2,\mathbf{r}_2,z)}{\Gamma_2(\mathbf{r}_1,\mathbf{r}_1,z)\Gamma_2(\mathbf{r}_2,\mathbf{r}_2,z)}, \tag{147}$$

where Γ_2 is the mutual coherence function for the optical field $U(\mathbf{r},z)$. For the cace $\mathbf{r}_1=\mathbf{r}_2=\mathbf{r}$ (147) reduces to the scintillation index

$$\sigma_I^2=\frac{\Gamma_4(\mathbf{r},\mathbf{r},\mathbf{r},\mathbf{r},z)}{[\Gamma_2(\mathbf{r},\mathbf{r},z)]^2}-1=\frac{\langle I^2(\mathbf{r},z)\rangle}{\langle I(\mathbf{r},z)\rangle^2}-1. \tag{148}$$

6.3 ZERO INNER SCALE MODEL

When the inner and outer scale effects can be ignored one can use the effective power spectrum (defined below) with $f(\kappa l_0)=g(\kappa L_0)=1$. For a special case when the inner scale of turbulent eddies is zero and the outer scale is infinite the scintillation index is given by [21, Ch. 9.4.1, 9.5.1]

$$\sigma_{I,pl}^2(z)=\exp\left[\frac{0.49\sigma_R^2}{(1+1.11\sigma_R^{12/5})^{7/6}}+\frac{0.51\sigma_R^2}{(1+0.69\sigma_R^{12/5})^{5/6}}\right]-1, \tag{149}$$

for a plane wave, and

$$\sigma_{I,sp}^2(z)=\exp\left[\frac{0.2\sigma_R^2}{(1+0.19\sigma_R^{12/5})^{7/6}}+\frac{0.2\sigma_R^2}{(1+0.23\sigma_R^{12/5})^{5/6}}\right]-1, \tag{150}$$

for a spherical wave. Both expressions are valid under all fluctuation regimes ($0\le\sigma_R^2<\infty$).

Now we are going to calculate the scintillation index and the covariance function for the two photon field from spontaneous parametric down-conversion in paraxial regime. The functions $\Gamma_2(\mathbf{r},\mathbf{r},z)$, $\Gamma_4(\mathbf{r},\mathbf{r},\mathbf{r},\mathbf{r},z)$ and $\Gamma_4(\mathbf{r}_1,\mathbf{r}_1,\mathbf{r}_2,\mathbf{r}_2,z)$ have been calculated using the extended Huygens-Fresnel principle [138]. They are given by Eqs.(64), (72) and (69)

$$\begin{aligned}\Gamma_2(\mathbf{r},\mathbf{r},z)&=\left(\frac{k}{2\pi z}\right)^2\exp\left[2\sigma_r^2-T\right]\int d\mathbf{r}'|E_p(\mathbf{r}')|^2\\&=\left(\frac{k}{2\pi z}\right)^2\exp\left[2\sigma_r^2-T\right]\times I_p|_{z=0}\\&\approx\left(\frac{k}{2\pi z}\right)^2\frac{W_{lt}^2}{W^2}\exp\left[-\frac{2r^2}{W_{lt}^2}\right],\end{aligned} \tag{151}$$

$$\Gamma_4(\mathbf{r},\mathbf{r},\mathbf{r},\mathbf{r},z)=\frac{e^{\sigma_{I,sp}^2(z)}}{2\pi W_{LT}^2}\exp\left[-\frac{2r^2}{W_{LT}^2}\right]\sum_{k=0}^{m}\sum_{l=0}^{n}\binom{m}{k}\binom{n}{l}\frac{(W/W_{LT})^{2k+2l}}{2^{k+l}k!\,l!}H_{2k}\left[\frac{\sqrt{2}}{W_{LT}}r_x\right]H_{2l}\left[\frac{\sqrt{2}}{W_{LT}}r_y\right], \tag{152}$$

and

$$\Gamma_4(\mathbf{r}_1,\mathbf{r}_1,\mathbf{r}_2,\mathbf{r}_2,z) = \frac{e^{-2r^2/W_{LT1}^2}}{2\pi W_{LT1}^2}\exp\left[\left(\frac{1.58\sigma_{R,p}^2}{\Lambda_p W^2}-\frac{2}{3\rho_{pl}^2}\right)p^2 - 0.043\pi^2 C_n^2 z^3 p^{-7/3}\right]$$
$$\times\sum_{k=0}^{m}\sum_{l=0}^{n}\binom{m}{k}\binom{n}{l}\frac{(W/W_{LT1})^{2k+2l}}{2^{k+l}k!\,l!}H_{2k}\left[\frac{\sqrt{2}}{W_{LT1}}\left(\frac{r_{x2}+r_{x1}}{2}\right)\right]H_{2l}\left[\frac{\sqrt{2}}{W_{LT1}}\left(\frac{r_{y1}+r_{y2}}{2}\right)\right], \tag{153}$$

where

$$\begin{aligned} W_{lt} &\equiv W_p\sqrt{1+T} = W_p\sqrt{1+1.33\sigma_R^2\Lambda^{5/6}},\\ W_{LT} &\equiv W\sqrt{1+6.32\sigma_{R,p}^2\Lambda},\\ W_{LT1} &\equiv W\sqrt{1+6.32\sigma_{R,p}^2\Lambda+4\Lambda^2W^2/(3\rho_{pl}^2)}. \end{aligned} \tag{154}$$

In the three Eqs. above E_p is the pump's field profile at the nonlinear crystal, k_p is the pump's wavenumber, D_{sp} is the wave structure function, $\rho_{pl} = (1.45C_n^2k^2z)^{-3/5}$ is the coherence radius for the plane wave, $\sigma_{R,p}^2 = 1.23C_n^2k_p^{7/6}z^{11/6}$ is the Rytov variance for the pump, σ_r^2 describes the atmospherically induced change in the mean intensity profile in the transverse direction, and T describes the change in the on-axis mean intensity at the receiver plane caused by turbulence, $\Lambda_{0,p} = 2z/(k_pW_0^2)$ is the pump's input beam parameter, $2\mathbf{s} = \mathbf{r}'+\mathbf{r}''$, $\mathbf{Q} = \mathbf{r}'-\mathbf{r}''$, $2\mathbf{r} = \mathbf{r}_1+\mathbf{r}_2$, and $p = |\mathbf{r}_1-\mathbf{r}_2|$. For the case of Eq.(152) it readily follows

$$\begin{aligned} \sigma_{I,sp}^2 &= 1.83788 + 2\ln[W_{LT}] + \ln[\Gamma_4^{00}(\mathbf{r},\mathbf{r},\mathbf{r},\mathbf{r},z)] + \frac{2r^2}{W_{LT}^2},\\ &= 1.83788 + 2\ln[W] + \ln[\Gamma_4^{00}(\mathbf{r},\mathbf{r},\mathbf{r},\mathbf{r},z)]\\ &\quad + \ln[1+6.32\sigma_{R,p}^2\Lambda] + \frac{2r^2}{W^2(1+6.32\sigma_{R,p}^2\Lambda)},\\ W_{LT} &= W\sqrt{1+6.32\sigma_{R,p}^2\Lambda}, \end{aligned} \tag{155}$$

where $\Gamma_4^{00}(\mathbf{r},\mathbf{r},\mathbf{r},\mathbf{r},z)$ stands for the case when the pump is a TEM_{00} mode. Considering the definition (148), Eq.(155) connects the measurable quantities $\Gamma_4^{00}(\mathbf{r},\mathbf{r},\mathbf{r},\mathbf{r},z)$ and $\Gamma_2(\mathbf{r},\mathbf{r},z)$ with the strength of turbulence $\sigma_{R,p}^2$

$$\begin{aligned} \ln[1+6.32\sigma_{R,p}^2\Lambda] + \frac{2r^2}{W^2(1+6.32\sigma_{R,p}^2\Lambda)} &= \ln[1.84W^2] + \ln[\Gamma_4^{00}(\mathbf{r},\mathbf{r},\mathbf{r},\mathbf{r},z)]\\ &\quad - \frac{\Gamma_4^{00}(\mathbf{r},\mathbf{r},\mathbf{r},\mathbf{r},z)}{[\Gamma_2(\mathbf{r},\mathbf{r},z)]^2} + 1. \end{aligned} \tag{156}$$

When the detectors are on the optical axis ($r = 0$), one deduces from (156) that

$$\sigma_{R,p}^2 = \frac{1.84W^2\Gamma_4^{00}(0,0,0,0,z)\exp\left[1-\Gamma_4^{00}(0,0,0,0,z)/[\Gamma_2(0,0,z)]^2\right]-1}{6.32\Lambda}. \tag{157}$$

Thus, by measuring single and coincident counts one can deduce the Rytov variance which is a measure of the strength of turbulence.

The presence of a finite inner scale generally has a strong effect on the scintillation index, particularly under weak-to-moderate irradiance fluctuations. For example, a finite inner scale based on the modified atmospheric spectrum leads to a corresponding bump in the scintillation index for certain values of the nondimensional parameter $Q_l = 10.89L/kl_0^2$ as compared with the traditional Tatarskii spectrum. Inner scale plays a significant role in the scintillation index under weak fluctuations, but outer scale effects are insignificant for infinite plane waves and spherical waves in this regime.

6.4.1 *Inner Scale Effects: Strong Fluctuation Regime*

Scintillation theory that is valid from weak fluctuations through strong fluctuations, including deep saturation regime are reported in [139–143]. Experimental data reveal that the scintillation index σ_I^2 increases initially within the regime of weak irradiance fluctuations with increasing values of the Rytov variance $\sigma_R^2 = 1.23C_n^2k^{7/6}z^{11/6}$, where C_n^2 is the refractive index structure constant. It then increases beyond unity and reaches its maximum value in the so-called focusing regime (possibly becoming as large as 5 or 6). With increasing path length, or increasing C_n^2, the focusing effect is weakened by the loss of spatial coherence and the scintillation index gradually decreases toward a value of unity as the Rytov variance increases without bound.

The conventional Rytov approximation is limited to weak fluctuation conditions in describing optical scintillation because it does not account for the role of the decreasing transverse spatial coherence radius of the propagating wave. A model for irradiance fluctuations that is applicable in moderate-to-strong fluctuation regimes is a modification of the Rytov method called the extended Rytov theory [21]. Another model that is valid for both the weak and strong fluctuation regimes is the so called *asymptotic theory* [72–76].

6.4.2 *Inner and Outer Scale Effects*

To take inner and outer scale effects into account, a specific power spectrum model is used, from which one can deduce large-scale and small-scale scintillation. The power spectrum mentioned above is the so called *effective atmospheric spectrum*

$$\Phi_e(\kappa) = \Phi(\kappa)G(\kappa, l_0, L_0) = 0.033C_n^2\kappa^{-11/3}G(\kappa, l_0, L_0), \tag{158}$$

where l_0 is the inner scale, L_0 is the outer scale, and $G(\kappa, l_0, L_0)$ is an *amplitude spatial filter*. The role of $G(\kappa, l_0, L_0)$ is to eliminate the ineffective scale sizes on scintillation under strong fluctuation conditions. It only permits low-pass ($\kappa < \kappa_X$) and high-pass ($\kappa > \kappa_Y$) frequencies at a given

propagation distance z. For horizontal paths C_n^2 is essentially constant, the spatial filter is given by [21]

$$G(\kappa, l_0, L_0) = f(\kappa l_0) g(\kappa L_0) \exp\left(-\frac{\kappa^2}{\kappa_X^2}\right) + \frac{\kappa^{11/3}}{(\kappa^2 + \kappa_Y^2)^{11/6}}, \tag{159}$$

where κ_X is a large-scale (or refractive) spatial frequency cutoff, κ_Y is a small-scale (or diffractive) spatial spatial frequency cutoff, $f(\kappa l_0)$ and $g(\kappa L_0)$ are factors that describe inner and outer scale modifications of the basic Kolmogorov power law, respectively. $f(\kappa l_0)$ and $g(\kappa L_0)$ are assumed to have following forms

$$f(\kappa l_0) = \exp\left(-\kappa^2/\kappa_l^2\right)\left[1 + 1.802(\kappa/\kappa_l) - 0.254(\kappa/\kappa_l)^{7/6}\right], \tag{160}$$

$$g(\kappa L_0) = 1 - \exp\left(-\kappa^2/\kappa_0^2\right), \tag{161}$$

where

$$\kappa_l = 3.3/l_0, \qquad \kappa_0 = 8\pi/L_0.$$

$$\therefore$$

To this point we have sketched a possible approach to solve the current problem. Thereof, it remains as an open problem to be considered in the future.

A

HG AND LG BEAMS

A.1 OVERVIEW.

In this Appendix we want to briefly examine other beam shapes that may have important propagation characteristics for certain applications. For our applications it is sufficient to use the scalar theory and the paraxial approximation. The basic beam characteristics at the transmitter ($z = 0$) are its wave number $k = 2\pi/\lambda$ (where λ is wavelength), spot size radius W_0 and phase front radius of curvature F_0.

By studying the lowest-order Gaussian-beam wave, it is easy to deduce results for the plane wave and spherical wave limits by simply specifying certain values of the Gaussian-beam parameters. However, there are other types of beams that are used in some applications, but their properties in atmospheric turbulence are not well known. These other beams include higher-order Hermite and Laguerre Gaussian beams, super Gaussian beams, flattened Gaussian profiles, and Bessel beams. Here we wish to examine higher-order Hermite and Laguerre Gaussian beam shapes .

A.2 HIGHER-ORDER GAUSSIAN BEAMS.

In certain applications it may be advantageous to use other beams such as higher-order Gaussian beams, among other shapes. Some investigators have discussed the general propagation characteristics of these higher-order Gaussian beams in free space [144], [145].

HERMITE-GAUSSIAN BEAMS. The higher-order Hermite-Gaussian modes TEM_{mn} of a collimated beam at the exit aperture $z = 0$ of a laser are described by

$$U_{mn}(x, y, 0) = H_m\left(\frac{\sqrt{2}x}{W_{x,0}}\right) H_n\left(\frac{\sqrt{2}y}{W_{y,0}}\right) \exp\left(-\frac{x^2}{W_{x,0}^2} - \frac{y^2}{W_{y,0}^2}\right) \tag{162}$$

where $m, n = 0, 1, 2, \ldots$, the TEM_{00} spot size along the x and y axes at the transmitter is given by $W_{x,0}$ and $W_{y,0}$, respectively, and $H_n(x)$ is the nth Hermite polynomial. However, the higher-order modes always form a pattern of spots or the intensity rather than a single spot as exhibited by the TEM_{00} mode. Note also that the intensity pattern of any

given TEM_{nm} mode changes size but not shape as it propagates forward in z – a given TEM_{nm} mode looks exactly the same, except for scaling, at every point along the z axis.

To find the field of a Hermite-Gaussian beam at distance z from the transmitter is to use the Huygens-Fresnel integral which yields

$$\begin{aligned} U_{mn}(x,y,z) = \frac{\exp(ikz)}{\sqrt{p_x(z)p_y(z)}} H_m\left(\frac{\sqrt{2}x}{W_x}\right) H_n\left(\frac{\sqrt{2}y}{W_y}\right) \exp[i\phi_m(z) - i\phi_n(z)] \\ \times \exp\left(-\frac{x^2}{W_x^2} - \frac{y^2}{W_y^2} - i\frac{kx^2}{2F_x} - i\frac{ky^2}{2F_y}\right), \quad m,n = 0,1,2,... \end{aligned} \tag{163}$$

where $W_{x,y}$ and $F_{x,y}$ are the spot size and phase front radius of curvature of the lowest-order Gaussian-beam wave in x and y directions, and $p_s(z) = 1 - z/F_{0s} + 2iz/(kW_{0s}^2)$. However, because higher-order beams always form a pattern of spots, rather than a single spot of light, we need a new definition of spot size of these higher-order modes. The spot size of the pth mode is defined by [147]

$$\sigma_{s,p}^2(z) = \frac{4\int\int_{\infty}^{-\infty} s^2 I_{m,n}(x,y,z)dxdy}{\int\int_{\infty}^{-\infty} I_{m,n}(x,y,z)dxdy} \tag{164}$$

where s represents either x or y and p denotes either m or n. The irradiance of the Hermite-Gaussian beam is given by

$$\begin{aligned} I_{mn}(x,y,z) = \frac{W_{x,0}W_{y,0}}{W_xW_y} H_m^2\left(\frac{\sqrt{2}x}{W_x}\right) H_n^2\left(\frac{\sqrt{2}y}{W_y}\right) \exp\left(-\frac{x^2}{W_x^2} - \frac{y^2}{W_y^2}\right) \\ m,n = 0,1,2,... \end{aligned} \tag{165}$$

By substituting (55) into (54), we find that the "effective spot size" is given by the rectangular domain $\sigma_{x,m}(z), \times\sigma_{y,n}(z)$, where

$$\begin{aligned} \sigma_{x,m}(z) &= \sqrt{2m+1}W_x(z), \qquad m = 0,1,2,... \\ \sigma_{y,n}(z) &= \sqrt{2n+1}W_y(z), \qquad n = 0,1,2,... \end{aligned} \tag{166}$$

LAGUERRE-GAUSSIAN BEAMS. By assuming cylindrical symmetry, higher-order modes of a collimated beam at the exit aperture $(z = 0)$ of a laser can be described in cylindrical coordinates (r,θ,z) by

$$U_{pl}^{LG}(r,\theta,0) = C(l,p)\left(\frac{\sqrt{2}r}{W_0}\right)^{|l|} \exp(il\theta)\exp\left(-\frac{r^2}{W_0^2}\right) L_l^{|l|}\left(\frac{2r^2}{W_0^2}\right), \tag{167}$$

where $C(l,p) = \sqrt{\frac{2p!}{\pi(|l|+p)!}}$ is the normalization factor, r is the modulus of a vector in the transverse plane at angle θ, W_0 is the radius of the TEM_{00} mode beam, $L_p^{|l|}(x)$ is the *associated Laguerre polynomial*, and l and m are the radial and angular mode numbers. The field described by (60) is called a *Laguerre-Gaussian beam*. By using the Huygens-Fresnel integral, it can be shown that the field of the Laguerre-Gaussian beam at distance z from the transmitter is given by

$$\begin{aligned} U_{pl}^{LG}(r,\theta,z) = \sqrt{\frac{2p!}{\pi(|l|+p)!}} \frac{W_0}{W(z)} \left(\frac{\sqrt{2}r}{W(z)}\right)^{|l|} L_p^{|l|}\left(\frac{2r^2}{W^2(z)}\right) e^{il\theta} \\ \times \exp[i(2p+|l|+1)\phi(z)] \exp\left(ikz - \frac{r^2}{W^2(z)} + i\frac{kr^2}{2F(z)}\right) \\ l,p = 0,1,2,... \end{aligned} \tag{168}$$

where W and F denote the spot size and phase front radius of curvature for a TEM_{00} beam. When $l \neq 0$, because of their azimuthal dependence $e^{il\theta}$, they have a helicoidal wavefront around the z-axis. This implies that these modes carry an orbital angular momentum proportional to the integer l.

The irradiance is

$$I(r,\theta,z) = \frac{2p!}{\pi(|l|+p)!}\frac{W_0^2}{W^2}\left(\frac{2r^2}{W^2}\right)^l \left[L_p^{|l|}\left(\frac{2r^2}{W^2}\right)\right]^2 \exp\left(-\frac{2r^2}{W^2}\right) \tag{169}$$

The spot pattern for Laguerre-Gaussian functions consists of multiple rings. Similar to the Hermite-Gaussian case, the spot size associated with a Laguerre-Gaussian beam can be defined by

$$\sigma_{l,p}(z) = \sqrt{2p+|l|+1}W(z); \qquad p,l = 0,1,2,... \tag{170}$$

The significance of this definition for spot size and that in (166) is that the spot size so defined contains all the irradiance maxima of the various polynomials.

A.3 GENERATION OF LG BEAMS WITH Q-PLATES

An electromagnetic field can have a definite orbital angular momentum (OAM) in the paraxial approximation when one uses Laguerre-Gauss modes to decompose the orbital angular momentum operator [52]. The orbital angular momentum is defined by the phase structure of the complex electric field [146, 148]. OAM is associated with the possibility of having a helical shape of the beam wavefront [149] and may take any of the infinite values $m = 0, \pm 1, \pm 2, ...$ It must be emphasized that this angular momentum, although labelled orbital, is still an "internal" kind of angular momentum according to the standard mechanical definition, i.e. its value is fully independent of the choice of the origin.

To generate and manipulate orbital angular momentum, tools have been developed, including pitchfork holograms [150], spiral phase plates [151, 152], Dove prisms eventually inserted in interferometers, [153] and cylindrical lens mode converters [91]. These devices and techniques have limitations in terms of efficiency, modulation speed, working wavelength, alignment, and constraints imposed on the input and output beams.

Another optical device for OAM manipulation has been introduced by [93, 154]. It is called a "q-plate", made from a birefringent liquid crystal plate having an azimuthal distribution of the local optical axis in the transverse plane.

Consider a planar liquid crystal cell having a thickness and material birefringence chosen so as to induce a homogeneous phase retardation of $\delta = \pi$ (corresponding to half-wave), at the working wavelength λ, for light propagation perpendicular to the cell plane walls (z

axis). Also consider a specific pattern geometry, given by the following law:

$$\alpha(r, \phi) = \alpha_0 + q\phi, \tag{171}$$

where α and ϕ are constants. This equation implies a presence of a topological defect in the medium localized at the cell center, i.e., at $r = 0$. A topological defect occurs where different regions, here $r = 0$ and $r > 0$ regions, come into contact with each other. It is formed because of symmetry breakdown at the center. If q is an integer or a semi-integer there will be no discontinuity line in the cell. Liquid-crystal cells having the above specified geometry are referred as q-plates (QP).

Suppose we have an input circularly polarized plane wave, described by the Jones electric-field vector [155, 156]

$$\mathbf{E}_{in}(x, y) = E_0 \begin{pmatrix} 1 \\ \pm i \end{pmatrix}, \tag{172}$$

where the $+$ is for the left-circular case and $-$ for the right-circular one. The Jones matrix $\mathbf{M}$ describing the cell action on the field at each transverse position x, y is the following:

$$\mathbf{M}(x, y) = \begin{pmatrix} \cos 2\alpha(x, y) & \sin 2\alpha(x, y) \\ \cos 2\alpha(x, y) & -\sin 2\alpha(x, y) \end{pmatrix}. \tag{173}$$

By the action of the cell into the following field (up to an overall phase):

$$\mathbf{E}_{out}(x, y) = \mathbf{M}(x, y)\mathbf{E}_{in}(x, y) = E_0 e^{\pm 2i\alpha(x,y)} \begin{pmatrix} 1 \\ \mp i \end{pmatrix}. \tag{174}$$

We see that the output wave is polarized with the opposite handedness. This is expected, as any half-wave plate inverts the handedness of circular polarization and the output field wavefront has acquired a nonuniform phase retardation $\pm 2\alpha(x, y)$. For the particular choice (65) for $\alpha(x, y)$, (68) takes the form

$$\mathbf{E}_{out}(x, y) = E_0 e^{\pm 2iq\phi \pm 2i\alpha_0} \begin{pmatrix} 1 \\ \mp i \end{pmatrix}. \tag{175}$$

This output field corresponds to a helical mode with helicity number

$$m = \pm 2q. \tag{176}$$

In other words the output wavefront is helical and the sign of the helicity is controlled by the input polarization handedness. The helicity magnitude $|m|$ is instead fixed by the LC cell geometry, via its characteristic integer or semi-integer parameter q. The $q = 1$ geometry presents a particular property: it is rotationally symmetric

around the coordinate origin. Thus, a left circularly polarized ($+\hbar$ spin angular momentum) incident wave having no orbital angular momentum will emerge from the q-plate as right circularly polarized ($-\hbar$ spin angular momentum) having helical wavefront with $m = 2q$. The total angular momentum is therefore $(2q-1)\hbar$ and the variation $\Delta J_z = (2q-1)\hbar - \hbar = 2(q-1)\hbar$ must be exchanged with the medium, i.e. with the q-plate.

The case $q = 1$ leads to a special result: the photon after the q-plate does not change its total angular momentum, and therefore no torque is generated on the medium. However, the spin and orbital angular momenta of the photon are both varied in the q-plate: the spin switches sign, passing from $+\hbar$ to $-\hbar$, while the orbital angular momentum passes from zero to $2\hbar$. The two variations exactly cancel each other. This phenomenon in which angular momentum of light changes its nature, exploiting the interaction with the medium but remaining entirely within the optical field, was called "spin-to-orbital angular momentum conversion" [93].

For the case $\delta \neq \pi$ the q-plate transformation is the following (in ket notation):

$$|\psi\rangle_{in} = |\pm 1, m\rangle \longrightarrow |\psi\rangle_{out} = \cos\frac{\delta}{2}|\pm 1, m\rangle + i\sin\frac{\delta}{2}e^{\pm 2i\alpha_0}|\mp 1, m \pm 2q\rangle. \tag{177}$$

The final state is the superposition of a "unmodified" photon and a "converted" photon states. In both states of the superposition the overall photon angular momentum is conserved, although the angular momentum conversion in the photon occurs only with a finite probability, given by $\sin^2\delta/2$.

One can also use an equivalent description of QP in terms of effective Hamiltonian. One writes the bosonic operator $a_{\sigma,l}$, where σ stands for the polarization (left- or right-circular) and l for the orbital angular momentum. Then for integer values of $2q$ the effective Hamiltonian has the form

$$H = \sum \left(c_{Ll} a^\dagger_{Ll} a_{Rl+2q} + c_{Rl} a^\dagger_{Rl} a_{Ll-2q} + H.C. \right), \qquad 2q = \text{integer}. \tag{178}$$

The coefficients c can be fixed from the Jones matrix (173). This Hamiltonian is especially useful in studying the transformation of nonclassical fields by systems having spin-orbit coupling.

B

SOME DERIVATIONS

B.1 EVALUATION OF THE INTEGRAL IN (59):

$$I = 4\pi^2 z^3 \int_0^1 d\xi \int_0^\infty d\kappa \kappa^5 \Phi(\kappa) J_0(\kappa\xi p)\xi^2(1-\xi)^2. \tag{179}$$

Using Tatarskii spectrum (13)

$$\Phi(\kappa) = 0.033 C_n^2 \kappa^{-11/3} \exp\left(-\frac{\kappa^2}{\kappa_m^2}\right), \tag{180}$$

we have

$$\int_0^\infty \kappa^{4/3} \exp\left[-\frac{\kappa^2}{\kappa_m^2}\right] J_0(\kappa\xi p) d\kappa = 0.033 C_n^2 \frac{\Gamma(7/6)\kappa^{7/3}}{2} {}_1F_1\left(\frac{7}{6}; 1; -\frac{\xi^2 p^2 \kappa_m^2}{4}\right), \tag{181}$$

where we used the integral 14 of [21, Appendix II]. ${}_1F_1(a;c;-z)$ is the Confluent Hypergeometric Function.

Now, using the asymptotic form of the Hypergeometric Function for the case $\mathrm{Re}(z) \gg 1$, viz.,

$${}_1F_1(a;c;-z) \sim \frac{\Gamma(c)}{\Gamma(c-a)} z^{-a}, \qquad \mathrm{Re}(z) \gg 1,$$

we can simplify (181) further:

$$\begin{aligned} \int_0^\infty \kappa^{4/3} \exp\left[-\frac{\kappa^2}{\kappa_m^2}\right] J_0(\kappa\xi p) d\kappa &\approx 0.033 C_n^2 \frac{\Gamma(7/6)}{2\Gamma(1-7/6)} \left(\frac{\xi^2 p^2}{4}\right)^{-7/6} \\ &\approx -0.016 C_n^2 \xi^{-7/3} p^{-7/3}. \end{aligned} \tag{182}$$

This approximation is valid since $\xi^2 p^2 \kappa_m^2/4 \gg 1$ for the following reasons: ξ is a variable that changes between 0 and 1, p is the distance between the detectors, so it can be chosen appropriately and finally and most importantly, $\kappa_m \equiv 5.29/l_0 \gg 1$ for the inner scale l_0 is a small quantity.

Finally, Eq.(179) takes the form

$$I = -0.046\pi^2 z^3 C_n^2 p^{-7/3} \int_0^1 \xi^{-1/3}(1-\xi)^2 d\xi = -0.043\pi^2 z^3 C_n^2 p^{-7/3}. \tag{183}$$

$$
\begin{aligned}
P_2(x,x) = \frac{k^2 e^{-\sigma_{sp}^2(z)}}{4\pi^2 z^2} \iint d\mathbf{S} d\mathbf{Q} H_m \left[\frac{\sqrt{2}}{W_0}\left(S_x + \frac{Q_x}{2}\right)\right] H_m \left[\frac{\sqrt{2}}{W_0}\left(S_x - \frac{Q_x}{2}\right)\right] \\
\times H_n \left[\frac{\sqrt{2}}{W_0}\left(S_y + \frac{Q_y}{2}\right)\right] H_n \left[\frac{\sqrt{2}}{W_0}\left(S_y - \frac{Q_y}{2}\right)\right] \\
\times \exp\left[-\frac{2}{W_0^2}\left(S_x^2 + S_y^2\right)\right] \exp\left[-\frac{1}{2W_0^2}\left(Q_x^2 + Q_y^2\right)\right] \\
\times \exp\left[\frac{ik_p}{z}\left(S_x Q_x + S_y Q_y\right)\right] \exp\left[-\frac{ik_p}{z}\left(r_x Q_x + r_y Q_y\right)\right] \\
\times \exp\left[-\frac{3.16\sigma_{R,p}^2}{\Lambda_{0,p} W_0^2}\left(Q_x^2 + Q_y^2\right)\right].
\end{aligned} \tag{184}
$$

All the integrals' limits are $\pm\infty$ unless stated otherwise.

INTEGRATION IN S_x AND S_y VARIABLES. Separating the s_x integral and calling it I_x we have

$$
I_x = \int dS_x H_m \left[\frac{\sqrt{2}}{W_0}\left(S_x + \frac{Q_x}{2}\right)\right] H_m \left[\frac{\sqrt{2}}{W_0}\left(S_x - \frac{Q_x}{2}\right)\right] \exp\left[-\left(\frac{2}{W_0^2}S_x^2 - \frac{ik_p Q_x}{z}S_x\right)\right]. \tag{185}
$$

The expression in the exponent can be written as

$$
\frac{2}{W_0^2}S_x^2 - \frac{ik_p Q_x}{z}S_x = \left(\frac{\sqrt{2}}{W_0}S_x - \frac{ik_p W_0}{2\sqrt{2}z}Q_x\right)^2 + \frac{k_p^2 Q_x^2 W_0^2}{8z^2}.
$$

We define $\xi = \frac{\sqrt{2}}{W_0}S_x - \frac{ik_p W_0}{2\sqrt{2}z}Q_x$ so that $dS_x = \frac{W_0}{\sqrt{2}}d\xi$ and

$$
\frac{\sqrt{2}}{W_0}\left(S_x \pm \frac{Q_x}{2}\right) = \xi + \frac{Q_x}{\sqrt{2}W_0}\left(i\frac{k_p W_0^2}{2z} \pm 1\right).
$$

Now I_x looks like

$$
I_x = \frac{W_0}{\sqrt{2}} \exp\left[-\frac{1}{2}\left(\frac{k_p Q_x W_0}{2z}\right)^2\right] \int d\xi H_m\left[\xi + \eta\right] H_m\left[\xi + \zeta\right] e^{-\xi^2}, \tag{186}
$$

where we also defined $\eta = \frac{Q_x}{\sqrt{2}W_0}\left(i\frac{k_p W_0^2}{2z} + 1\right)$ and $\zeta = \frac{Q_x}{\sqrt{2}W_0}\left(i\frac{k_p W_0^2}{2z} - 1\right)$. Using [127, formula 7.377], viz.,

$$
\int d\xi H_m\left[\xi + \eta\right] H_n\left[\xi + \zeta\right] e^{-\xi^2} = 2^n \sqrt{\pi} m!\, \zeta^{n-m} L_m^{n-m}(-2\eta\zeta), \qquad [m \le n],
$$

where L_m^α are the generalized Laguerre polynomials, $L_m^0 \equiv L_m$, one arrives at

$$
I_x = \frac{W_0}{\sqrt{2}} \exp\left[-\frac{1}{2}\left(\frac{k_p Q_x W_0}{2z}\right)^2\right] 2^m \sqrt{\pi} m!\, L_m\left[\left(\frac{1}{W_0^2} + \left(\frac{k_p W_0}{2z}\right)^2\right) Q_x^2\right]. \tag{187}
$$

Similar steps bring us to the expression for I_y, viz.,

$$
I_y = \frac{W_0}{\sqrt{2}} \exp\left[-\frac{1}{2}\left(\frac{k_p Q_y W_0}{2z}\right)^2\right] 2^n \sqrt{\pi} n!\, L_n\left[\left(\frac{1}{W_0^2} + \left(\frac{k_p W_0}{2z}\right)^2\right) Q_y^2\right]. \tag{188}
$$

Now (184) has the form (note that the coefficients exactly cancel $B_{m,n}^2$)

$$
\begin{aligned}
P_2(x,x) = \frac{k^2 e^{-\sigma_{sp}^2(z)}}{4\pi^2 z^2} \iint dQ_x dQ_y L_m(\alpha Q_x^2) L_n(\alpha Q_y^2) \exp[-\beta(Q_x^2 + Q_y^2)] \\
\times \exp\left[-\frac{ik_p}{z}(r_x Q_x + r_y Q_y)\right],
\end{aligned} \tag{189}
$$

where we defined

$$\alpha \equiv \frac{1}{W_0^2} + \left(\frac{k_p W_0}{2z}\right)^2,$$
$$\beta \equiv \frac{3.16\sigma_{R,p}^2}{\Lambda_{0,p} W_0^2} + \frac{1}{2W_0^2} + \frac{1}{2}\left(\frac{k_p W_0}{2z}\right)^2 = \frac{3.16\sigma_{R,p}^2}{\Lambda_{0,p} W_0^2} + \frac{\alpha}{2}.$$

INTEGRATION IN Q_x AND Q_y VARIABLES. The integral in Q_x, which we call J_x, is the following

$$\begin{aligned} J_x &= \int dQ_x L_m[\alpha Q_x^2] \exp\left[-\left(\beta Q_x^2 + \frac{ik_p r_x}{z} Q_x\right)\right] \\ &= \exp\left[-\frac{1}{\beta}\left(\frac{k_p r_x}{2z}\right)^2\right] \int dQ_x L_m[\alpha Q_x^2] \exp\left[-\left(\sqrt{\beta} Q_x + \frac{ik_p r_x}{2\sqrt{\beta} z}\right)^2\right]. \end{aligned} \tag{190}$$

Changing the variables

$$\xi \equiv \sqrt{\beta} Q_x, \qquad \eta \equiv -\frac{ik_p r_x}{2\sqrt{\beta} z}$$

we have

$$J_x = \frac{1}{\sqrt{\beta}} \exp\left[-\frac{1}{\beta}\left(\frac{k_p r_x}{2z}\right)^2\right] \int d\xi L_m\left(\frac{\alpha}{\beta}\xi^2\right) e^{-(\xi-\eta)^2}. \tag{191}$$

Now we use the series representation of the Laguerre polynomial [128]

$$L_m(x) = \sum_{k=0}^{m} \binom{m}{k} \frac{(-1)^k}{k!} x^k,$$

to write the above integral as

$$J_x = \frac{1}{\sqrt{\beta}} \exp\left[-\frac{1}{\beta}\left(\frac{k_p r_x}{2z}\right)^2\right] \sum_{k=0}^{m} \binom{m}{k} \frac{(-1)^k}{k!} \left(\frac{\alpha}{\beta}\right)^k \int d\xi e^{-(\xi-\eta)^2} \xi^{2k}. \tag{192}$$

Using formula $3.462-4$ of Ref. [127],

$$\int dx e^{-(x-y)^2} x^n = (2i)^{-n} \sqrt{\pi} H_n(iy),$$

we arrive at

$$J_x = \frac{1}{\sqrt{\beta}} \exp\left[-\frac{1}{\beta}\left(\frac{k_p r_x}{2z}\right)^2\right] \sum_{k=0}^{m} \binom{m}{k} \frac{(-1)^k}{k!\,(2i)^{2k}} \left(\frac{\alpha}{\beta}\right)^k H_{2k}\left[\frac{k_p r_x}{2\sqrt{\beta} z}\right]. \tag{193}$$

Integration in Q_y brings us to a similar expression,

$$J_y = \frac{1}{\sqrt{\beta}} \exp\left[-\frac{1}{\beta}\left(\frac{k_p r_x}{2z}\right)^2\right] \sum_{l=0}^{n} \binom{n}{l} \frac{(-1)^l}{l!\,(2i)^{2l}} \left(\frac{\alpha}{\beta}\right)^l H_{2l}\left[\frac{k_p r_x}{2\sqrt{\beta} z}\right]. \tag{194}$$

Finally, Eq.(189) takes the following form

$$P_2(x,x) = \frac{k^2 e^{-\sigma_{sp}^2(z)}}{4\pi z^2 \beta} \exp\left[-\frac{1}{\beta}\left(\frac{k_p r}{2z}\right)^2\right] \sum_{k=0}^{m}\sum_{l=0}^{n} \binom{m}{k}\binom{n}{l} \frac{(\alpha/\beta)^{k+l}}{k!\,l!\,2^{2k+2l}} H_{2k}\left[\frac{k_p r_x}{2\sqrt{\beta} z}\right] H_{2l}\left[\frac{k_p r_x}{2\sqrt{\beta} z}\right]. \tag{195}$$

One can write this expression in terms of output pump-beam parameters. To do so, notice that

$$W = W_0\sqrt{1+\Lambda_{0,p}^2} = W_0\Lambda_{0,p}\sqrt{1+\frac{1}{\Lambda_{0,p}^2}} = \frac{2z}{k_p W_0}\sqrt{1+\frac{1}{\Lambda_{0,p}^2}},$$

where we used Eqs.(37) and (38) with $\Theta_0 = 1$ for a collimated beam,

$$\alpha = \frac{1}{W_0^2}\left(1+\frac{1}{\Lambda_0^2}\right) = \frac{W^2k_p^2}{4z^2}, \qquad \beta = \frac{3.16\sigma_{R,p}^2}{\Lambda_{0,p}W_0^2} + \frac{\alpha}{2} = \frac{3.16\sigma_{R,p}^2}{\Lambda_p W^2} + \frac{W^2k_p^2}{8z^2},$$

$$\frac{k_p}{2\sqrt{\beta}z} = \frac{k_p}{2z\sqrt{\frac{3.16\sigma_{R,p}^2}{\Lambda_p W^2} + \frac{W^2k_p^2}{8z^2}}} = \frac{\sqrt{2}}{W\sqrt{1+\frac{3.16\sigma_{R,p}^2}{\Lambda_p W^2}\frac{8z^2}{k_p^2W^2}}} \equiv \frac{\sqrt{2}}{W_{LT}},$$

where

$$W_{LT} \equiv W\sqrt{1+6.32\sigma_{R,p}^2\Lambda},$$

and

$$\frac{\beta}{\alpha} = \frac{1}{2}\left(1+6,32\sigma_{R,p}^2\Lambda\right) = \frac{W_{LT}^2}{2W^2}$$

With these formulas, Eq.(195) takes the form

$$P_2(x,x) = \frac{e^{-\sigma_{sp}^2(z)}}{2\pi W_{LT}^2}\exp\left[-\frac{2r^2}{W_{LT}^2}\right]\sum_{k=0}^{m}\sum_{l=0}^{n}\binom{m}{k}\binom{n}{l}\frac{(W/W_{LT})^{2k+2l}}{2^{k+l}k!\,l!}H_{2k}\left[\frac{\sqrt{2}}{W_{LT}}r_x\right]H_{2l}\left[\frac{\sqrt{2}}{W_{LT}}r_y\right]. \tag{196}$$

B.3 Evaluation of the integral (116) for a Gaussian pump and Hermite-Gaussian mode functions.

To calculate (116) and (117), we write the two-photon wavefunction in the form [37]

$$\begin{aligned} E_p\left(\frac{\mathbf{x}_1+\mathbf{x}_2}{2}\right)V(\mathbf{x}_1-\mathbf{x}_2) = \frac{1}{\lambda^2z^2}\int d\mathbf{r}'\int d\mathbf{r}''E_p\left(\frac{\mathbf{r}'+\mathbf{r}''}{2}\right)\delta(\mathbf{r}'-\mathbf{r}'') \\ \times\exp\left[\frac{ik}{2z}\left[|\mathbf{x}_1-\mathbf{r}'|^2+|\mathbf{x}_2-\mathbf{r}''|^2\right]\right]\exp[\psi(\mathbf{x}_1,\mathbf{r}')+\psi(\mathbf{x}_2,\mathbf{r}'')], \end{aligned} \tag{197}$$

where $\psi(\mathbf{x},\mathbf{r})$ is a random function representing phase and amplitude distortions of signal and idler fields. With the help of (197) the probability (116) takes the form

$$\begin{aligned} P(M_1,M_2) = \mathscr{C}_0\int d\mathbf{x}_1\int d\mathbf{x}_1'\int d\mathbf{x}_2\int d\mathbf{x}_2'\int d\mathbf{r}'\int d\mathbf{r}'' \\ \times M_1^*(\mathbf{x}_1)M_1(\mathbf{x}_1')M_2^*(\mathbf{x}_2)M_2(\mathbf{x}_2')E_p(\mathbf{r}')E_p^*(\mathbf{r}'') \\ \times\exp\left[\frac{ik}{2z}\left(|\mathbf{x}_1-\mathbf{r}'|^2-|\mathbf{x}_1'-\mathbf{r}''|^2+|\mathbf{x}_2-\mathbf{r}'|^2-|\mathbf{x}_2'-\mathbf{r}''|^2\right)\right] \\ \times\left\langle\exp\left[\psi(\mathbf{x}_1,\mathbf{r}')+\psi^*(\mathbf{x}_1',\mathbf{r}'')+\psi(\mathbf{x}_2,\mathbf{r}')+\psi^*(\mathbf{x}_2',\mathbf{r}'')\right]\right\rangle, \end{aligned} \tag{198}$$

where $\mathscr{C}_0 = 1/(\lambda^4z^4)$. The ensemble averaging, again, can be made using the theory developed in [21, Ch.7]

$$\begin{aligned} \langle\exp[\ldots]\rangle = \exp\Big[4E_1(0)+E_2(\mathbf{x}_1,\mathbf{x}_1';\mathbf{r}',\mathbf{r}'')+E_2(\mathbf{x}_1,\mathbf{x}_2';\mathbf{r}',\mathbf{r}'')+E_2(\mathbf{x}_2,\mathbf{x}_1';\mathbf{r}',\mathbf{r}'') \\ +E_2(\mathbf{x}_2,\mathbf{x}_2';\mathbf{r}',\mathbf{r}'')+E_3(\mathbf{x}_1,\mathbf{x}_2;0,0)+E_3^*(\mathbf{x}_1',\mathbf{x}_2';0,0)\Big]. \end{aligned} \tag{199}$$

Using the definitions of the functions in (199) from [21, Ch.7], one can write

$$
\begin{aligned}
[...] = &- 8\pi^2 k^2 z \int_0^\infty \kappa\Phi(\kappa)d\kappa + \left(8\pi^2 k^2 z \int_0^\infty \kappa\Phi(\kappa)d\kappa - 8\pi^2 k^2 z \int_0^\infty \kappa\Phi(\kappa)d\kappa\right) \\
&+ 4\pi^2 k^2 z \int_0^1 d\xi \int_0^\infty d\kappa\kappa\Phi(\kappa) J_0\left[\kappa|(1-\xi)(\mathbf{x}_1 - \mathbf{x}_1') + \xi(\mathbf{r}' - \mathbf{r}'')|\right] \\
&+ 4\pi^2 k^2 z \int_0^1 d\xi \int_0^\infty d\kappa\kappa\Phi(\kappa) J_0\left[\kappa|(1-\xi)(\mathbf{x}_1 - \mathbf{x}_2') + \xi(\mathbf{r}' - \mathbf{r}'')|\right] \\
&+ 4\pi^2 k^2 z \int_0^1 d\xi \int_0^\infty d\kappa\kappa\Phi(\kappa) J_0\left[\kappa|(1-\xi)(\mathbf{x}_2 - \mathbf{x}_1') + \xi(\mathbf{r}' - \mathbf{r}'')|\right] \\
&+ 4\pi^2 k^2 z \int_0^1 d\xi \int_0^\infty d\kappa\kappa\Phi(\kappa) J_0\left[\kappa|(1-\xi)(\mathbf{x}_2 - \mathbf{x}_2') + \xi(\mathbf{r}' - \mathbf{r}'')|\right] \\
&- 4\pi^2 k^2 z \int_0^1 d\xi \int_0^\infty d\kappa\kappa\Phi(\kappa) J_0\left[\kappa(1-\xi)|(\mathbf{x}_1 - \mathbf{x}_2)|\right] \exp\left[-i\frac{z\kappa^2}{k}\xi(1-\xi)\right] \\
&- 4\pi^2 k^2 z \int_0^1 d\xi \int_0^\infty d\kappa\kappa\Phi(\kappa) J_0\left[\kappa(1-\xi)|(\mathbf{x}_1' - \mathbf{x}_2')|\right] \exp\left[i\frac{z\kappa^2}{k}\xi(1-\xi)\right].
\end{aligned}
\tag{200}
$$

One can identify the sum of the first term in the first line and the terms in the second and third lines with two-point wave structure function's definition [21]

$$
-\frac{1}{2}\left[D_{sp}(\mathbf{x}_1 - \mathbf{x}_1', \mathbf{r}' - \mathbf{r}'') + D_{sp}(\mathbf{x}_1 - \mathbf{x}_2', \mathbf{r}' - \mathbf{r}'')\right],
$$

the sum of the third term in the first line and the terms in the fourth and fifth lines with

$$
-\frac{1}{2}\left[D_{sp}(\mathbf{x}_2 - \mathbf{x}_1', \mathbf{r}' - \mathbf{r}'') + D_{sp}(\mathbf{x}_2 - \mathbf{x}_2', \mathbf{r}' - \mathbf{r}'')\right].
$$

Now we make the geometrical optics approximation $(z\kappa^2/k \ll 1)$ to replace the exponential functions in the sixth and seventh lines of (200) with one. With that, the two approximated terms and the remaining second term in the first line of Eq.(200) one can identify the wave structure functions for a spherical wave

$$
\frac{1}{2}\left[D_{sp}(|\mathbf{x}_1' - \mathbf{x}_2'|) + D_{sp}(|\mathbf{x}_1 - \mathbf{x}_2|)\right].
$$

With this (200) takes a simpler form

$$
\begin{aligned}
[...] = &- \frac{1}{2}\left[D_{sp}(\mathbf{x}_1 - \mathbf{x}_1', \mathbf{r}' - \mathbf{r}'') + D_{sp}(\mathbf{x}_1 - \mathbf{x}_2', \mathbf{r}' - \mathbf{r}'')\right] \\
&- \frac{1}{2}\left[D_{sp}(\mathbf{x}_2 - \mathbf{x}_1', \mathbf{r}' - \mathbf{r}'') + D_{sp}(\mathbf{x}_2 - \mathbf{x}_2', \mathbf{r}' - \mathbf{r}'')\right] \\
&+ \frac{1}{2}\left[D_{sp}(|\mathbf{x}_1' - \mathbf{x}_2'|) + D_{sp}(|\mathbf{x}_1 - \mathbf{x}_2|)\right].
\end{aligned}
\tag{201}
$$

Finally, using the expressions for wave structure functions evaluated in the quadratic approximation [21] we have

$$
\begin{aligned}
[...] = &- \frac{1}{3\rho_{pl}^2}\left[|\mathbf{x}_1 - \mathbf{x}_1'|^2 + |\mathbf{r}' - \mathbf{r}''|^2 + (\mathbf{x}_1 - \mathbf{x}_1')\cdot(\mathbf{r}' - \mathbf{r}'')\right] \\
&- \frac{1}{3\rho_{pl}^2}\left[|\mathbf{x}_1 - \mathbf{x}_2'|^2 + |\mathbf{r}' - \mathbf{r}''|^2 + (\mathbf{x}_1 - \mathbf{x}_2')\cdot(\mathbf{r}' - \mathbf{r}'')\right] \\
&- \frac{1}{3\rho_{pl}^2}\left[|\mathbf{x}_2 - \mathbf{x}_1'|^2 + |\mathbf{r}' - \mathbf{r}''|^2 + (\mathbf{x}_2 - \mathbf{x}_1')\cdot(\mathbf{r}' - \mathbf{r}'')\right] \\
&- \frac{1}{3\rho_{pl}^2}\left[|\mathbf{x}_2 - \mathbf{x}_2'|^2 + |\mathbf{r}' - \mathbf{r}''|^2 + (\mathbf{x}_2 - \mathbf{x}_2')\cdot(\mathbf{r}' - \mathbf{r}'')\right] \\
&+ \frac{1}{3\rho_{pl}^2}\left[|\mathbf{x}_1' - \mathbf{x}_2'|^2 + |\mathbf{x}_1 - \mathbf{x}_2|^2\right],
\end{aligned}
\tag{202}
$$

where $\rho_{pl} = (1.46C_n^2k^2z)^{-3/5}$ is the plane-wave coherence radius.

Let us make a change of variables

$$\mathbf{Q} = \mathbf{r}' - \mathbf{r}'', \qquad 2\mathbf{S} = \mathbf{r}' + \mathbf{r}'' \tag{203}$$

for the source plane, and

$$\mathbf{p} = \mathbf{x}_1 - \mathbf{x}_2, \qquad \mathbf{p}' = \mathbf{x}_1' - \mathbf{x}_2', \qquad 2\mathbf{X} = \mathbf{x}_1 + \mathbf{x}_2, \qquad 2\mathbf{X}' = \mathbf{x}_1' + \mathbf{x}_2' \tag{204}$$

for the observation plane. Then, (202) can be expressed in the form

$$-\frac{4}{3\rho_{pl}^2}\left[Q^2 + |\mathbf{X} - \mathbf{X}'|^2 + \mathbf{Q}\cdot(\mathbf{X} - \mathbf{X}')\right]. \tag{205}$$

It is more convenient to express this result in terms of the Rytov variance $\sigma_R^2 = 1.23C_n^2k^{7/6}z^{11/6}$, that is,

$$\frac{4}{3\rho_{pl}^2} = 1.63(\sigma_R^2)^{6/5}\frac{k}{z} \equiv \gamma\frac{k}{z}. \tag{206}$$

The exponent in the second line of Eq. (198) can also be expressed in the new variables, viz.

$$\exp\left\{\frac{ik}{2z}\left[4\mathbf{S}\cdot\mathbf{Q} - 4\mathbf{S}\cdot(\mathbf{X} - \mathbf{X}') - 2\mathbf{Q}\cdot(\mathbf{X} + \mathbf{X}') + 2(X^2 - X'^2) + \frac{1}{2}(p^2 - p'^2)\right]\right\}. \tag{207}$$

Putting this all together, (198) takes the following form

$$\begin{aligned} P(M_1, M_2) = \mathscr{C}_0 \int d\mathbf{X} \int d\mathbf{X}' \int d\mathbf{p} \int d\mathbf{p}' \int d\mathbf{Q} \int d\mathbf{S}\; & M_1^*\left(\mathbf{X} + \frac{\mathbf{p}}{2}\right) M_1\left(\mathbf{X}' + \frac{\mathbf{p}'}{2}\right) \\ & \times M_2^*\left(\mathbf{X} - \frac{\mathbf{p}}{2}\right) M_2\left(\mathbf{X}' - \frac{\mathbf{p}'}{2}\right) E_p\left(\mathbf{S} + \frac{\mathbf{Q}}{2}\right) E_p^*\left(\mathbf{S} - \frac{\mathbf{Q}}{2}\right) \\ & \times \exp\left\{\frac{ik}{z}\left[2\mathbf{S}\cdot\mathbf{Q} - 2\mathbf{S}\cdot(\mathbf{X} - \mathbf{X}') - \mathbf{Q}\cdot(\mathbf{X} + \mathbf{X}') + (X^2 - X'^2) + \frac{1}{4}(p^2 - p'^2)\right]\right\} \\ & \times \exp\left\{-\frac{\gamma k}{z}\left[Q^2 + |\mathbf{X} - \mathbf{X}'|^2 + \mathbf{Q}\cdot(\mathbf{X} - \mathbf{X}')\right]\right\}. \end{aligned} \tag{208}$$

All the integrals' limits are $\pm\infty$ unless stated otherwise.

INTEGRATING THE S VARIABLE WITH A GAUSSIAN PUMP FIELD.

$$I_S \equiv \int d\mathbf{S} E_p\left(\mathbf{S} + \frac{\mathbf{Q}}{2}\right) E_p^*\left(\mathbf{S} - \frac{\mathbf{Q}}{2}\right) \exp\left\{\frac{2ik}{z}\left[\mathbf{S}\cdot\mathbf{Q} - \mathbf{S}\cdot(\mathbf{X} - \mathbf{X}')\right]\right\}. \tag{209}$$

Considering a normalized Gaussian pump field without diffraction

$$E_p(\mathbf{r}) = \sqrt{\frac{2}{\pi W_{0p}^2}}\exp\left(-\frac{r^2}{W_{0p}^2}\right), \tag{210}$$

Eq.(209) evaluates to

$$I_S = \exp\left[-\frac{Q^2}{2W_{0p}^2} - \frac{k^2W_{0p}^2}{2z^2}|\mathbf{Q} - (\mathbf{X} - \mathbf{X}')|^2\right]. \tag{211}$$

INTEGRATING THE $\mathbf{Q}$ VARIABLE. After combining Eqs.(208) – (211), the integral in $\mathbf{Q}$ is

$$I_Q \equiv \int d\mathbf{Q}\ \exp\left[-B_1 Q^2 + (B_2\mathbf{X} - B_2^*\mathbf{X}')\cdot\mathbf{Q}\right], \tag{212}$$

where

$$\begin{aligned} B_1 &= \frac{k}{z}\left(\frac{\Lambda_0}{2} + \frac{1}{2\Lambda_0} + \gamma\right), \\ B_2 &= \frac{k}{z}\left(\frac{1}{\Lambda_0} - \gamma - i\right), \\ \Lambda_0 &= \frac{2z}{kW_0^2}, \text{ with } W_0 = \sqrt{2}W_{0p}, \end{aligned} \tag{213}$$

which evaluates to

$$I_Q = \mathscr{C}_Q \exp\left[\frac{1}{4B_1}\left(B_2^2 X^2 + B_2^{*2} X'^2 - 2|B_2|^2 \mathbf{X}\cdot\mathbf{X}'\right)\right]. \tag{214}$$

where $\mathscr{C}_Q = \pi/B_1$. After combining the two results of integrations, we get

$$\begin{aligned} P(M_1, M_2) = \mathscr{C}_0\mathscr{C}_Q \int d\mathbf{X}\int d\mathbf{X}'\int d\mathbf{p}\int d\mathbf{p}'\, M_1^*\left(\mathbf{X}+\frac{\mathbf{p}}{2}\right) M_1\left(\mathbf{X}'+\frac{\mathbf{p}'}{2}\right) \\ \times M_2^*\left(\mathbf{X}-\frac{\mathbf{p}}{2}\right) M_2\left(\mathbf{X}'-\frac{\mathbf{p}'}{2}\right) \exp\left[\frac{ik}{4z}(p^2 - p'^2)\right] \\ \times \exp\left[\left(\frac{B_2^2}{4B_1} - B_3\right) X^2 + \left(\frac{B_2^{*2}}{4B_1} - B_3^*\right) X'^2\right] \\ \times \exp\left[\left(-\frac{|B_2|^2}{2B_1} + B_4\right)\mathbf{X}\cdot\mathbf{X}'\right], \end{aligned} \tag{215}$$

where

$$\begin{aligned} B_3 &= \frac{k}{z}\left(\frac{1}{2\Lambda_0} + \gamma - i\right), \\ B_4 &= \frac{k}{z}\left(\frac{1}{\Lambda_0} + 2\gamma\right). \end{aligned}$$

Next, we introduce the normalized mode functions $M_j(\mathbf{X})$ as Hermite-Gaussians:

$$M_j(\mathbf{X}) = U^{HG}_{m_j n_j}(X_x, X_y, 0) = B_{m_j n_j} H_{m_j}\left(\frac{\sqrt{2}}{W}X_x\right) H_{n_j}\left(\frac{\sqrt{2}}{W}X_y\right)\exp\left(-\frac{X^2}{W^2}\right), \tag{216}$$

where $H_n(\rho)$ are Hermite polynomials, $B_{m,n} = 1/\left(W\sqrt{\pi 2^{m+n-1} m!\, n!}\right)$, and $W = W_0\sqrt{1+\Lambda_0^2}$. Notice that we have chosen $W_0 = \sqrt{2}\,W_{0p}$ so that we consider HG modes with the same Fresnel ratio Λ of the SPDC pump beam.

$$\begin{aligned} P(HG_{m_s n_s}, HG_{m_i n_i}) = \mathscr{C}_0\mathscr{C}_Q\mathscr{C}_M \int dX_x \int dX_y \int dX'_x \int dX'_y \int dp_x \int dp_y \int dp'_x \int dp'_y \\ \times H_{m_s}\left[\frac{\sqrt{2}}{W}\left(X_x + \frac{p_x}{2}\right)\right] H_{m_i}\left[\frac{\sqrt{2}}{W}\left(X_x - \frac{p_x}{2}\right)\right]\exp\left[-A_1 p_x^2\right] \\ \times H_{n_s}\left[\frac{\sqrt{2}}{W}\left(X_y + \frac{p_y}{2}\right)\right] H_{n_i}\left[\frac{\sqrt{2}}{W}\left(X_y - \frac{p_y}{2}\right)\right]\exp\left[-A_1 p_y^2\right] \\ \times H_{m_s}\left[\frac{\sqrt{2}}{W}\left(X'_x + \frac{p'_x}{2}\right)\right] H_{m_i}\left[\frac{\sqrt{2}}{W}\left(X'_x - \frac{p'_x}{2}\right)\right]\exp\left[-A_1^{*2} p_x'^2\right] \\ \times H_{n_s}\left[\frac{\sqrt{2}}{W}\left(X'_y + \frac{p'_y}{2}\right)\right] H_{n_i}\left[\frac{\sqrt{2}}{W}\left(X'_y - \frac{p'_y}{2}\right)\right]\exp\left[-A_1^{*2} p_y'^2\right] \\ \times \exp\left[-A_2 X^2\right]\exp\left[-A_2^* X'^2\right]\exp\left[A_3 X_x X'_x\right]\exp\left[A_3 X_y X'_y\right], \end{aligned} \tag{217}$$

where

$$\mathscr{C}_M = \frac{4}{\pi^2 W^4 m_s!\, m_i!\, n_s!\, n_i!\, 2^{m_s+m_i+n_s+n_i}}, \tag{218}$$

$$A_1 = \frac{k}{4z}(\Lambda - i), \tag{219}$$

$$A_2 = -\frac{B_2^2}{4B_1} + B_3 + \frac{k}{z}\Lambda, \tag{220}$$

$$A_3 = -\frac{|B_2|^2}{2B_1} + B_4, \tag{221}$$

$$\Lambda = \frac{\Lambda_0}{1+\Lambda_0^2}. \tag{222}$$

All the integrals in (215) are separable in x and y. The X or X' types look alike, also the p and p' ones. One can start by integrating the p_x variable,

$$I_{p_x} = \int dp_x H_{m_s}\left[\frac{\sqrt{2}}{W}\left(X_x + \frac{p_x}{2}\right)\right] H_{m_i}\left[\frac{\sqrt{2}}{W}\left(X_x - \frac{p_x}{2}\right)\right] \exp\left[-A_1 p_x^2\right]. \tag{223}$$

Using the Taylor expansion of Hermite polynomials and Formula 7.374-5 of Ref. [127], viz.,

$$H_n(x+y) = \sum_{k=0}^{n} \binom{n}{k} H_k(x)(2y)^{n-k} \tag{224}$$

and

$$\begin{aligned}\int dx H_k(x) H_l(x) \exp[-2\alpha^2 x^2] &= 2^{\frac{k+l-1}{2}} \alpha^{-k-l-1}(1-2\alpha^2)^{\frac{k+l}{2}} \\ &\times \Gamma\left(\frac{k+l+1}{2}\right) {}_2F_1\left(-k,-l;\frac{1-k-l}{2};\frac{\alpha^2}{2\alpha^2-1}\right), \\ &\mathrm{Re}(\alpha^2) > 0, \quad \alpha^2 \neq 1/2, \quad k+l = \text{even},\end{aligned} \tag{225}$$

the integral (223) evaluates to

$$I_{p_x} = \frac{W}{\sqrt{2}} \sum_{k_1=0}^{m_s} \sum_{l_1=0}^{m_i} \mathscr{F}(m_s, m_i, k_1, l_1) X_x^{m_s+m_i-k_1-l_1}, \tag{226}$$

with

$$\begin{aligned}\mathscr{F}(\mu,\nu,k,l) = &\binom{\mu}{k}\binom{\nu}{l} 2^{\mu+\nu} i^{k+l} \sigma(k,l)\, \Gamma\left(\frac{k+l+1}{2}\right)\left(\frac{\sqrt{2}}{W}\right)^{\mu+\nu-k-l} \\ &\times \sqrt{1-\zeta}\left(\sqrt{\zeta}\right)^{k+l} {}_2F_1\left(-k,-l;\frac{1-k-l}{2};\frac{1}{2\zeta}\right),\end{aligned} \tag{227}$$

where $\zeta = 1/(1+i\Lambda)$, $\sigma(k,l) = [(-1)^k + (-1)^l]/2$ and ${}_2F_1(a,b;c;z)$ is the hypergeometric function. The integrations in p_y, p'_x and p'_y are straightforward. They are

$$I_{p_y} = \frac{W}{\sqrt{2}} \sum_{k_2=0}^{n_s} \sum_{l_2=0}^{n_i} \mathscr{F}(n_s, n_i, k_2, l_2) X_y^{n_s+n_i-k_2-l_2}, \tag{228}$$

$$I_{p'_x} = \frac{W}{\sqrt{2}} \sum_{k_3=0}^{m_s} \sum_{l_3=0}^{m_i} \mathscr{F}^*(m_s, m_i, k_3, l_3) X_x'^{m_s+m_i-k_3-l_3}, \tag{229}$$

$$I_{p'_y} = \frac{W}{\sqrt{2}} \sum_{k_4=0}^{n_s} \sum_{l_4=0}^{n_i} \mathscr{F}^*(n_s, n_i, k_4, l_4) X'^{n_s+n_i-k_4-l_4}_y. \tag{230}$$

Now we integrate the X_j and X'_j $(j = x, y)$ variables, which are all in the form

$$\mathscr{K}(\mu, \nu) = \int dx \int dx' \; x^\mu x'^\nu \exp(-A_2 x^2 - A_2^* x'^2 + A_3 x x'), \tag{231}$$

which evaluates to

$$\begin{aligned}
\mathscr{K}(\mu,\nu) = & \frac{1}{4}\left(\frac{1}{\sqrt{2}}\right)^{\mu+\nu} \sum_{p=0}^{\mu}\sum_{q=0}^{\nu}\binom{\mu}{p}\binom{\nu}{q}(-1)^{\nu-q}\left(\frac{1}{\sqrt{C_1}}\right)^{2+p+q}\left(\frac{1}{\sqrt{C_2}}\right)^{\mu+\nu-p-q} \\
& \times \left\{\sigma(0,p+q)\sigma(0,\mu+\nu-p-q)\sqrt{\frac{C_1}{C_2}}\;\Gamma\left(\frac{1+p+q}{2}\right)\right. \\
& \times \Gamma\left(\frac{1+\mu+\nu-p-q}{2}\right) {}_2F_1\left(\frac{1+p+q}{2}; \frac{1+\mu+\nu-p-q}{2}, \frac{1}{2}; C_4\right) \\
& - \frac{i\sigma(1,p+q)\sigma(1,\mu+\nu-p-q)(4C_1C_2+C_3^2)}{C_2C_3(1+p+q)(1+\mu+\nu-p-q)}\Gamma\left(\frac{2+p+q}{2}\right) \\
& \times \Gamma\left(\frac{2+\mu+\nu-p-q}{2}\right) {}_2F_1\left(\frac{2+p+q}{2}; \frac{2+\mu+\nu-p-q}{2}, -\frac{1}{2}; C_4\right) \\
& + \frac{i\sigma(1,p+q)\sigma(1,\mu+\nu-p-q)[4C_1C_2+C_3^2(4+\mu+\nu)]}{C_2C_3(1+p+q)(1+\mu+\nu-p-q)}\Gamma\left(\frac{2+p+q}{2}\right) \\
& \left. \times \Gamma\left(\frac{2+\mu+\nu-p-q}{2}\right) {}_2F_1\left(\frac{2+p+q+}{2}; \frac{2+\mu+\nu-p-q}{2}, \frac{1}{2}; C_4\right)\right\},
\end{aligned} \tag{232}$$

where

$$C_1 = ReA_2 - \frac{A_3}{2} \tag{233}$$

$$C_2 = ReA_2 + \frac{A_3}{2} \tag{234}$$

$$C_3 = ImA_2 \tag{235}$$

$$C_4 = -\frac{C_3^2}{4C_1C_2}. \tag{236}$$

So, the four integrals in the X_j and X'_j $(j = x, y)$ variables are

$$\begin{aligned}
\int dX_x \int dX_y \int dX'_x \int dX'_y \ldots = & \mathscr{K}(m_s + m_i - k_1 - l_1, m_s + m_i - k_3 - l_3) \\
& \times \mathscr{K}(n_s + n_i - k_2 - l_2, n_s + n_i - k_4 - l_4).
\end{aligned} \tag{237}$$

Then, we finally arrive at

$$P(HG_{m_s n_s}, HG_{m_i n_i}) = \Pi(m_s, m_i)\Pi(n_s, n_i), \tag{238}$$

where

$$\begin{aligned}
\Pi(\mu,\nu) = & \left(\frac{\sqrt{2}}{W_0}\right)^{\mu+\nu} \frac{1}{\mu!\,\nu!} \sum_{k_1=0}^{\mu}\sum_{l_1=0}^{\nu}\sum_{k_3=0}^{\mu}\sum_{l_3=0}^{\nu} \mathscr{F}(\mu,\nu,k_1,l_1)\mathscr{F}^*(\mu,\nu,k_3,l_3) \\
& \times \mathscr{K}(\mu+\nu-k_1-l_1, \mu+\nu-k_3-l_3),
\end{aligned} \tag{239}$$

It should be noticed that since the two-photon wavefunction in Eq. (197) is written in the paraxial approximation and, therefore, not properly normalizable, $\sum_{m_s}\sum_{n_s}\sum_{m_i}\sum_{n_i} P(HG_{m_s n_s}, HG_{m_i n_i})$ does not converge to 1.

This Thesis is a continuation of the work done in the Prof. Dr. C. H. Monken's group in Physics Department of Federal University of Minas Gerais. In the last decade there have been written Theses and Dissertations exploring various features of the field from the spontaneous parametric down-conversion (SPDC) source in the two photon regime. Particularly, in 2004, Stephen Walborn defended his PhD Thesis "The Brothers Q: Multimode Entangled Photons with Parametric Down Conversion", in a theoretical and experimental study of the quantum properties of multimode entangled photons created by spontaneous parametric down-conversion. In his MSc Dissertation "Associação de um Feixe de Correlação ao Campo Gerado pela Conversão Paramétrica Descendente" Pablo Lima Saldanha arrived to the concept of the *Correlation Beam* by showing that for SPDC field the fourth order correlation function is directly related to second order correlation function of the pump beam that generates the SPDC field in a nonlinear crystal, thus, having a beam-like behaviour. He also verified it experimentally. In 2014, Marcelo Vítor da Cunha Pereira in his PhD Thesis "Propagação de feixes ópticos de correlação em atmosféra turbulenta" investigated numerically the atmospheric propagation of the Correlation Beam. He also made in-lab experiments by setting up a turbulence chamber which emulates real atmospheric conditions. In 2015, Luísa Amorim Perez Filpi in her PhD Thesis "Cancelamento de aberrações ópticas utilizando feixes de correlao" studied the aberration effects of the Correlation Beam.

In this Thesis I investigated analytically the atmospheric propagation features of *higher order* Correlation Beams, as well as tubulence effects on multimode properties of the quantum state of SPDC. Higher order Correlation Beams are those produced when higher order Hermite or Laguerre-Gaussian laser modes pump the crystal. As the twin photons produced by SPDC process are entangled in transverse spatial modes, one can use these modes as a basis (alphabet) to expand the SPDC state. These modes can be used to encode more information, also have more secure quantum communication. Thus, for global quantum communication purposes, as well as for fundamental (large-scale) tests of quantum mechanics, it is of great importance studying atmospheric effects on the (higher order) Correlation Beams.

With intrductions to the theories of SPDC, the Correlation Beam and optical turbulence I put ground for the development of atmospheric propagation of the Correlation Beam. In many calculations the Extended Huygens-Fresnel Principle is used which is valid for both, weak and strong turbulence conditions. The two-photon joint

probability density function which is proportional to the measurable fourth order correlation function is calculated for Hermite-Gaussian as well as partially coherent Gaussian-Schell model pump cases. Because of mathematical difficulty, a direct calculation for Laguerre-Gaussian modes has not been done but owing to transformation properties between Hermite- and Laguerre-Gaussian modes it is possible to generalize the results for Laguerre-Gaussian pump. The partially coherent pump case is particularly important because it has been shown that partially coherent beams are less affected by turbulence than coherent beams in a sense that their relative spreading due to atmosphere is less than that of coherent case. An important property has been revealed between the two cases: the joint detection probability density function for the partially coherent pump case is expressed as a convex sum of those of coherent probability density. These results are reported in Optics Express 24, 2318 (2016).

Then, expressing the SPDC state as an entangled state in Hermite-Gaussian modes, a mode analysis is made. Again, for mathematical convenience only a conventional Gaussian pump is considered. Here, the two-mode joint detection probability function is calculated. While there are restrictions on both the parity and mode order of downconverted photons in the vacuum case, it no longer holds when turbulence effects are added. The crosstalk between modes that takes place when propagating through the atmosphere is quantified in terms of probabilities of those modes that were forbidden to be populated. Some information on Hermite- and Laguerre-Gaussian modes as well as mathematical derivations of the main results are provided in the Appendices.

Finally, approaches for solving two problems is given. One concerns the correction of SPDC wave phase corrupted by turbulence. The ABCD ray matrix formalism and Zernike polynomials are needed to fulfill the task. The method is provided in the Thesis leaving open the calculations of considered quantities. The second problem has an inverse purpose as opposed to the rest of the Thesis: the inference of atmospheric parameters from measurements of the Correlation Beam. The procedure is given and a partial result is produced.

[1] J. H. Shapiro, "The quantum theory of optical communications," IEEE journal of selected topics in Quantum Electronics 15, 1547 (2009).

[2] Z.-S. Yuan, X.-H. Bao, C-Y. Lu, J. Z., C.-Z. Peng, J.-W. Pan, "Entangled photons and quantum communication," Physics Reports 497, 140 (2010).

[3] A. Mair, A. Vaziri, G. Weihs, and A. Zeilinger, "Entanglement of the orbital angular momentum states of photons," Nature (London) 412, 313 (2001).

[4] D. Bruss, L. Faoro, C. Macchiavello, and G. M. Palma, "Quantum entanglement and classical communication through a depolarising channel," J. Mod. Opt. 47, 325 (2000).

[5] C. King, "The capacity of the quantum depolarizing channel," IEEE Trans. Inform. Theory 49, 221 (2003).

[6] C. Paterson, "Atmospheric turbulence and orbital angular momentum of single photons for optical communication," Phys. Rev. Lett. 94, 153901 (2005).

[7] F. S. Roux, "Infinitesimal-propagation equation for decoherence of an orbital-angular-momentum-entangled biphoton state in atmospheric turbulence," Phys. Rev. A 83, 053822 (2011); 88, 049906(E) (2013).

[8] D. J. Sanchez and D. W. Oesch, "Orbital angular momentum in optical waves propagating through distributed turbulence," Opt. Express 19, 24596 (2011).

[9] M. Malik, M. O'Sullivan, B. Rodenburg, M. Mirhosseini, J. Leach, M. P. J. Lavery, M. J. Padgett, and R. W. Boyd, "Influence of atmospheric turbulence on optical communications using orbital angular momentum for encoding," Opt. Express 20, 13195 (2012).

[10] F. Tamburini, E. Mari, A. Sponselli, B. Thide, A. Bianchini, and F. Romanato, "Encoding many channels on the same frequency through radio vorticity: first experimental test," New J. Phys. 14, 033001 (2012).

[11] G. Gibson, J. Courtial, M. Padgett, M. Vasnetsov, V. Pas'ko, S. Barnett, and S. Franke-Arnold, "Free-space information transfer

using light beams carrying orbital angular momentum," Opt. Express 12, 5448 (2004).

[12] N. Gisin, G. Ribordy, W. Tittel, and H. Zbinden, "Quantum cryptography," Rev. Mod. Phys. 74, 145 (2002).

[13] B.-J. Pors, C. H. Monken, E. R. Eliel, and J. P. Woerdman, "Transport of orbital-angular-momentum entanglement through a turbulent atmosphere," Opt. Express 19, 6671 (2011).

[14] G. Vallone, V. D'Ambrosio, A. Sponselli, S. Slussarenko, L. Marrucci, F. Sciarrino, and P. Villoresi, "Free-space quantum key distribution by rotation-invariant twisted photons," Phys. Rev. Lett. 113, 060503 (2014).

[15] M. Krenn, J. Handsteiner, M. Fink, R. Fickler, A. Zeilinger, "Twisted photon entanglement through turbulent air across Vienna," PNAS 112, 14197 (2015).

[16] O. Keskin, L. Jolissaint, and C. Bradley, "Hot-air optical turbulence generator for the testing of adaptive optics systems: principles and characterization.," Appl. Opt. 45, 4888 (2006).

[17] B. J. Smith and M.G. Raymer, "Two-photon wave mechanics," Phys. Rev. A 74, 062104 (2006).

[18] G. A. Tyler and R. W. Boyd, "Influence of atmospheric turbulence on the propagation of quantum states of light carrying orbital angular momentum," Opt. Lett. 34, 142 (2009).

[19] A. H. Ibrahim, F. S. Roux, M. McLaren, T. Konrad, and A. Forbes, "Orbital-angular-momentum entanglement in turbulence," Phys. Rev. A 88, 012312 (2013).

[20] N. D. Leonhard, V. N. Shatokhin, and A. Buchleitner, "Universal entanglement decay of photonic-orbital-angular-momentum qubit states in atmospheric turbulence," Phys. Rev. A 91, 012345 (2015).

[21] L. C. Andrews and R. L. Phillips, *Laser Beam Propagation Through Random Media*, SPIE, 2005.

[22] F. S. Roux, "The Lindblad equation for the decay of entanglement due to atmospheric scintillation," J. Phys. A: Math. Theor. 47, 195302 (2014).

[23] A. L. Moustakas, H. U. Baranger, L. Balents, A. M. Sengupta, S. H. Simon, "Communication through a diffusive medium: coherence and capacity," Science 287, 287 (2000).

[24] S. E. Skipetrov, "Information transfer through disordered media by diffuse waves," Phys. Rev. E 67, 036621 (2003).

[25] D. Elser, T. Bartley, B. Heim, Ch. Wittmann, D. Sych and G Leuchs, "Feasibility of free space quantum key distribution with coherent polarization states," New J. Phys. **11**, 045014 (2009).

[26] B. Heim, D. Elser, T. Bartley, M. Sabuncu, C. Wittmann, D. Sych, C. Marquardt, G. Leuchs, "Atmospheric channel characteristics for quantum communication with continuous polarization variables," Appl. Phys. B **98** 635 (2010).

[27] A. A. Semenov, F. Toppel, D. Yu. Vasylyev, H. V. Gomonay, and W. Vogel, "Homodyne detection for atmosphere channels," Phys. Rev. A **85**, 013826 (2012).

[28] B. Heim, C. Peuntinger, N. Killoran, I. Khan, C. Wittmann, Ch. Marquardt and G. Leuchs, "Atmospheric continuous-variable quantum communication," New J. Phys. **16**, 113018 (2014).

[29] M. Mafu, A. Dudley, S. Goyal, D. Giovannini, M. McLaren, M. J. Padgett, T. Konrad, F. Petruccione, N. Lutkenhaus, and A. Forbes, "Higher-dimensional orbital-angular-momentum-based quantum key distribution with mutually unbiased bases," Phys. Rev. A **88**, 032305 (2013).

[30] S. E. Skipetrov, "Quantum theory of dynamic multiple light scattering in fluctuating disordered media," Phys. Rev. A **75**, 053808 (2007).

[31] S. Smolka, A. Huck, U. L. Andersen, A. Lagendijk, and P. Lodahl, "Observation of spatial quantum correlations induced by multiple scattering of nonclassical light," Phys. Rev. Lett. **102**, 193901 (2009).

[32] J. R. Ott, N. A. Mortensen, and P. Lodahl, "Quantum interference and entanglement induced by multiple scattering of light," Phys. Rev. Lett. **105**, 090501 (2010).

[33] C. W. J. Beenakker, J. W. F. Venderbos, and M. P. van Exter, "Two-photon speckle as a probe of multi-dimensional entanglement," Phys. Rev. Lett. **102**, 193601 (2009).

[34] W. H. Peeters, J. J. D. Moerman, and M. P. van Exter, "Observation of two-photon speckle patterns," Phys. Rev. Lett. **104**, 173601 (2010).

[35] H. Di Lorenzo Pires, J. Woudenberg, and M. P. van Exter, "Statistical properties of two-photon speckles," Phys. Rev. A **85**, 033807 (2012).

[36] M. Cande and S. E. Skipetrov, "Quantum versus classical effects in two-photon speckle patterns," Phys. Rev. A **87**, 013846 (2013).

[37] M. V. da Cunha Pereira, L. A. P. Filpi and C. H. Monken, "Cancellation of atmospheric turbulence effects in entangled two-photon beams," Phys. Rev. A, 88, 053836 (2013).

[38] S. Smolka, J. R. Ott, A. Huck, U. L. Andersen, and P. Lodahl, "Continuous-wave spatial quantum correlations of light induced by multiple scattering," Phys. Rev. A 86, 033814 (2012).

[39] D. V. Strekalov, A. V. Sergienko, D. N. Klyshko, and Y. H. Shih, "Observation of Two-Photon "Ghost" Interference and Diffraction," Phys. Rev. Lett. 74, 3600 (1995).

[40] J. Cheng, "Ghost imaging through turbulent atmosphere," Opt. Express 17, 7916 (2009).

[41] A. K. Jha and R. W. Boyd, "Effects of atmospheric turbulence on the entanglement of spatial two-qubit states," Phys. Rev. A 81, 0 53832 (2010).

[42] C. Li, T. Wang, J. Pu, W. Zhu, R. Rao, "Ghost imaging with partially coherent light radiation through turbulent atmosphere," Appl. Phys. B 99, 599 (2010).

[43] P. Zhang, W. Gong, X. Shen, and S. Han, "Correlated imaging through atmospheric turbulence," Phys. Rev. A 82, 033817 (2010).

[44] K. W. C. Chan, D. S. Simon, A. V. Sergienko, N. D. Hardy, J. H. Shapiro, P. B. Dixon, G. A. Howland, J. C. Howell, J. H. Eberly, M. N. OSullivan, B. Rodenburg, and R. W. Boyd, "Theoretical analysis of quantum ghost imaging through turbulence," Phys. Rev. A 84, 043807 (2011).

[45] S. Smolka, O. L. Muskens, Ad Lagendijk, and P. Lodahl, "Angle-resolved photon-coincidence measurements in a multiple-scattering medium," Phys. Rev. A 83, 043819 (2011).

[46] M. P. van Exter, J. Woudenberg, H. Di Lorenzo Pires, and W. H. Peeters, "Bosonic, fermionic, and anyonic symmetry in two-photon random scattering," Phys. Rev. A 85, 033823 (2012).

[47] M. Mirhosseini, O. S. Magaa-Loaiza, M. N. O'Sullivan, B. Rodenburg, M. Malik, M. P. J. Lavery, M. J. Padget, D. J. Gauthier and R. W. Boyd, "High-dimensional quantum cryptography with twisted light," New J. Phys. 17, 033033 (2015).

[48] S. P. Walborn, C.H. Monken, S. Pádua, P. H. Souto Ribeiro, "Spatial correlations in parametric down-conversion," Phys. Rep. 495, 87 (2010).

[49] G. Gbur and E. Wolf, "Spreading of partially coherent beams in random media," J. Opt. Soc. Am. A 19, 1592 (2002).

[50] T. Shirai, A. Dogariu, and E. Wolf, "Mode analysis of spreading of partially coherent beams propagating through atmospheric turbulence," J. Opt. Soc. Am. A 20, 1094 (2003).

[51] M. Salem, T. Shirai, A. Dogariu, E. Wolf, "Long-distance propagation of partially coherent beams through atmospheric turbulence," Opt. Commun. 216, 261 (2003).

[52] G. Grynberg, A. Aspect, C. Fabre, *Introduction to Quantum Optics*, Cambridge University Press, New York, 2010.

[53] D. C. Burnham and D. L. Weinberg, "Observation of Simultaneity in Parametric Production of Optical Photon Pairs," Phys. Rev. Lett. 25, 84 (1970).

[54] C. K. Hong, Z. Y. Ou, and L. Mandel, "Measurement of subpicosecond time intervals between two photons by interference," Phys. Rev. Lett. 59, 2044 (1987).

[55] W. H. Louisell, A. Yariv, A. E. Siegman, "Quantum Fluctuations and Noise in Parametric Processes. I," Phys. Rev. 124, 1646 (1961).

[56] J. P. Gordon, W. H. Louisell, and L. R. Walker, "Quantum Fluctuations and Noise in Parametric Processes. II," Phys. Rev. 129, 481 (1963).

[57] B. R. Mollow, "Photon Correlations in the Parametric Frequency Splitting of Light," Phys. Rev. A 8, 2684 (1973).

[58] L. Mandel and E. Wolf, *Optical Coherence and Quantum Optics*, Cambridge, New York, 1995.

[59] P. L. Saldanha, *Associação de um Feixe de Correlação ao Campo Gerado pela Conversão Paramétrica Descendente*, Master's Dissertation, UFMG, 2006.

[60] C. H. Monken, P. S. Ribeiro, and S. Padua, "Transfer of angular spectrum and image formation in spontaneous parametric down-conversion" Phys. Rev. A. 57, 3123 (1998).

[61] A. N. Kolmogorov, "The local structure of turbulence in an incompressible viscous fluid for very large Reynolds numbers," C. R. (Doki) Acad. Sci. U.S.S.R. 30, 301305 (1941).

[62] J. C. Owens, "Optical refractive index of air: dependence on pressure, temperature and composition," Appl. Opt. 6, 51 (1967).

[63] V. I. Tatarskii, *The Effects of the Turbulent Atmosphere on Wave Propagation* (transl. for NOAA by Israel Program for Scientific Translations, Jerusalem, 1971).

[64] V. I. Tatarskii. *Wave propagation in a turbulent medium*. McGraw-Hill, New York, 1961.

[65] V. I. Tatarskii, A. Ishimaru, and V. U. Zavorotny. *Wave propagation in random media (Scintillation)*. SPIE, Bellingham, 1993.

[66] M. C. Roggemann and B. Welsh. *Imaging Through Turbulence.* CRC Press, Boca Raton, 1996.

[67] R. L. Fante, "Wave propagation in random media: a system approach," Progress in Optics 22, 342 (1985).

[68] T. von Kármán, "Progress in the Statistical Theory of Turbulence," Proceedings of the National Academy of Sciences 34, 530 (1948).

[69] L. C. Andrews, "An analytical model for the refractive index power spectrum and its application to optical scintillations in the atmosphere," J. Mod. Opt. 39, 1849 (1992).

[70] J. W. Strohbehn, "Lino-of-sight wave propagation through the turbulent atmosphere," Proc. IEEE 56, 1301 (1968).

[71] S. M. Rytov, "Diffraction of light by ultrasonic waves," Izvestiya Akademii Nauk SSSR, Seriya Fizicheskaya (Bulletin of the Academy of Sciences of the USSR, Physical Series) 2, 223259 (1937).

[72] A. M. Prokhorov, F. V. Bunkin, K. S. Gochelashvily, and V. I. Shishov, "Laser irradiance propagation in turbulent media," Proc. IEEE 63, 790 (1975).

[73] K. S. Gochelashvili and V. I. Shishov, "Saturated fluctuations in the laser radiation intensity in a turbulent medium," Sov. Phys. JETP 39, 605 (1974).

[74] R. L. Fante, "Inner-scale size effect on the scintillations of light in the turbulent atmosphere," J. Opt. Soc. Am. 73, 277 (1983).

[75] R. G. Frehlich, "Intensity covariance of a point source in a random medium with a Kolmogorov spectrum and an inner scale of turbulence," J. Opt. Soc. Am. A 4, 360 (1987); Errata: J. Opt. Soc. Am. A 4, 1324 (1987).

[76] V. I. Tatarskii and V. U. Zavorotnyi, "Strong fluctuations in light propagation in a randomly inhomogeneous medium," in Progress in Optics III, (W. Wolf, ed.) Elsevier, New York, 1980.

[77] H. Yura, "Mutual coherence function of a finite cross section optical beam propagating in a turbulent medium," Appl. Opt. 11, 1399 (1972).

[78] R. Lutomirski and H. T. Yura, "Propagation of a finite optical beam in an inhomogeneous medium," Appl. Opt. 10, 1652 (1971).

[79] Z. I. Feizulin and Yu. A. Kravtsov, "Expansion of a laser beam in a turbulent medium," Izv. Vyssh., Uchebn. Zaved. Radiofiz. 24, 1351-1355 (1967).

[80] A. Ishimaru, *Wave Propagation and Scattering in Random Media*, IEEE Press, Piscataway, New Jersey, 1997.

[81] R. Dashen, "Path integrals for waves in random media," J. Math. Phys. 20, 894 (1979).

[82] H. T. Yura, S. G. Hanson, "Second-order statistics for wave propagation through complex optical systems," J. Opt. Soc. Am. A 6, 564 (1989).

[83] Monin and Yaglom, *Stat. Fluid Mechanics, vol. 1*, (MIT Press, Cambridge, Mass.) 1971.

[84] Monin and Yaglom, *Stat. Fluid Mechanics, vol. 2*, 1975.

[85] A. H. Ibrahim, F. S. Roux, M. McLaren, T. Konrad, and A. Forbes, "Orbital-angular-momentum entanglement in turbulence," Phys. Rev. A 88, 012312 (2013).

[86] B. E. A. Saleh, M. C. Teich, and A. V. Sergienko, "Wolf equations for two-photon light," Phys. Rev. Lett. 94, 223601 (2005).

[87] H. van Cittert, "Die wahrscheinliche schwingungsverteilung in einer von einer lichtquelle direkt oder mittels einer linse beleuchteten ebene," Physica 1, 201 (1934).

[88] F. Zernike, "The concept of degree of coherence and its application to optical problems," Physica V, 785 (1938).

[89] B. E. A. Saleh, A. F. Abouraddy, A. V. Sergienko, and M. C. Teich, "Duality between partial coherence and partial entanglement," Phys. Rev. A 62, 043816 (2000).

[90] C. Ho, A. Lamas-Linares, C. Kurtsiefer, "Clock synchronization by remote detection of correlated photon pairs," New J. Phys. 11, 045011 (2009).

[91] L. Allen, M. W. Beijersbergen, R. J. C. Spreeuw, and J. P. Woerdman, "Orbital angular momentum of light and the transformation of Laguerre-Gaussian laser modes," Phys. Rev. A 45, 8185 (1992).

[92] A. T. O'Neil, J. Courtial, "Mode transformations in terms of the constituent HermiteGaussian or LaguerreGaussian modes and the variable-phase mode converter," Opt. Comm. 181, 35 (2000).

[93] L. Marrucci, C. Manzo, and D. Paparo, "Optical spin-to-orbital angular momentum conversion in inhomogeneous anisotropic media," Phys. Rev. Lett. 96, 163905 (2006).

[94] A. Yang, E. Zhang, X. Ji and B. Lü, "Angular spread of partially coherent Hermite-cosh-Gaussian beams propagating through atmospheric turbulence ," Opt. Express 16, 8366 (2008).

[95] O. Korotkova, L. C. Andrews, and R. L. Phillips, "A model for a partially coherent Gaussian beam in atmospheric turbulence with application in lasercom," Opt. Eng. 43, 330341 (2004).

[96] J. H. Shapiro, B. A. Capron, R. C. Harney, "Imaging and target detection with a heterodyne-reception optical radar," Appl. Opt. 20, 3292 (1981).

[97] R. K. Tyson, *Principles of Adaptive Optics* (Academic Press, San Diego, 1991).

[98] M. Born and E. Wolf, *Principles of Optics*, 7th ed. (Cambridge University, 1999).

[99] R. J. Noll, "Zernike polynomials and atmospheric turbulence," J. Opt. Soc. Am. 73, 207 (1976).

[100] A. Siegman, *Lasers* (University Science, Mill Valley, Calif., 1986).

[101] Y. Cai, "Generation of various partially coherent beams and their propagation properties in turbulent atmosphere: A review," Proc. of SPIE 7924, 792402 (2011).

[102] P. H. Souto Ribeiro, "Partial coherence with twin photons," Phys. Rev. A 56, 4111 (1997).

[103] M. A. Olvera, S. Franke-Arnold, "Two photon amplitude of partially coherent partially entangled electromagnetic fields," arXiv:1507.08623v1.

[104] Collett and E. Wolf, "Is complete spatial coherence necessary for the generation of highly directional light beams?," Opt. Lett. 2, 27 (1978).

[105] E. Wolf and E. Collett, "Partially coherent sources which produce the same far-field intensity distribution as a laser," Opt. Comm. 25, 293 (1978).

[106] F. Gori, "Mode propagation of the field generated by Collett-Wolf Schell-model sources," Opt. Comm. 46, 149 (1983).

[107] P. De Santis, F. Gori, G. Guattari and C. Palma, "An example of a Collett-Wolf source," Opt. Comm. 29, 256 (1979).

[108] J.D. Farina, L.M. Narducci and E. Collett, "Generation of highly directional beams from a globally incoherent source," Opt. Comm. 32, 203 (1980).

[109] S. P. Walborn, *The Brothers Q: Multimode Entangled Photons with Parametric Down Conversion*, PhD Thesis, UFMG, 2004.

[110] Arlt, K. Dholakia, L. Allen, M.J. Padgett, "The production of multiringed LaguerreGaussian modes by computer-generated holograms," J. Mod. Opt. 45, 1231 (1998).

[111] A. Vaziri, G. Weihs, A. Zeilinger, "Experimental two-photon, three-dimensional entanglement for quantum communication," Phys. Rev. Lett. 89, 240401 (2002).

[112] V. D. Salakhutdinov, E. R. Eliel, and W. Löffler, "Full-field quantum correlations of spatially entangled photons," Phys. Rev. Lett. 108, 173604 (2012).

[113] M. Krenn, M. Huber, R. Fickler, R. Lapkiewicz, S. Ramelow, and A. Zeilinger, "Generation and confirmation of a (100 100)-dimensional entangled quantum system", PNAS 111, 6243 (2014).

[114] G. S. Agarwal, *Quantum Optics*, Cambridge University Press, The Edinburgh Building, Cambridge CB2 8RU, UK, 2013.

[115] D. Bhatti, J. von Zanthier, G. S. Agarwal, "Entanglement of Polarization and Orbital Angular Momentum,"arXiv:1502.01906 (2015).

[116] H. Di Lorenzo Pires, H. C. B. Florijn, and M. P. van Exter, "Measurement of the spiral spectrum of entangled two-photon states," Phys. Rev. Lett. 104, 020505 (2010).

[117] F. S. Roux and Y. Zhang, "Projective measurements in quantum and classical optical systems," Phys. Rev. A 90, 033835 (2014).

[118] D. F. V. James, P. G. Kwiat, W. J. Munro, and A. G. White, "Measurement of qubits," Phys. Rev. A 64, 052312 (2001).

[119] B. Jack, J. Leach, H. Ritsch, S. M. Barnett, M. J. Padgett, and S. Franke-Arnold, "Precise quantum tomography of photon pairs with entangled orbital angular momentum," New J. Phys. 11, 103024 (2009).

[120] M. Agnew, J. Leach, M. McLaren, F. S. Roux, and R. W. Boyd, "Tomography of the quantum state of photons entangled in high dimensions," Phys. Rev. A 84, 062101 (2011).

[121] J. P. Torres, A. Alexandrescu, and L. Torner, "Quantum spiral bandwidth of entangled two-photon states," Phys. Rev. A 68, 050301 (2003).

[122] C. K. Law and J. H. Eberly, "Analysis and interpretation of high transverse entanglement in optical parametric down conversion," Phys. Rev. Lett. 92, 127903 (2004).

[123] F. M. Miatto, A. M. Yao, and S. M. Barnett, "Full characterization of the quantum spiral bandwidth of entangled biphotons," Phys. Rev. A 83, 033816 (2011).

[124] Sonja Franke-Arnold, Stephen M. Barnett, Miles J. Padgett, L. Allen, "Two-photon entanglement of orbital angular momentum states," Phys. Rev. A 65, 033823 (2002).

[125] S. P. Walborn, A. N. de Oliveira, R. S. Thebaldi, and C. H. Monken, "Entanglement and conservation of orbital angular momentum in spontaneous parametric down-conversion," Phys. Rev. A 69, 023811 (2004).

[126] S. P. Walborn, S. Pádua, and C. H. Monken, "Conservation and entanglement of Hermite-Gaussian modes in parametric down-conversion," Phys. Rev. A 71, 053812 (2005).

[127] I.S. Gradshteyn and I.M. Ryzhik, *Table of Integrals, Series, and Products*, 7th ed., Academic Press, San Diego, Calif., 2007.

[128] N.N.Lebedev, *Special Functions and their Applications*, Physico-Technical Institute Academy of Sciences, U.S.S.R, Prentice-Hall,Inc. Englewood Cliffs, N.J., 1965.

[129] M. C. W. van Rossum and Th. M. Nieuwenhuizen, "Multiple scattering of classical waves: microscopy, mesoscopy, and diffusion," Rev. Mod. Phys. 71, 313 (1999).

[130] A. F. Abouraddy, B. E. A. Saleh, A. V. Sergienko, and M. C. Teich, "Role of Entanglement in Two-Photon Imaging," Phys. Rev. Lett. 87, 123602 (2001).

[131] Di Lorenzo Pires, C.H. Monken, and M.P. van Exter, "Direct measurement of transverse-mode entanglement in two-photon states," Phys. Rev. A 80, 022307 (2009).

[132] D. Branning, W. P. Grice, R. Erdmann, and I. A. Walmsley, "Engineering the indistinguishability and entanglement of two photons," Phys. Rev. Lett. 83, 955 (1999).

[133] A. G. da Costa Moura, W. A. T. Nogueira, S. P. Walborn, C. H. Monken, "Transverse spatial and frequency properties of two-photon states generated by spontaneous parametric down-conversion," arXiv:0806.4624v1 (2008).

[134] A. Consortini, R. Cochetti, J. H. Churnside, and R. J. Hill, "Inner-scale effect on irradiance variance measured for weak-to-strong atmospheric scintillation," J. Opt. Soc. Am. A 10, 2354–2362 (1993).

[135] V. A. Klückers, N. J. Wooder, M. J. Nichols, I. Munro, J. C. Dainty, "Profiling of atmospheric turbulence strength and velocity using a generalised SCIDAR technique," A&AS, 130, 141 (1998).

[136] R. W. Wilson, "SLODAR: measuring optical turbulence altitude with a Shack-Hartmann wavefront sensor," Mon. Not. R. Astron. Soc. 337, 103 (2002).

[137] D. T. Wayne, R. L. Phillips, L. C. Andrews, F. S. Vetelino, B. Griffis, M. R. Borbath, D. J. Galus, C. Visone, "Measuring optical turbulence parameters with a three-aperture receiver" Proc. SPIE 6709, 67090L (2007).

[138] H. Avetisyan, C. H. Monken, "Higher order correlation beams in atmosphere under strong turbulence conditions," Optics Express, 24, 2318 (2016).

[139] L. C. Andrews, R. L. Phillips, C. Y. Hopen, and M. A. Al-Habash, "Theory of optical scintillation," J. Opt. Soc. Am. A 16, 1417 (1999).

[140] L. C. Andrews, R. L. Phillips, and C. Y. Hopen, "Scintillation model for a satellite communication link at large zenith angles," Opt. Eng. 39, 3272 (2000).

[141] L. C. Andrews, R. L. Phillips, and C. Y. Hopen, "Aperture averaging of optical scintillations: power fluctuations and the temporal spectrum," Waves Random Media 10, 5370 (2000).

[142] L. C. Andrews, M. A. Al-Habash, C. Y. Hopen, and R. L. Phillips, "Theory of optical scintillation: Gaussian-beam wave model," Waves Random Media 11, 271 (2001).

[143] L. C. Andrews, R. L. Phillips, and C. Y. Hopen, *Laser Beam Scintillation with Applications*, SPIE, Bellingham, Wash., 2001.

[144] B.E.A. Saleh, M.C. Teich, *Fundamentals of Photonics*, John Wiley and Sons, Hoboken, 2007.

[145] A. E. Siegman, *Lasers*, University Science Books 20 Edgehill Road, Mill Valley, CA 94941, 1986.

[146] L. Allen, S. M. Barnett, and M. J. Padgett, *Optical Angular Momentum*, Institute of Physics, Bristol, 2003.

[147] W. H. Carter, "Spot size and divergence for Hermite-Gaussian beams of any order," Appl. Opt. 19, 1027 (1980).

[148] S. Franke-Arnold, L. Allen, and M. J. Padgett, "Advances in optical angular momentum," Laser Photonics Rev. 2, 299 (2008).

[149] M. J. Padgett, J. Courtial, L. Allen. "Light's orbital angular momentum," Phys. Today, 57, 35, (2004).

[150] Y. Bazhenov, M. V. Vasnetsov, and M. S. Soskin, "Laser beams with screw dislocations in their wavefronts," JETP Lett. 52, 429 (1990).

[151] M. W. Beijersbergen, R. P. C. Coerwinkel, M. Kristensen, and J. P. Woerdman, "Helical-wavefront laser beams produced with a spiral phaseplate," Opt. Com. 112, 321 (1994).

[152] K. Sueda, G. Miyaji, N. Miyanaga, and M. Nakatsuka, "Laguerre-Gaussian beam generated with a multilevel spiral phase plate for high intensity laser pulses," Opt. Express 12, 3548 (2004).

[153] J. Leach, J. Courtial, K. Skeldon, S. M. Barnett, S. F. Arnold, and M. J. Padgett, "Interferometric methods to measure orbital and spin, or the total angular momentum of a single photon," Phys. Rev. Lett. 92, 013601 (2004).

[154] L. Marrucci, C. Manzo, and D. Paparo, "Pancharatnam-Berry phase optical elements for wave front shaping in the visible domain: Switchable helical mode generation," Appl. Phys. Lett. 88, 221102 (2006).

[155] J. W. Goodman. *Introduction to Fourier Optics*, McGraw-Hill, Stanford University, 2nd edition, 1996.

[156] G.R. Fowles, *Introduction to Modern Optics*, Dover, New York, 1989.